

**CYCLONE CHARACTERIZATION USING ISRO'S
EOS06 SCATTEROMETER DATA**

*A Report submitted
in partial fulfilment for the Degree of*

B. Tech
in
Information Technology

by
BHUVAN KANDHI

pursued in
Department of Earth & Climate Sciences Area
National Remote Sensing Centre

Jeedimetla

To



**VIGNAN INSTITUTE OF TECHNOLOGY AND SCIENCE
HYDERABAD**
APRIL 2024

CERTIFICATE

This is to certify that the project report entitled **Cyclone Characterization using ISRO's EOS06 Scatterometer Data** submitted by **Bhuvan Kandhi** to the National Remote Sensing Centre, Jeedimetla, in partial fulfilment for the award of the degree of **B. Tech in Information Technology** is a bona fide record of project work carried out by him under our supervision. The contents of this report, in full or in parts, have not been submitted to any other Institution or University for the award of any degree or diploma.

Shashank Kumar Mishra

Guide

Scientist -'SE',

ECSA

Jeedimetla

Hyderabad

April,2024

DECLARATION

I declare that this project report titled **Cyclone Characterization using ISRO's EOS06 Scatterometer Data** submitted in partial fulfilment of the degree of **B. Tech in Information Technology** is a record of original work carried out by me under the supervision of **Mr. Shashank Kumar Mishra and Dr. Rajesh Sikhakoli** and has not formed the basis for the award of any other degree or diploma, in this or any other Institution or University. In keeping with the ethical practice in reporting scientific information, due acknowledgements have been made wherever the findings of others have been cited.

Bhuvan Kandhi

Hyderabad
April,2024

Acknowledgement

With a deep sense of gratitude and respect, I would like to extend my sincere thanks to the members of Mr. Shashank Kumar Mishra (Scientist-SE), Physical Oceanography Division of Earth & Climate Sciences Area at the National Remote Sensing Centre (NRSC) for their kind attention and guidance which have made this project successful. To Dr. Rajesh Sikhakoli (Head, Physical Oceanography Division) , I am grateful for giving me the opportunity to pursue this project in the premises of the prestigious NRSC.

Bhuvan Kandhi

Table of Contents

Keywords.....	5
Abstract.....	6
1. Introduction.....	8
1.1 Atmospheric Pressure.....	10
1.1.1 Horizontal Distribution of Pressure.....	10
1.1.2 Vertical Variation of Pressure.....	11
1.1.3 Global Distribution of Sea Level Pressure.....	12
1.2 Wind Circulation.....	12
1.2.1 Forces Affecting the Velocity and Direction of Wind.....	12
1.2.2 Seasonal Winds.....	16
1.2.3 Tropical Cyclones.....	17
1.2.4 Life Cycle of Tropical Cyclones.....	23
1.2.5 Formation or Genesis Stage.....	24
1.2.6 Movement of Cyclones.....	25
1.2.7 Classification of Cyclonic Disturbances.....	26
1.3 EOS06-SCAT.....	29
1.4 Why this Study.....	31
2. Products Background.....	33
2.1. EOS06-SCAT Winds.....	33
2.2. Wind Curl(RV).....	33
3. Methodology.....	35
3.1. Wind Velocity.....	37
3.2. Wind Curl(RV).....	37
3.3. Binarizations.....	38
3.4. Centre Identification.....	43
3.4.1 RV Mawar.....	43
3.4.2 Binarization Mawar.....	43
3.4.3 RV Biparjoy.....	44
3.4.5 Binarization Biparjoy.....	44
3.5. Characteristics along different quadrants.....	45
3.5.1. RV.....	45
3.5.2. Binarization.....	48
4. Results.....	49
4.1. RV.....	50
4.2. Binarization.....	67
4.3. Track Plot.....	83
4.4. Contour R34, R50, R60.....	86
5. Conclusion.....	87
7. References.....	88
Process DataSet.....	89

Table of Figures

Figure 1.1- Global Isobars, pressure and wind systems	11
Figure 1.2- Geostrophic Wind.....	14
Figure 1.3- Convergence and divergence of winds	14
Figure 1.4- Simplified general circulation of the atmosphere.....	15
Figure 1.5- Vertical section of the tropical cyclone.....	18
Figure 1.6- Global tropical cyclone tracks.....	22
Figure 1.7- Global wind patterns	26
Figure 1.8- Observation/operating geometry of the proposed O3SCAT.....	29
Figure 1.9- Image view of EOS06-SCAT.....	30
Figure 1.10- Details of different levels EOS06-SCAT Data Product.....	31
Figure 3.1- Flow chart Relative Vorticity.....	36
Figure 3.2- Flow chart Binarization.....	36
Figure 3.3- Wind Velocity.....	37
Figure 3.4- RV snippet.....	38
Figure 3.5- Binarization snippet.....	39
Figure 3.6- Binarized largest group of ones.....	40
Figure 3.7- Grayscale scaled image.....	40
Figure 3.8- Binarized image.....	41
Figure 3.9- Binarized largest group of ones.....	41
Figure 3.10- Binarized largest group of ones.....	42
Figure 3.11- Binarized largest group of ones.....	42
Figure 3.12- RV Mawar.....	43
Figure 3.13- Binarization Mawar.....	44
Figure 3.14- RV Biparjoy.....	44
Figure 3.15- Binarization Biparjoy.....	45
Figure 3.16- RV - Mawar, Quadrant Wise - Max.....	47
Figure 3.17- RV - Mawar, Quadrant Wise - Mean.....	47
Figure 3.18- RV - Mawar, Quadrant Wise - Max.....	47
Figure 3.19- RV - Mawar, Quadrant Wise - Mean.....	47
Figure 3.20- Binarization - Mawar, Quadrant Wise - Max.....	48
Figure 3.21- Binarization - Mawar, Quadrant Wise - Mean.....	48
Figure 3.22- Binarization - Mawar, Quadrant Wise - Max.....	48
Figure 3.23- Binarization - Mawar, Quadrant Wise - Mean.....	48
Figure 4.1- Day 142-162 Pass with max wind speed in each quadrants.....	49
Figure 4.2- Day 157,9-161-163 Pass with max wind speed in each quadrants....	49
Figure 4.3- Day 142-162 Pass with max wind speed in each quadrants.....	49
Figure 4.4- Day 157,9-161-163 Pass with max wind speeds in each quadrants....	49
Figure 4.5- Day 22 142 Pass with min 11.39 , max 33.36, vorticity 12.29 ws.....	51
Figure 4.1.2- Day 23 143 Pass with min 8.57, max 36.58, vorticity 21.92 ws.....	52

Figure 4.6- Day 24 144 Pass with min 10.41, max 47.34, vorticity 13.80 ws.....	53
Figure 4.7- Day 25 145 Pass with min 12.1, max 38.65, vorticity 15.79 ws.....	54
Figure 4.8- Day 26 146 Pass with min 13.66, max 46.16, vorticity 18.41.....	55
Figure 4.9- Day 27 147 Pass with min 11.91, max 37.59, vorticity 14.69 ws.....	56
Figure 4.10- Day 28 148 Pass with min 8.91, max 36.99, vorticity 4.57 ws.....	57
Figure 4.11- Day 29 149 Pass with min 11.21, max 44.54, vorticity 17.66 ws....	58
Figure 4.12- Day 30 150 Pass with min 12.52, max 41.91, vorticity 6.98 ws....	59
Figure 4.13- Day 31 151 Pass with min 10.62, max 35.77, vorticity 12.69 ws....	60
Figure 4.14- Day 01 152 Pass with min 11.32, max 30.51, vorticity 12.36 ws....	61
Figure 4.15- Day 06 157 Pass with min 7.92, max 39.34, vorticity 13.24 ws....	62
Figure 4.16- Day 08 159 Pass with min 7.55, max 33.96, vorticity 11.69 ws....	63
Figure 4.17- Day 10 161 Pass with min 10.17, max 37.35, vorticity 11.27 ws....	64
Figure 4.18- Day 11 162 Pass with min 8.66, max 44.17, vorticity 21.77 ws....	65
Figure 4.19- Day 12 163 Pass with min 7.76, max 33.13, vorticity 11.87 ws....	66
Figure 4.20- Day 22 142 Pass with min 11.39, max 33.46, vorticity 12.21 ws....	67
Figure 4.21- Day 23 143 Pass with min 11.93, max 36.58, vorticity 21.92 ws....	68
Figure 4.22- Day 24 144 Pass with min 12.99, max 47.34, vorticity 13.80 ws....	69
Figure 4.23- Day 25 145 Pass with min 12.1, max 38.65 , vorticity 15.79 ws....	70
Figure 4.24- Day 26 146 Pass with min 13.66 , max 46.16, vorticity 18.41 ws....	71
Figure 4.25- Day 27 147 Pass with min 10.74, max 37.59, vorticity 14.96 ws....	72
Figure 4.26- Day 28 148 Pass with min 8.91, max 36.99, vorticity 7.44 ws....	73
Figure 4.27- Day 29 149 Pass with min 11.21, max 44.54, vorticity 17.66 ws....	74
Figure 4.28- Day 30 150 Pass with min 10.35, max 33.21, vorticity 5.22 ws....	75
Figure 4.29- Day 31 151 Pass with min 10.62, max 35.77, vorticity 12.19 ws....	76
Figure 4.30- Day 32 152 Pass with min 11.32, max 28.69, vorticity 12.36 ws....	77
Figure 4.31- Day 06 157 Pass with min 11.11, max 39.34, vorticity 13.24 ws....	78
Figure 4.32- Day 08 159 Pass with min 10.4, max 33.96, vorticity 11.69 ws....	79
Figure 4.33- Day 10 161 Pass with min 10.17, max 37.35, vorticity 11.27 ws....	80
Figure 4.34- Day 11 162 Pass with min, max, vorticity ws.....	81
Figure 4.35- Day 12 162 Pass with min 8.95, max 44.17, vorticity 21.77 ws....	82
Figure 4.36- Track data of RV and binarization for mawar.....	83
Figure 4.37- Track data of RV and binarization for biparjoy.....	83
Figure 4.38- Track data of RV and binarization for mawar.....	84
Figure 4.39- Track data of RV and binarization for biparjoy.....	84
Figure 4.40- Track data of centre between IMD and RVand BI for Marwr.....	85
Figure 4.41- Track data of centre between IMD and RVand BI for Biparjoy.....	85

List of Tables

Table 1.1- Keywords.....	6
Table 1.2- Standard Pressure and Temperature at Selected (Atmospheric circulation and weather systems [3]).....	12
Table 1.3- Hurricane Scale (Atmospheric circulation and weather systems [3])...22	
Table 1.4- Cyclone Classification(Richard Ryan Halterman [7]).....	28
Table 1.5- Vmax-Direction.....	47
Table 1.6- Vmax-Direction.....	47

Keywords

Keyword	Context
RV	Relative Vorticity
EOS06	Earth Observation Satellite
V_{max}	Maximum wind speed
R_{max}	Distance between centre and maximum wind speed.
$V_{Direction}$	maximum wind speed direction
Center_ws	wind speed at the centre of the cyclone
N	NORTH
S	SOUTH
W	WEST
E	EAST
NE	NORTH EAST
NW	NORTH WEST
SE	SOUTH EAST
SW	SOUTH WEST
km	Kilometre
m/s	metres per second
kt	knots
C	Celsius
F	Fahrenheit

Table 1.1- Keywords.

Abstract

In this report, we delve into the criticality of enhancing the precision of tropical cyclone analysis and forecasting to mitigate the devastating impacts of these natural disasters. With tropical cyclones being among the most severe natural calamities, the locus and intensity of these cyclones significantly influence their impact. Thus, it becomes imperative to refine our methodologies for assessing and predicting tropical cyclones. This report focuses on two innovative methods aimed at enhancing cyclone centre positioning accuracy by leveraging the L2B scatterometer data of EOS06 SCAT sensor as a case study to scrutinise the distribution characteristics of Relative Vorticity during cyclones and the binarization of scatterometer data to estimate V_{max} distribution. Subsequently, these methods are meticulously compared to ascertain their efficacy. The ultimate aim is to provide an automated process for analysing the cyclone characteristics and monitor its behaviour and minimise the disparity in cyclone centre positioning by refining proposed methodologies. To validate the proposed methods, remote sensing data pertaining to Typhoon "Mawar" and Cyclone "Biparjoy" are employed. Through comprehensive analysis, it becomes evident that these proposed methods yield more accurate cyclone centre positioning compared to conventional techniques (Aircraft Reconnaissance, Buoy Data, Radar Observations). This advancement holds profound implications for disaster management and preparedness, as it enables more precise forecasting and timely interventions in the face of tropical cyclones.

Project Outline

This project is organised into five chapters with one appendix.

Chapter 1 covers the introduction and description of the problem.

Chapter 2 provides background on tropical cyclones, cyclogenesis and a brief history of scatterometry.

Chapter 3 provides details about EOS06-SCAT, and purpose of the study along with description about product background for EOS06-SCAT winds and Relative Vorticity (RV).

Chapter 4 is a summary look at tropical cyclone wind retrievals. The Oceansat-3-derived wind images are evaluated for their usefulness in observing tropical cyclone parameters of interest. Two different methods are proposed: Relative Vorticity and Binarization for centre identification, and characteristics of the cyclone in different quadrants.

Chapter 5 concludes the body of this report by summarising results and with additional information on the automated tropical cyclone data set generation tools created for this study.

Chapter 1

1. Introduction

One of the most disruptive of natural disasters, tropical cyclones have long garnered significant attention from the scientific community. Early meteorologists were limited in their tropical cyclone observations to near coastal and sporadic ship-based measurements. Beginning in 1945 with the 53rd Weather Reconnaissance Squadron, aerial observation of hurricanes became possible. Then, with the launch of the first weather satellites, in the 1950s and 1960s, scientists gained further tropical cyclone observation ability. Space-borne remote sensing has enabled much improvement in tropical cyclone understanding and prediction. This thesis focuses on the observation of tropical cyclones by wind scatterometers, a class of space-borne remote sensors [7].

A scatterometer is a scientific instrument to measure the return of a beam of light or radar waves scattered by diffusion in a medium such as air. Radar scatterometers use radio or microwaves to determine the normalised radar cross section (σ^0 , "sigma zero" or "sigma naught") of a surface. They are often mounted on weather satellites to find wind speed and direction, and are used in industries to analyse the roughness of surfaces.[1] Wind scatterometers are differentiated from other radars by their highly calibrated measurements of the returned pulse power from multiple azimuth angles. The pulse power backscattered by a distributed target such as the Earth's surface contains information about its roughness and dielectric properties. Surface roughness is generally direction dependent. Thus, multiple azimuth observations are required to fully characterise it. From the surface roughness at a variety of observation geometries, the near-surface ocean wind speed and direction can be inferred.

Description of the Problem

Modern advances enable researchers to monitor tropical cyclones in a variety of ways. In situ observation remains important for the most accurate measurements of atmospheric pressure, wind speed and direction, and other parameters, but such aerial reconnaissance of tropical cyclones on a global scale is prohibitively costly

and dangerous. Surface-based measurement by ship and buoy is used, but is inadequate for storm-scale observation because of its sparse and sporadic sampling. Space-borne observation using visible and infrared sensors, microwave radiometers, precipitation radars, and scatterometers contribute to a greater understanding of tropical cyclone conditions. They do so over expansive scales and without endangering in situ data collectors. Scatterometers can detect the centre of a cyclone by identifying the area of maximum wind rotation. This information is crucial for accurately determining the position and movement of the cyclone. Accurate data on wind speed and direction provided by scatterometers improves the accuracy of computer models used for forecasting cyclone tracks and intensities. This, in turn, helps in issuing timely warnings and advisories to potentially affected regions, allowing for better preparedness and mitigation efforts.

EOS satellite scatterometers provide data over large geographical areas, allowing for comprehensive coverage of cyclone-prone regions. This wide coverage enables researchers to monitor cyclones across vast ocean expanses where ground-based data may be scarce.

EOS satellite scatterometers can collect data remotely, eliminating the need for physical presence in the cyclone-affected area. This remote sensing capability is particularly beneficial for studying cyclones in remote or inaccessible regions where deploying ground-based instruments may be challenging. EOS satellite scatterometer data undergo rigorous validation and calibration processes to ensure accuracy and reliability. Researchers can have confidence in the quality of the data, making it suitable for scientific analysis and modelling purpose.

Chapter 2

Background

Spaceborne remote sensors have greatly increased in number and capability in recent years. They have also seen a commensurate increase in use and utility for monitoring tropical cyclones. This chapter provides basic background on tropical cyclones, cyclogenesis, and observation of tropical cyclones, and an overview of scatterometry algorithms for standard and enhanced resolution wind field retrieval.

1.1 Atmospheric Pressure

The weight of a column of air contained in a unit area from the mean sea level to the top of the atmosphere is called the atmospheric pressure. The atmospheric pressure is expressed in units of millibar (mb). At sea level the average atmospheric pressure is 1,013.2 mb. Due to gravity the air at the surface is denser and hence has higher pressure. The air pressure decreases with height. At any elevation it varies from place to place and its variation is the primary cause of air motion, i.e. wind which moves from high pressure areas to low pressure areas.

1.1.1 Horizontal Distribution of Pressure

Horizontal distribution of pressure is studied by drawing isobars at constant levels. Isobars are lines connecting places having equal pressure. In order to eliminate the effect of altitude on pressure, it is measured at any station after being reduced to sea level for purposes of comparison. The sea level pressure distribution is shown on weather maps. Low-pressure system is enclosed by one or more isobars with the lowest pressure in the centre. High-pressure system is also enclosed by one or more isobars with the highest pressure in the centre.

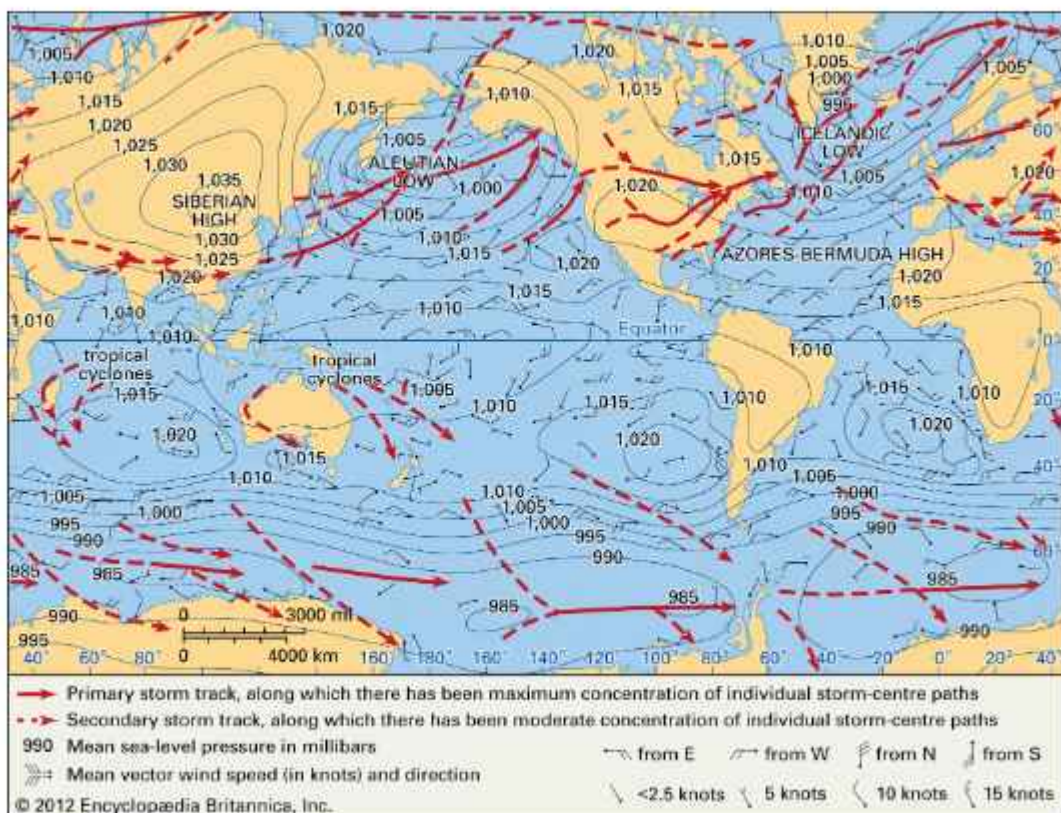


Figure 1.1- Global Isobars, pressure and wind systems (Atmospheric pressure and wind [2]).

1.1.2 Vertical Variation of Pressure

In the lower atmosphere the pressure decreases rapidly with height. The decrease amounts to about 1 mb for each 10 m increase in elevation. It does not always decrease at the same rate. Table 1.0 gives the average pressure and temperature at selected levels of elevation for a standard atmosphere.

Level	Pressure in mb	Temperature °C
Sea Level	1,013.25	15.2
1 km	898.76	8.7
5 km	540.48	-17.3
10 km	265.00	-49.7

Table 1.2- Standard Pressure and Temperature at Selected (Atmospheric circulation and weather systems [3]).

The vertical pressure gradient force is much larger than that of the horizontal pressure gradient. But, it is generally balanced by a nearly equal but opposite gravitational force. Hence, we do not experience strong upward winds.

1.1.3 Global Distribution of Sea Level Pressure

Near the equator the sea level pressure is low and the area is known as equatorial low. Along 30°N and 30°S are found the high-pressure areas known as the subtropical highs. Further polewards along 60°N and 60°S , the low-pressure belts are termed as the sub polar lows. Near the poles the pressure is high and it is known as the polar high. These pressure belts are not permanent in nature. They oscillate with the apparent movement of the sun. In the northern hemisphere in winter they move southwards and in the summer northwards.

1.2 Wind Circulation

A cyclone is a low-pressure weather system that forms over a tropical or subtropical ocean, usually accompanied by severe weather or oceanic phenomena such as strong winds, heavy rains and high waves, and can cause serious property damage and casualties if it invades coastal areas.

The impact of tropical cyclone disasters mainly depends on the intensity, movement path and vulnerability of the disaster-bearing bodies, so real-time and accurate information on the location and intensity of tropical cyclones is of great significance for disaster prevention and mitigation. At present, a tropical cyclone monitoring system combining ground radar, unmanned aerial vehicles (UAVs) or manned aircraft, and remote sensing satellites has been established at home and abroad. Among them, satellite remote sensing, as a large-scale dynamic monitoring method, is the most effective means to obtain information on the location and intensity of tropical cyclone centres at the same time.

All cyclones are characterised by:

- (1) low pressure at the centre,
- (2) winds spiralling toward the centre.

1.2.1 Forces Affecting the Velocity and Direction of Wind

The wind blows from high pressure to low pressure. The wind at the surface experiences friction. In addition, rotation of the earth also affects the wind movement. The force exerted by the rotation of the earth is known as the Coriolis force. Thus, the horizontal winds near the earth surface respond to the combined

effect of three forces – the pressure gradient force, the frictional force and the Coriolis force. In addition, the gravitational force acts downward.

Pressure Gradient Force

It refers to the force exerted on a fluid (such as air or water) due to differences in pressure over a distance. When there is a variation in pressure across a fluid, a pressure gradient is established, and the fluid tends to flow from areas of high pressure to areas of low pressure.

Wind Stress

Wind stress, also known as surface wind stress or wind drag, refers to the force exerted by the wind on the surface of a body of water, such as the ocean. It represents the transfer of momentum from the atmosphere to the ocean surface due to the frictional interaction between the air and the water. Therefore losing or gaining wind velocity depending upon the sea state encountered with winds.

Coriolis Force

The rotation of the earth about its axis affects the direction of the wind. This force is called the Coriolis force after the French physicist who described it in 1844. It deflects the wind to the right direction in the northern hemisphere and to the left in the southern hemisphere. The deflection is more when the wind velocity is high. The Coriolis force is directly proportional to the angle of latitude. It is maximum at the poles and is absent at the equator.

$$F_c = 2m(v \times \omega) \quad \text{Eq. 1.1}$$

m is the mass of the object, v is the velocity, and ω is the angular velocity of the Earth (7.27×10^{-5} rad/sec).

The Coriolis force acts perpendicular to the pressure gradient force. The pressure gradient force is perpendicular to an isobar. The higher the pressure gradient force, the more is the velocity of the wind and the larger is the deflection in the direction of wind. As a result of these two forces operating perpendicular to each other, in the low-pressure areas the wind blows around it. At the equator, the Coriolis force is zero and the wind blows perpendicular to the isobars. The low pressure gets filled instead of getting intensified. That is one of the reasons why tropical cyclones are not formed near the equator.

Pressure and Wind

The velocity and direction of the wind are the net result of the wind generating forces. The winds in the upper atmosphere, 2 - 3 km above the surface, are free from the frictional effect of the surface and are controlled mainly by the pressure gradient and the Coriolis force. When isobars are straight and when there is no friction, the pressure gradient force is balanced by the Coriolis force and the resultant wind blows parallel to the isobar.

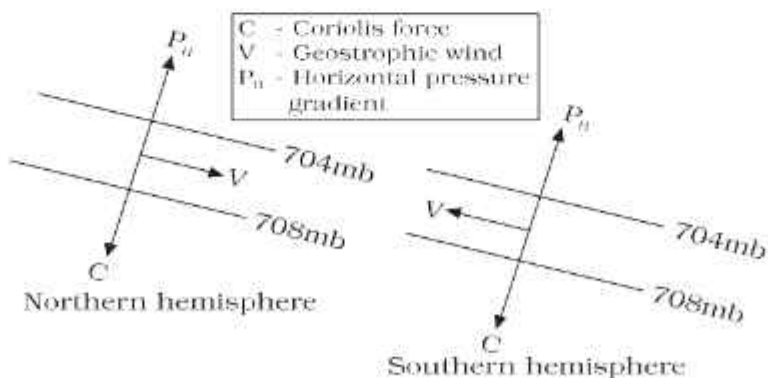


Figure 1.2- Geostrophic Wind (Atmospheric circulation and weather systems [3]).

The wind circulation around a low pressure system is called cyclonic circulation. Around a high pressure system it is called anticyclonic circulation. The direction of winds around such systems changes according to their location in different hemispheres. The wind circulation at the earth's surface around low and high on many occasions is closely related to the wind circulation at higher levels. Generally, over a low pressure area the air will converge and rise. Over high pressure areas the air will subside from above and diverge at the surface. Apart from convergence, some eddies, convection currents, orographic uplift and uplift along fronts cause the rising of air, which is essential for the formation of clouds and precipitation.

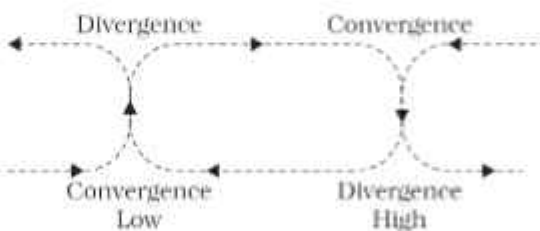


Figure 1.3- Convergence and divergence of winds (Atmospheric circulation and weather systems [3]).

General circulation of the atmosphere

The pattern of planetary winds largely depends on-

- (i) latitudinal variation of atmospheric heating;
- (ii) emergence of pressure belts;
- (iii) the migration of belts following apparent path of the sun;
- (iv) the distribution of continents and oceans;
- (v) the rotation of earth.

The pattern of the movement of the planetary winds is called the general circulation of the atmosphere. The general circulation of the atmosphere also sets in motion the ocean water circulation which influences the earth's climate.

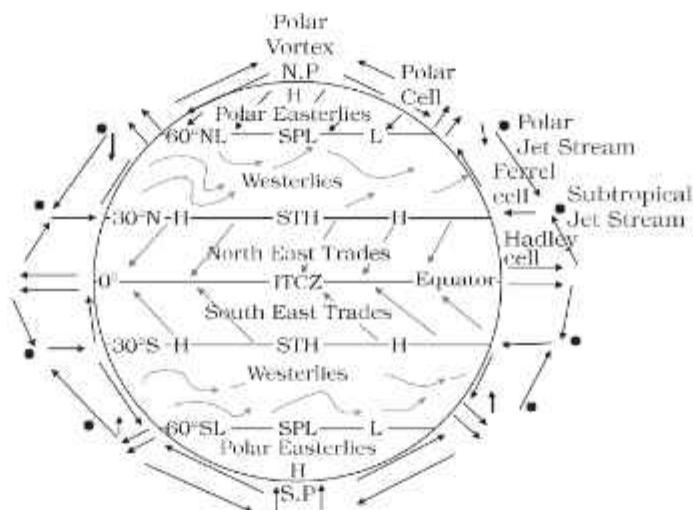


Figure 1.4- Simplified general circulation of the atmosphere (Atmospheric circulation and weather systems [3]).

The air at the Inter Tropical Convergence Zone (ITCZ) rises because of convection caused by high insolation and a low pressure is created. The winds from the tropics converge at this low pressure zone. The converged air rises along with the convective cell. It reaches the top of the troposphere up to an altitude of 14km. and moves towards the poles. This causes accumulation of air at about 30°N and 30°S. Part of the accumulated air sinks to the ground and forms a subtropical high. Another reason for sinking is the cooling of air when it reaches 30° N and 30°S latitudes. Down below near the land surface the air flows towards the equator as the easterlies. The easterlies from either side of the equator

converge in the Inter Tropical Convergence Zone (ITCZ). Such circulations from the surface upwards and vice-versa are called cells. Such a cell in the tropics is called Hadley Cell. In the middle latitudes the circulation is that of sinking cold air that comes from the poles and the rising warm air that blows from the subtropical high. At the surface these winds are called westerlies and the cell is known as the Ferrel cell. At polar latitudes the cold dense air subsides near the poles and blows towards middle latitudes as the polar easterlies. This cell is called the Polar cell. These three cells set the pattern for the general circulation of the atmosphere. The transfer of heat energy from lower latitudes to higher latitudes maintains the general circulation.

The general circulation of the atmosphere also affects the oceans. The large-scale winds of the atmosphere initiate large and slow moving currents of the ocean. Oceans in turn provide input of energy and water vapour into the air. These interactions take place rather slowly over a large part of the ocean.

1.2.2 Seasonal Winds

The pattern of wind circulation is modified in different seasons due to the shifting of regions of maximum heating, pressure and wind belts [3].

Global seasonal winds are large-scale atmospheric circulation patterns that change with the seasons due to variations in solar heating and the Earth's axial tilt. These winds play a crucial role in shaping regional climates, distributing heat, moisture, and atmospheric gases around the globe.

During the Northern Hemisphere winter, the temperature contrast between the equator and the poles strengthens, resulting in the intensification of the polar vortex and the formation of the subtropical jet stream. This leads to the dominance of westerly winds in the mid-latitudes and the onset of the northeast trade winds in the tropics.

Conversely, in the Northern Hemisphere summer, the temperature gradient weakens, causing the polar vortex to weaken and retreat poleward. This allows the subtropical jet stream to migrate northward, leading to the prevalence of easterly winds in the tropics and the establishment of the westerlies in the mid-latitudes.

Similar seasonal wind patterns occur in the Southern Hemisphere, albeit with opposite characteristics due to the reversed seasons. These global seasonal wind patterns influence weather phenomena such as monsoons, cyclones, and the migration of weather systems, impacting agriculture, transportation, and ecosystems worldwide. Understanding these wind patterns is essential for climate modelling, weather prediction, and mitigating the impacts of climate change.

1.2.3 Tropical Cyclones

Cyclones are powerful, rotating storm systems characterised by low atmospheric pressure at their centre, known as the eye. They typically form over warm ocean waters near the equator and can vary in size from tens to hundreds of kilometres across. The term tropical cyclone encompasses a wide variety of storms. It describes the weather system's formation in the tropics and the nature of wind circulation within the system counter-clockwise in the northern hemisphere and clockwise in the southern. Specifically, a tropical cyclone is a warm-core, synoptic scale cyclone with organised convection and closed circulation of surface winds about a well defined centre.

Tropical cyclones originate and intensify over warm tropical oceans. The conditions favourable for the formation and intensification of tropical storms are:

- (i) Large sea surface with temperature higher than 27° C ;
- (ii) Presence of the Coriolis force;
- (iii) Small variations in the vertical wind speed;
- (iv) A pre-existing weak- low-pressure area or low-level-cyclonic circulation;
- (v) Upper divergence above the sea level system.

The energy that intensifies the storm, comes from the condensation process in the towering cumulonimbus clouds, surrounding the centre of the storm. With continuous supply of moisture from the sea, the storm is further strengthened. On reaching the land the moisture supply is cut off and the storm dissipates. The place where a tropical cyclone crosses the coast is called the landfall of the cyclone. The cyclones, which generally cross 20° N latitude generally, recurve and they are more destructive.

A schematic representation of the vertical structure of a mature tropical cyclonic storm is shown in Figure 1.5. A mature tropical cyclone is characterised by the strong spirally circulating wind around the centre, called the eye. The diameter of the circulating system can vary between 150 and 250 km.

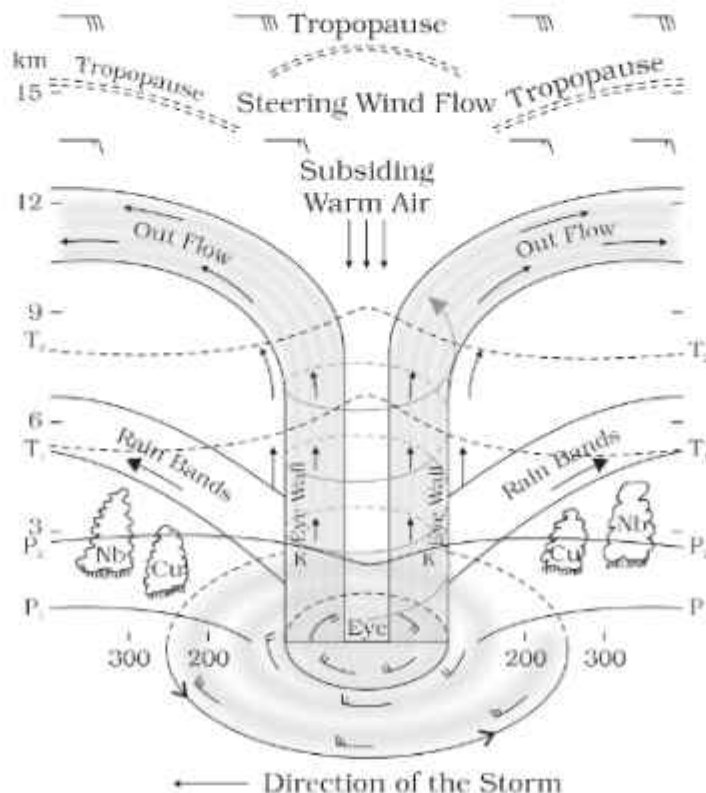


Figure 1.5- Vertical section of the tropical cyclone (after Rama Sastry) [3].

The eye is a region of calm with subsiding air. Around the eye is the eye wall, where there is a strong spiralling ascent of air to greater height reaching the tropopause. The wind reaches maximum velocity in this region, reaching as high as 250 km per hour. Torrential rain occurs here. From the eye wall rain bands may radiate and trains of cumulus and cumulonimbus clouds may drift into the outer region. The diameter of the storm over the Bay of Bengal, Arabian sea and Indian ocean is between 600 - 1200 km. The system moves slowly about 300 - 500 km per day. The cyclone creates storm surges and they inundate the coastal lowlands.

The direction of the spiral is unique because in the northern hemisphere the winds blow counterclockwise and in the southern hemisphere they blow clockwise. Cyclones are formed from simple thunderstorms. However, these thunderstorms can only grow to cyclone strength with cooperation from both the ocean and the

atmosphere. First of all, the ocean water itself must be warmer than a threshold, say, 28 °C. The heat and moisture from this warm water is the source of energy for cyclones. Cyclones will weaken rapidly when they travel over land or colder ocean waters locations where their heat and/or moisture sources do not exist. High relative humidities in the lower and middle troposphere are also required for cyclone development. These high humidities reduce the amount of evaporation in clouds and maximises the latent heat released because there is more precipitation. The vertical wind shear in a tropical cyclone's environment is also important. Wind shear is defined as the amount of change in the wind's direction or speed with increasing altitude. When the wind shear is weak, the storms that are part of the cyclone grow vertically, and the latent heat from condensation is released into the air directly above the storm, aiding in development. When there is stronger wind shear, the storms become more slanted and the latent heat release is dispersed over a much larger area.

The eye is rain-free with light winds. It is surrounded by a 'wall cloud' made up of tall cumulo-nimbus clouds rising up to an altitude of 15-18 km, the wall cloud thickness being about 10-15 km radially. Below the wall cloud are found the strongest surface winds of the cyclone (V_{max}) with heaviest rain. Beyond the wall cloud, surface wind speeds decrease gradually with the radial distance from the centre and rainfall is confined to the regions covered by the inward spiralling cloud-bands (composed of cumulo-nimbus clouds and some cumulus clouds at large distances from the centre) that are seen within a radial distance of about 400 km from the centre of the cyclone.

As one moves from the periphery to the centre of the cyclone, the sea level atmospheric pressure falls continuously, the largest radial pressure gradients of 2-4 hPa/km, occurring in the wall cloud region. Under the influence of frictional forces, the low-level wind direction, which is almost tangential to the nearly circular isobars of the cyclone field at about 1-km above sea level, cuts the isobars at about 25° towards low pressure at sea level. The low level winds rich in moisture thus possess strong tangential and radial components causing the air parcels to spiral inwards from the peripheral regions of the cyclone towards its centre. In consequence, their rotational velocity (tangential wind) increases

rapidly due to partial conservation of its angular momentum. The radial component of the wind converges large amounts of moisture to the central regions of the cyclone, which ascends and condenses in cloud formations there, keeping the central regions warmer than the surrounding tropical atmosphere. This warm anomaly which reaches a maximum of about 15°C at 300-200 hPa level (9-12 km altitude) reduces the radial pressure gradients at these high altitudes. The cyclically rotating air parcels rising up in the central regions of the cyclone move outwards in the upper troposphere, under the action of unbalanced centrifugal forces (with reduced pressure gradients) and conserving angular momentum, begin to reverse their cyclonic rotation as they move further away from the centre. Satellite pictures of tropical cyclones indeed show both the inward spiralling (anti-clockwise) low level clouds and the outward moving (clockwise) cirrus clouds at the upper levels in the northern hemisphere.

Precise sub-terms for tropical cyclones vary by the storm's intensity and location. For weaker storms, all basins use the same referencing scheme: tropical depression for storms with winds less than 33 kt (17 m/s) and tropical storm for storms with winds between 33-63 kt (17-32 m/s). For more intense tropical cyclones, referencing terms vary by basin. The principal basins of tropical cyclone formation monitored by US agencies. The National Hurricane Centre (NHC) is tasked with storms originating in the Northern Atlantic and Eastern Pacific. In these basins, tropical cyclones with winds exceeding 63 kt (32 m/s) are termed hurricanes after the Carib god of evil, Hurricane.

Tropical cyclone basins: 1) Eastern Pacific, 2) Northern Atlantic 3) Indian Ocean, 4) Western Pacific, and 5) Southern Pacific

Joint Typhoon Warning centre (JTWC) monitors tropical cyclones for US interests in the Indian Ocean, Western Pacific, and Southern Pacific. Within these basins, the JTWC designates storms exceeding 63 kt (32 m/s) as typhoons. This term is thought to originate from a Cantonese phrase meaning big wind . Other local agencies monitor these basins for their respective nations, but all reference data used herein is acquired from the NHC and JTWC.

Hurricanes are further classified according to maximum sustained winds (1 min average) by the Sa r-Simpson Hurricane Scale, see Table 1.2 This scale attempts

to estimate the expected damage to man-made structures from impacting storms. It originated in 1969 with Herbert Saffir, a civil engineer on commission by the United Nations to study low cost housing in hurricane prone areas. Bob Simpson, then director of the NHC, added expected storm surge values to the scale. Because classification is based on wind speeds alone, actual values of storm surge and resultant damage may vary widely due to related complexities. Other scales are used by local agencies to classify intense tropical cyclones in basins outside the Northern Atlantic and Eastern Pacific.

Category (Damage)	Wind Speed	Storm Surge
1 (Minimal)	64-82 kt (33-42 m/s)	4-5 ft (1.2-1.5 m)
2 (Moderate)	83-95 kt (43-49 m/s)	6-8 ft (1.8-2.4 m)
3 (Extensive)	96-113 kt (50-58 m/s)	9-12 ft (2.7-3.7 m)
4 (Extreme)	114-135 kt (59-69 m/s)	13-18 ft (4.0-5.5 m)
5(Catastrophic)	>135 kt (>69 m/s)	>18 ft (>5.5 m)

Table 1.3- Hurricane Scale (Atmospheric circulation and weather systems [3]).

In order for continued intensification, adequate linkage between the lower and upper troposphere must exist so that mass can be transported vertically and then dispersed horizontally. A potentially disruptive force in this linkage is the presence of strong vertical wind shear. In the Southern Atlantic basin, excessive wind shear is one of the primary factors in the absence of tropical cyclones. Wind shear a difference in wind speed or direction in excess of about 15 kt (8 m/s) prohibits the necessary structure for appropriate heat dissipation and mass dispersion. Without these two elements, the storm is unable to maintain a sufficiently low central pressure for cyclonic wind convergence. It should be noted that the above conditions are necessary, but not sufficient, for tropical cyclone formation and intensification. Frequently, all of the conditions appear to be met for cyclogenesis, yet the storm fails to materialise. This is one of the complications in tropical cyclone intensity forecasting.

Tropical cyclones are violent storms that originate over oceans in tropical areas

and move over to the coastal areas bringing about large scale destruction caused by violent winds, very heavy rainfall and storm surges. This is one of the most devastating natural calamities.

They are known as Cyclones in the Indian Ocean, Hurricanes in the Atlantic, Typhoons in the Western Pacific and South China Sea, and Willy-willies in the Western Australia. Cyclones are characterised as tornadoes, hurricanes and typhoons. A tornado is a smaller kind of cyclone. When a cyclone forms over tropical waters in the North Atlantic or eastern North Pacific oceans and has winds of 119 km/hr or more it is called a Hurricane. If the cyclone forms in the western Pacific with winds of 119 km/hr or more it is called a Typhoon. All of these storms are generally accompanied by high winds, heavy rains, severe thunder, and lightning. In the north Indian Ocean they are simply called tropical cyclones.

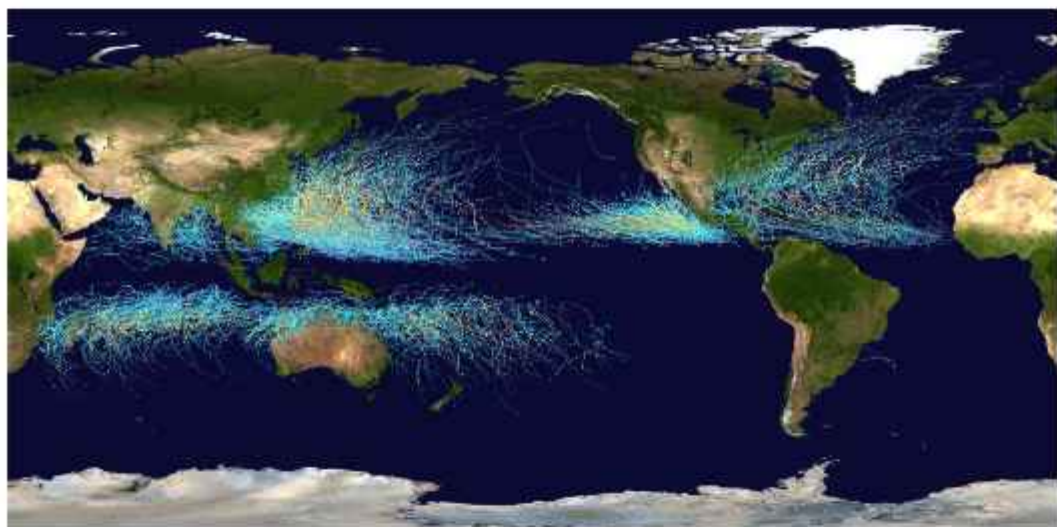


Figure 1.6- Global tropical cyclone tracks (Global tropical cyclone tracks) [4].

Our current knowledge of the structure of tropical cyclones has come from studies made over a hundred years of different cyclone-prone regions of the world. Early studies using ship reports and measurements from coastal Island observatories gave a reasonably good picture of the surface level features of the cyclone, but that of their three dimensional structure has been derived mainly from reconnaissance flights using specially equipped aircrafts that were flown into the cyclone at various levels, measuring winds, temperatures, humidity and pressure. Direct sensing as well as remote sensing methods were used. Compositing of data from routine balloon soundings of the atmosphere has also yielded a wealth of

information. Details regarding the eye, wall cloud and the spiral cloud bands were obtained from satellite pictures (polar orbiting and geo-stationary) as well as cyclone detection radar systems installed at coastal and island .

1.2.4 Life Cycle of Tropical Cyclones

Cyclones evolve through a life cycle of stages from genesis to dissipation. A tropical disturbance in time can grow to a more intense stage by attaining a specified sustained wind speed. Cyclones can often live for a long period of time as much as two to three weeks. They may initiate as a cluster of thunderstorms over the tropical ocean waters. Once a disturbance has become a tropical depression, the amount of time it takes to achieve the next stage, tropical storm, can take as little as half a day up to a couple of days. The same may occur for the amount of time a tropical storm needs to intensify into a cyclone. Atmospheric and oceanic conditions play the major role in determining these events.

There are several schemes that describe the life-cycle of an average TC. The four stages shown below are not really discrete entities, rather they represent a continuous process. Individual stages may even occur more than once during the life-cycle of a particular storm.

Though not fully understood, six conditions are generally necessary for tropical cyclone formation or tropical cyclogenesis: pre-existing atmospheric disturbance, warm ocean waters, high humidity, sufficient atmospheric vertical temperature gradient, adequate distance from the equator, and weak vertical wind shear.

Tropical cyclones do not spontaneously develop. They require pre existing disturbances with near-surface circulation. Cyclones may then intensify as the manifestation of a positive feedback heat engine. They are fueled by warmth requisite water temperatures above 26°C (79°F) and an essentially limitless supply of moisture from the ocean surface.

To permit the release of latent heat energy and fuel the tropical cyclone, the upper atmosphere must be sufficiently cool with respect to the rising warm moist air. The resultant saturation of the cool upper atmosphere contributes to the generation of cumulonimbus clouds which are effective transporters of additional heat and moisture to the upper atmosphere. Vertical transportation of warm air ceases at the

tropopause so rising air spreads out laterally once reaching this boundary. This dissipation of the vertical air column further lowers near-surface pressures at the storm core and enhances surface wind convergence.

Cyclonic circulation is initiated by the Coriolis effect. For the force to be sufficiently strong, the emergent storm must occur at least 4° - 5° (about 500 km) poleward. This cyclonic circulation further enhances wind convergence and the continued transportation of warm air to the storm's core.

1.2.5 Formation or Genesis Stage

Since the nature of Tropical Cyclone (TC) development is continuous, features associated with earliest stages of the TC life-cycle can overlap. To complicate the issue, there is no standard language for these initial stages. For example, some meteorologists prefer the term "genesis" to describe both the earliest stages of the life-cycle and progression to a mature hurricane or typhoon. Others use the term "genesis" to describe the earliest stages and "formation" to somewhat later stages in the life-cycle.

The development cycle of tropical cyclones may be divided into three stages:

Intensification or Deepening Stage

In this stage, the TC central pressure falls and the maximum surface wind speed increases. An eye may develop at the centre of the TC if the stage continues. The formation and initial development of a cyclonic storm depends upon various conditions. These are:

- (1). A warm sea (a temperature in excess of 26 degrees Celsius to a depth of 60 m) with abundant and turbulent transfer of water vapour to the overlying atmosphere by evaporation.
- (2). Atmospheric instability which encourages formation of massive vertical cumulus clouds due to convection with condensation of rising air above ocean surface.

Mature Stage

The mature stage of a TC is usually associated with the period in which the TC reaches maximum intensity. The central pressure has reached a minimum, and the surface winds have reached a maximum. When a tropical storm intensifies, the air rises in vigorous thunderstorms and tends to spread out horizontally at the tropopause level. Once air spreads out, a positive perturbation pressure at high levels is produced, which accelerates the downward motion of air due to convection. With the inducement of subsidence, air warms up by compression and a warm 'Eye' is generated. Generally, the 'Eye' of the storms has three basic shapes:

- (i) circular
- (ii) concentric
- (iii) elliptical.

The main physical feature of a mature tropical cyclone in the Indian Ocean is a concentric pattern of highly turbulent giant cumulus thundercloud bands.

Decay Stage

When a TC decays, the central pressure increases and the maximum surface winds weaken. Usually, the decaying process is the result of a TC moving over land, moving over cool water, recurving and assuming extratropical characteristics, or a combination of these processes. Even though the TC is decaying, it can produce high winds and heavy rains.

A tropical cyclone begins to weaken in terms of its central low pressure, internal warmth and extremely high speeds, as soon as its source of warm moist air begins to ebb, or is abruptly cut off. This happens after its landfall or when it passes over cold waters. The weakening of a cyclone does not mean that the danger to life and property is over.

1.2.6 Movement of Cyclones

Winds steer the cyclones. The global wind pattern is also known as the "general circulation" and the surface winds of each hemisphere are divided into three wind belts. Polar Easterlies: from 60-90 degrees latitude, prevailing westerlies: from

30-60 degrees latitude, tropical easterlies: from 0-30 degrees latitude. The easterly trade winds of both hemispheres converge at an area near the equator called the “Intertropical Convergence Zone (ITCZ)”, producing a narrow band of clouds and thunderstorms that encircle portions of the globe. The path of a cyclone greatly depends upon the wind belt in which it is located. A cyclone originating in the eastern tropical Pacific, for example, is driven westward by easterly trade winds in the tropics. Eventually, these storms turn northwestward around the subtropical high and migrate into higher latitudes. Sometimes the local steering winds may not exactly follow this pattern.

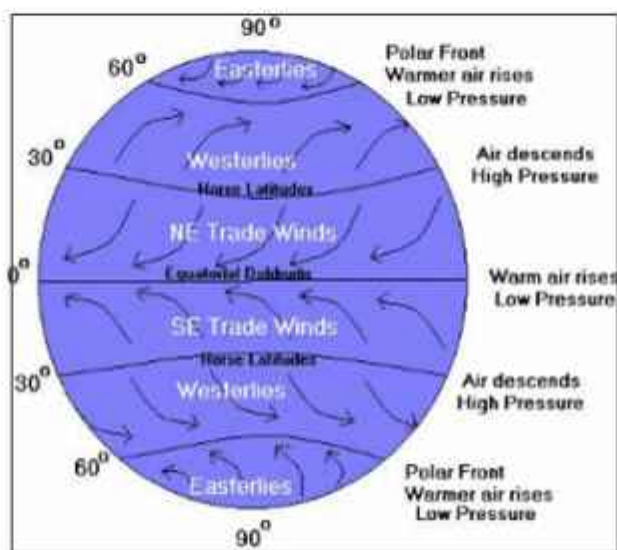


Figure 1.7- Global wind patterns (Atmospheric circulation and weather systems) [3].

1.2.7 Classification of Cyclonic Disturbances

Tropical cyclones have great socio-economic concern for the Indian subcontinent that is the only region in the world having two cyclone seasons within a year. A vast coastline of India with a high density of population is exposed to these natural threats, making it one of the worst cyclone-affected regions in the world in terms of the loss of lives. Due to the varying coastal bathymetry of the Indian coast, the severity of the storm surge created by the cyclones vary from place to place for the same intensity of the cyclone. Classifications of cyclonic disturbances for the Bay of Bengal and the Arabian Sea region for the exchange of messages among the panel countries are given below.

Weather system	Maximum wind speed
Low pressure area	Wind speed less than 17 kt (31 km/h)
Depression	Wind speed between 17 and 33 kt (31 & 61 km/h)
Cyclonic storm	Wind speed between 34 and 47 kt (62 & 88 km/h)
Severe cyclonic storm	Wind speed between 48 and 63 kt (89 & 118 km/h)
Severe cyclonic storm	Wind speed 64 kt (119 km/h) or more with a core of hurricane winds
Very severe cyclonic storm	Wind speed 64 and 119 kt (119 and 221 km/h)
Super cyclonic storm	Wind speed 120 kt and above (222 km/h)

Table 1.4- Cyclone Classification(Richard Ryan Halterman [7]).

Observation of Tropical Cyclones

Historically, observation of tropical cyclones has posed particular challenges. Surface level observations from weather stations are generally only available near coastal areas or from ships venturing into their path. Even in these cases, most useful observations are toward the storm exterior where conditions are less violent and do not damage the sensing platform. As such, it is difficult to obtain a full picture of tropical cyclones from surface measurements alone.

Reconnaissance flights into tropical cyclones have recently become possible, however. Large, specially-equipped cargo planes WC-130 Hercules and WP-3D Orions are able to penetrate into the centre of even intense storms. From there, a number of direct and remote sensing instruments are used to measure temperature, pressure, humidity, and wind speed. Among the available on-board sensors are flight level instruments, weather radars, and GPS dropsondes.

The latter of these, GPS dropsondes, provide a storm profile from flight level to the surface. Each of up to four simultaneous sondes parachutes to Earth while relaying temperature, pressure, humidity, and wind speed and direction back to the plane. Measurements of winds are achieved by using GPS derived positions to calculate the wind speed and direction causing the sound to deviate from a vertical path.

Storms near land in many areas are observed by Doppler weather radars. Excellent storm characterizations are available from their high temporal and spatial resolution. At sea and in most basins, however, neither surface-based Doppler radars nor reconnaissance flights are available. In such cases, space-borne observation fills the gap.

Optical and infrared data from geostationary satellites, along with microwave radar and radiometer data from polar-orbiting satellites, significantly enhance the observation and tracking of tropical cyclones. For instance, the GOES series, including GOES-16 and GOES-17, delivers real-time imagery, aiding in monitoring cyclones like Hurricane Dorian in 2019. Similarly, Japan's Himawari satellites, exemplified by Himawari-8, have been pivotal in tracking cyclones such as Super Typhoon Haiyan in 2013. Furthermore, NOAA's polar-orbiting satellites like NOAA-20 and Suomi NPP furnish microwave imagery, vital for deciphering a cyclone's internal structure, as observed during Hurricane Irma in 2017. Additionally, the European Space Agency's Sentinel satellites, such as Sentinel-1 and Sentinel-3, contribute essential data on environmental parameters like sea surface temperature and ocean currents, crucial for understanding cyclone behaviour.

Chapter 3

ISRO's advanced active microwave radar sensor, exemplified by OSCAT aboard SCATSAT-1, adds significant value to our cyclone tracking endeavours. This technology complements existing satellite systems, offering enhanced insights into cyclones.

1.3 EOS06-SCAT

EOS-06 (Oceansat-3), a mission launched by the ISRO in November 2022, aims to maintain the continuity of services provided by Oceansat-2 (OSCAT) and SCATSAT-1 missions while offering enhanced payload specifications and expanded application areas. As the third-generation satellite in the Oceansat series, EOS-06 is equipped with three payloads. Firstly, the Ocean Colour Monitor (OCM-3) offers improved radiometric and spectral performance, featuring a greater number of VNIR bands compared to its predecessor, Oceansat-2. Secondly, the Sea Surface Temperature Monitor (SSTM-1) is a new payload specifically designed for this mission. Lastly, the scatterometer (EOS06-SCAT) is an advanced version with enhanced features in comparison to OSCAT and SCATSAT, providing more comprehensive and accurate data.

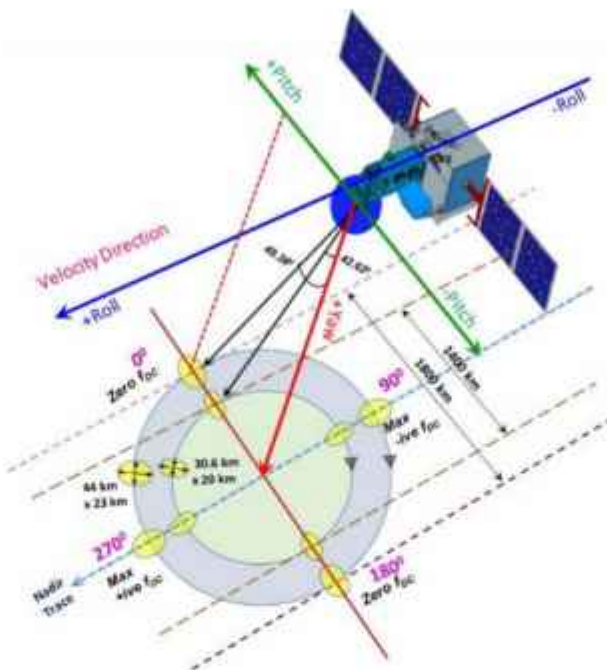


Figure 1.8- Observation/operating geometry of the proposed O3SCAT (EOS06).

EOS06-SCAT, an active microwave radar scatterometer, serves as a follow-up to the SCATSAT-1—(Launched in September, 2016) and Oceansat-2 satellite (Launched in September, 2009) missions. Its primary objective is to ensure the continuity of global ocean wind vector data acquisition. The Ku-band scatterometer EOS06-SCAT closely resembles SCATSAT-1, with the main difference being an increase in the antenna size from 1m to 1.4m. This upgrade allows EOS06-SCAT to introduce a high spatial resolution product for ocean surface wind vectors, achieving a resolution of 12.5 km for the first time, in addition to the standard 25 km nominal mode. Moreover, an experimental mode with even higher resolution wind data at 5 km is also included.

EOS06-SCAT is expected to deliver enhanced accuracy in wind speed measurements, improving its RMSE to approximately ~1.5 m/s and by ~15° for wind speed and direction respectively. Additionally, the Noise Equivalent Sigma-0 (NESZ) is projected to be improved by around 4dB, a crucial advancement that will benefit various other applications reliant on precise wind data.



Figure 1.9- Image view of EOS06-SCAT(EOS06-SCAT-3 Wind Products V1).

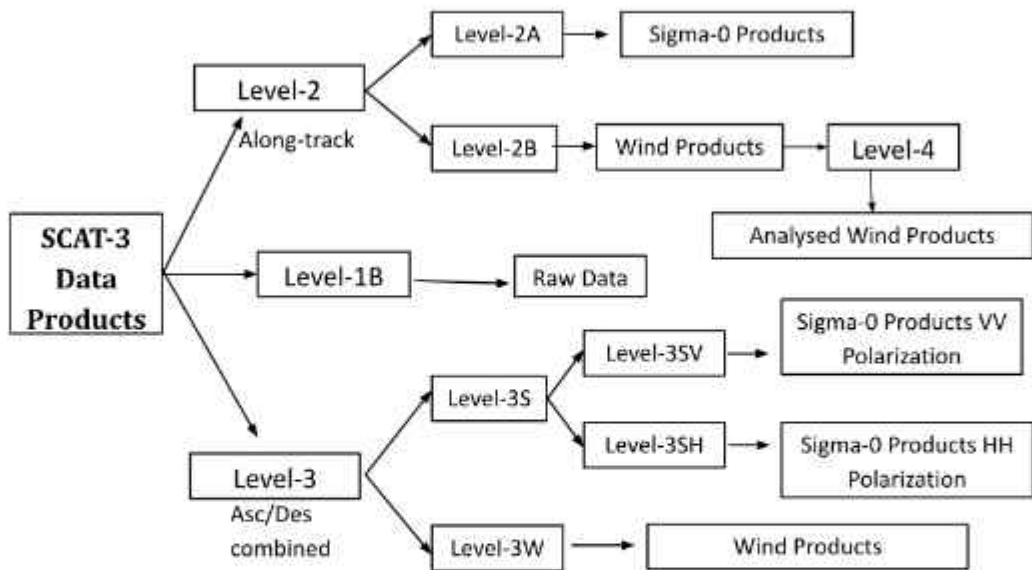


Figure 1.10- Details of different levels EOS06-SCAT Data Product (EOS06-SCAT-3 Wind Products).

1.4 Why this Study

This study delves into a critical aspect of meteorological science: the precision of tropical cyclone analysis and forecasting. Tropical cyclones, among the most severe natural disasters, can wreak havoc on communities, infrastructure, and ecosystems. Their intensity and trajectory significantly influence the extent of their impact, making it imperative to continually refine methodologies for assessing and predicting their behaviour.

At the heart of this study lies the recognition of the importance of enhancing cyclone analysis accuracy, particularly in terms of centre positioning. The precision of this aspect directly affects the effectiveness of early warning systems, evacuation procedures, and resource allocation for disaster response. By scrutinising the distribution characteristics of wind curl and employing innovative binarization techniques on scatterometer data, this research aims to address existing gaps in cyclone analysis methodologies.

One of the primary contributions of this study is the exploration of the L2B scatterometer as a case study. By leveraging this advanced technology, researchers gain insights into the intricate details of wind patterns associated with tropical

cyclones. This detailed understanding forms the basis for proposing two novel methods aimed at improving cyclone centre positioning accuracy.

The significance of this research extends beyond academic curiosity; it has direct implications for disaster management and preparedness. By refining methodologies for cyclone analysis and forecasting, this study enables more accurate predictions of cyclone trajectories and intensities. This, in turn, facilitates timely interventions, allowing communities to better prepare for and respond to impending cyclones.

To validate the proposed methods, the study utilises remote sensing data from real-world cyclone events, including Typhoons "Mawar" and "Biparjoy." This empirical approach ensures that the findings are grounded in real-world scenarios, enhancing the credibility and applicability of the research outcomes.

The results of this study demonstrate a clear improvement in cyclone centre positioning accuracy compared to conventional techniques. Such advancements in cyclone analysis hold profound implications for disaster management agencies, policymakers, and vulnerable communities. By providing more precise forecasts, this research equips decision-makers with the information needed to implement proactive measures, thereby reducing the human and economic toll of tropical cyclones.

Furthermore, the methodologies developed in this study have the potential for broader application beyond tropical cyclones. The insights gained from analysing wind patterns and refining data processing techniques could be leveraged in other meteorological phenomena, such as extratropical cyclones or severe thunderstorms. This interdisciplinary approach underscores the versatility and significance of the research findings.

In conclusion, this study represents a significant contribution to the field of meteorology and disaster management. By enhancing the precision of tropical cyclone analysis and forecasting, it empowers stakeholders to make informed decisions and take proactive measures in mitigating the devastating impacts of

these natural disasters. As climate change continues to influence the frequency and intensity of tropical cyclones, the importance of such research endeavours cannot be overstated.

2. Products Background

Surface winds over oceans play a crucial role in various operational oceanographic, atmospheric, and climatological studies, enhancing numerical weather prediction, ocean state forecasting, and research on monsoons and cyclones. Winds act as a fundamental driving parameter in influencing the upper ocean circulation. Therefore, information on wind velocity, wind stress, and wind stress curl is vital for major ocean circulation models, and these parameters are derived from the sea surface (or nearby) wind field. Wind stress refers to the force exerted by the wind on the sea surface in a direction parallel to it. This force causes a vertical transfer of horizontal momentum, leading to the transfer of momentum from the atmosphere to the ocean. The computation of wind stress relies on bulk formulae based on standard meteorological data.

2.1. EOS06-SCAT Winds

There are three levels of data products available from EOS06-SCAT: Level-1B (Raw data), Level-2B (Along-track data) and Level-3 (Global gridded data). The EOS06-SCAT data from the NRSC is available in HDF5 (.h5) file format. We have used the .h5 data as an input to generate an automated process to obtain cyclone characteristics by using techniques mentioned below finally to obtain the characteristics of the cyclone.

2.2. Wind Curl(RV)

Relative vorticity refers to the rotation of air parcels relative to their surrounding environment within the atmosphere. It's a measure of the local spin of the air mass, either clockwise or counterclockwise, with respect to a reference frame. There are two main components of relative vorticity: vertical vorticity and horizontal vorticity.

Vertical vorticity is the spin of the air parcel around a vertical axis. It's caused by features like troughs, ridges, and other embedded waves in the atmosphere.

Troughs are regions where the air flow is cyclonic (counterclockwise in the Northern Hemisphere), while ridges are areas of anticyclonic (clockwise in the Northern Hemisphere) flow. When air flows through these features, it experiences changes in wind speed and direction with respect to a vertical axis, leading to the development of vertical vorticity. Positive vorticity advection (PVA) occurs in regions of increasing vertical vorticity, which contributes to rising air and can lead to the development of clouds and precipitation.

Horizontal vorticity, on the other hand, is the spin of the air parcel around a horizontal axis. It's most significant in the planetary boundary layer (PBL), which encompasses the lower levels of the atmosphere. Horizontal vorticity arises from changes in wind speed and direction with height, such as wind shear. For example, if winds at the surface are south easterly and stronger than winds aloft, which are westerly, there will be a significant amount of horizontal vorticity due to the speed and directional shear. This horizontal vorticity can influence the development of mesoscale weather phenomena like tornadoes and severe thunderstorms.

Overall, relative vorticity provides valuable insights into the dynamics of atmospheric circulation and the development of weather systems, helping meteorologists forecast and understand the behaviour of the atmosphere.

Chapter 4

3. Methodology

EOS06 Scatterometer data provides the data in multiple forms here the data are:

- 1). Latitude: Latitude is the angular distance of a location north or south of the Earth's equator, measured in degrees. It ranges from 0° at the equator to 90°N at the North Pole and 90°S at the South Pole.
- 2). Longitude: Longitude is the angular distance of a location east or west of the Prime Meridian, which passes through Greenwich, England. It is measured in degrees, ranging from 0° at the Prime Meridian to 180°E and 180°W at the International Date Line.
- 3). Wind Direction: Wind direction is the direction from which the wind is blowing, expressed in degrees clockwise from true north. For example, a wind direction of 0° indicates a north wind, 90° indicates an east wind, 180° indicates a south wind, and 270° indicates a west wind.
- 4). Zonal Wind Speed: Zonal wind speed represents the component of the wind speed that is parallel to lines of latitude, typically in the east-west direction. It is also referred to as the eastward wind component. Zonal wind speed is often denoted by the symbol u .
- 5). Meridional Wind Speed: Meridional wind speed represents the component of the wind speed that is parallel to lines of longitude, typically in the north-south direction. It is also referred to as the northward wind component. Meridional wind speed is often denoted by the symbol v .

Parameters, namely latitude, longitude, zonal wind speed, meridional wind speed were derived from the scatterometer data received from EOS06.

The RV (Relative Vorticity) computed is the maximum vorticity at a given instant.

$$\text{Vorticity} = (\text{Longitude} / \text{Meridional}) - (\text{Latitude} / \text{Zonal}) \quad \text{Eq. 1.2}$$

For, Binarization after extracting wind speed applying binarization to it and extracting the largest group of ones and then mapping it back to the binarized data.

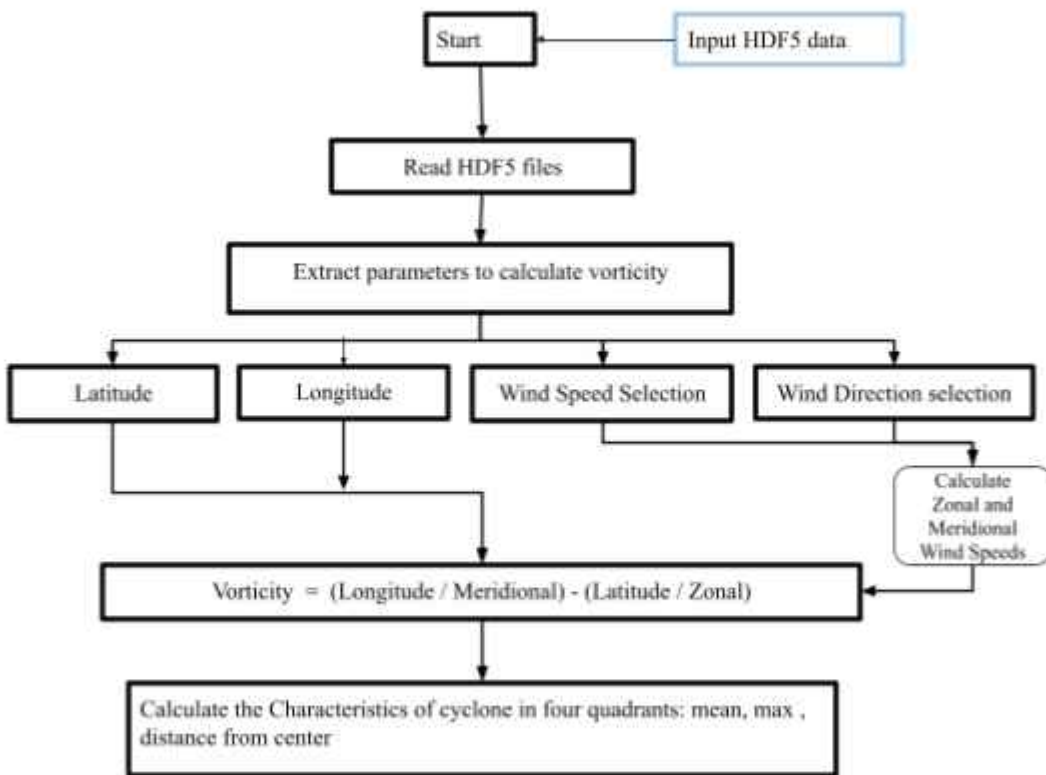


Figure 3.1- Flow chart Relative Vorticity

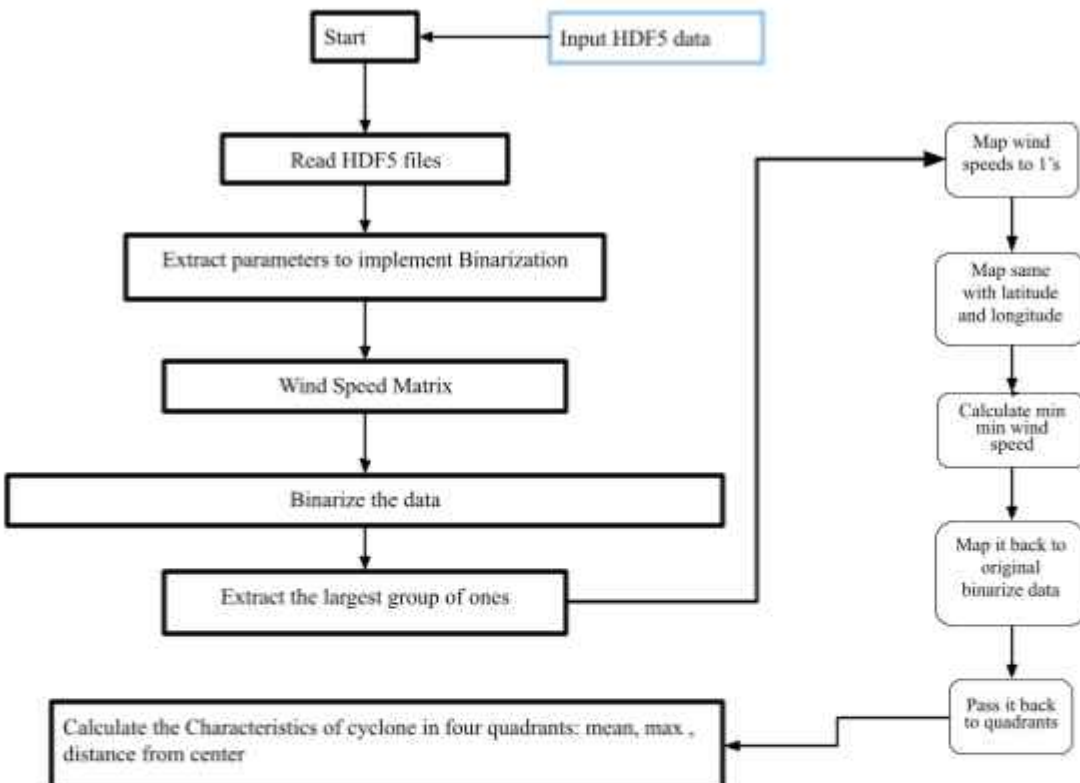


Figure 3.2- Flow chart Binarization

3.1. Wind Velocity

Wind velocity, also referred to simply as wind speed, is a measure of the rate at which air is moving horizontally past a particular point in the atmosphere. It is typically expressed in units such as metres per second (m/s), kilometres per hour (km/h), miles per hour (mph), or knots (nautical miles per hour). So, the wind velocity is extracted from the Level 2b (L2B) products.

```
file_path = 'E065CTI202023149_02660_02661_N5_12km_2023-149T20-1d-48_v1.0.2.h5' # filename - 29may2023
#file_path = 'E065CTI202023149_02660_02661_N5_12km_2023-149T20-1d-48_v1.0.2.h5'

z = 0

#colorbar_ticks = [0,0.2,0.4,0.6,0.8,1,1.5,2,4,5,6,7,8,9,14,16,18,20,22,24,28]
colorbar_ticks = [0, 4, 8, 12, 16, 20]
colorbar_labels = ['0', '4', '8', '12', '16', '20'] # corresponding labels
levels = np.linspace(0,0,20)
#levels = [0,4,8,12,16,20,24,28]
#levels = np.concatenate(([0,1,5],[1,10,10],[10,24,16]))
```

Open the h5 file

```
with h5py.File(file_path, 'r') as hs_file:
    # Access the variables (same as before)
    LATITUDE_125 = hs_file['science_data'][1]['latitude'][::]
    LONGITUDE_125 = hs_file['science_data'][1]['longitude'][::]
    ws = hs_file['science_data'][1]['wind_speed_selection'][::] # Wind Speed
    wd = hs_file['science_data'][1]['wind_direction_selection'][::] # Wind Direction

    # Scaling Parameters
    LATITUDE_125 = LATITUDE_125.astype(float) / 100
    LONGITUDE_125 = LONGITUDE_125.astype(float) / 100
    wd = wd.astype(float) / 100
    ws = ws.astype(float) / 100

    LATITUDE_125[LATITUDE_125 == 327.67] = np.nan
    LONGITUDE_125[LONGITUDE_125 == -655.35] = np.nan
    ws[ws == 327.67] = np.nan
    wd[wd == -655.35] = np.nan
```

Figure 3.3- Wind Velocity

3.2. Wind Curl(RV)

The RV value (in per second) is calculated from the wind observations, defined by four adjacent scatterometer vectors, by determining the circulation around each box and then dividing by the area. The mathematical expression for estimating the RV is given as follows:

with inputs taken from wind speed selection, wind direction selection.

$$\zeta = \partial v / \partial x - \partial u / \partial y \quad \text{Eq. 1.3}$$

where x and y refer to the longitudinal and latitudinal positions and u and v are the zonal and meridional components of the surface wind vector (in metres per second). As the TCs normally form above $\pm 5^\circ$ from the equator. The point of maximum vorticity was selected.

Zonal and Meridional wind stress components are computed as:

V as wind speed and θ as wind direction angle.

$$u = V \cdot \cos(\theta) \quad \text{Eq. 1.4}$$

$$v = V \cdot \sin(\theta) \quad \text{Eq. 1.5}$$

```
u_x = np.zeros((lat.shape[0] + 2, lat.shape[1] + 2))
u_y = np.zeros((lat.shape[0] + 2, lat.shape[1] + 2))

u_x[1:-1, 1:-1] = u
u_y[1:-1, 1:-1] = v

u_x[0,:] = u_x[-2,:]
u_x[-1,:] = u_x[1,:]
u_x[:, 0] = u_x[:, -2]
u_x[:, -1] = u_x[:, 1]

u_y[0,:] = u_y[-2,:]
u_y[-1,:] = u_y[1,:]
u_y[:, 0] = u_y[:, -2]

u_y[:, -1] = u_y[:, 1]
wca1 = u_y[2:, 1:-1] - u_y[:-2, 1:-1]
wca2 = u_x[1:-1, 2:] - u_x[1:-1, -2]

vorticity = (wca1) / (2 * DX) - (wca2) / (2 * DY)
vorticity[vorticity == 0] = np.nan
vorticity = vorticity * 10***4
```

Figure 3.4- RV snippet

When maximum vorticity was selected the surrounding 100 km is considered and min wind speed is calculated and that is used as a centre.

3.3. Binarizations

Binarization is a technique used in image processing to convert a grayscale or colour image into a binary image, where each pixel is represented as either black (0) or white (1). This is achieved by applying a threshold value to the intensity

levels of the pixels in masked wind speed. Pixels with intensity values below the threshold are set to black value set to 0, while those above the threshold are set to white value set 1. Here the threshold is considered to be 17.6 m/s (can be considered the average wind speed which could be used to determine the cyclonic and non cyclonic regions) for Mawar and Biparjoy for Michaung threshold is 17.0.

```
def binarize_image(matrix, threshold):
    binarized_matrix = np.where(matrix >= threshold, 1, 0)
    return binarized_matrix

threshold = 17.6
# Binarize the image
binarized_image = binarize_image(matrix, threshold)

# extracting largest group of ones
Largest_group_of_ones,bi_indices,lar_grp=extract_largest_group_of_ones(binarized_image)
```

Figure 3.5- Binarization snippet

In the given code snippet, a 2D array named 'matrix' represents the image, and a threshold value of 17.6 is applied using the 'binarize_image' function. This function processes the matrix, assigning black or white values to each pixel based on whether its intensity is below or above the threshold, respectively, resulting in a binary image stored in 'binarized_image'.

After creating a binarized Image (matrix) we are going to find the largest group of ones to exactly determine the cyclone region and then extract the group of ones.

BI (Th = 17.6) all1s

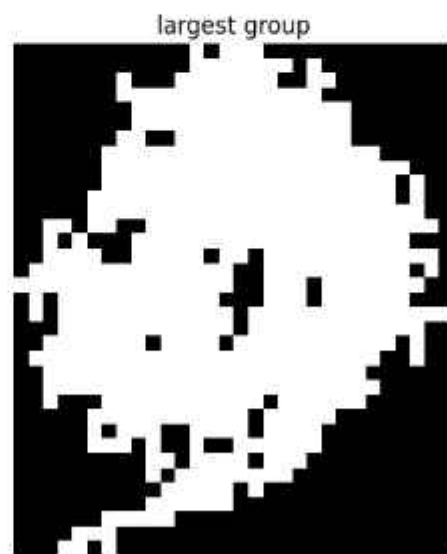


Figure 3.6- Binarized largest group of ones.

It follows a process in the binarization process the example (L2B) pass below can be considered.

EOS-06 SCAT matrix



Figure 3.7- Grayscale scaled image.

This is the first step in which the grayscale scaled image is converted from the colour image that depicts the cyclone region which can be extracted down the line.

EOS-06 SCAT binarized_image



Figure 3.8- Binarized image.

This is the second step in which the grayscale scaled image is converted to a binarized image that depicts the cyclone region in either 0 or 1.

EOS-06 SCAT largest_group_of_ones

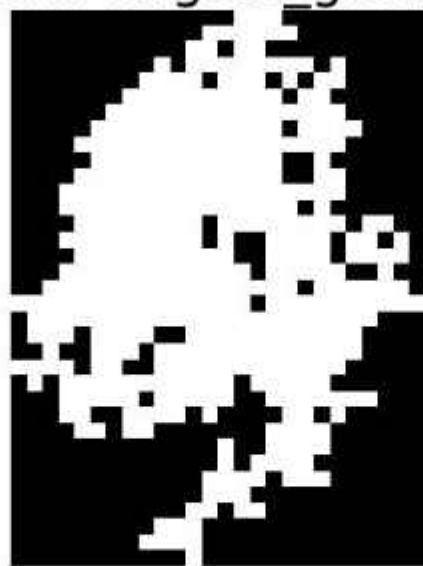


Figure 3.9- Binarized largest group of ones.

This is the third step in which the binarized image is analysed and the largest group of 1 which gives the cyclone region is extracted.

EOS-06 SCAT cycbione

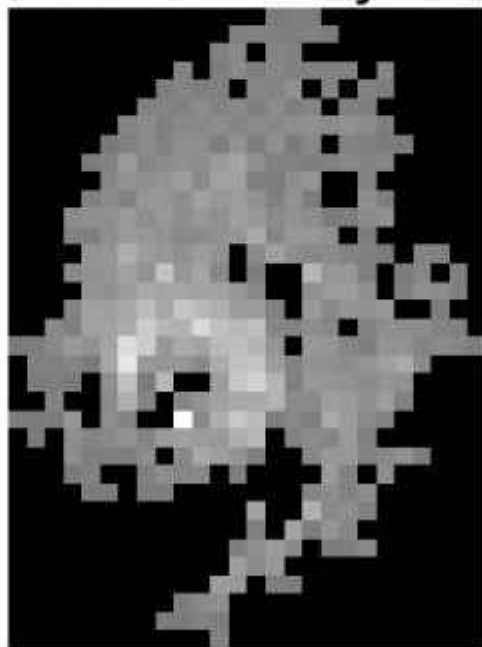


Figure 3.10- Binarized largest group of ones.

This is the fourth step in which the largest group of 1 values is mapped with the wind speed selection and the wind speed at their locations are replaced with 1's.

EOS-06 SCAT cycb



Figure 3.11- Binarized largest group of ones.

This is the fifth step final in which the largest group of 1 values is mapped with the wind speed selection and the wind speed at their locations are replaced with 1's. After that this region is mapped to the binarized region. When extracting the largest group of ones even the indices are also extracted so later the wind velocity values are mapped to these indices and create a new matrix in which we find the min wind speed, max wind speed. Based on that we locate the lat and lon of the cyclones centre.

3.4. Centre Identification

3.4.1 RV Mawar

When analysing the Mawar Cyclone, we determine the RV by identifying its peak vorticity [5]. To locate the centre of the cyclone, we survey the surrounding area within a radius of 100 km, pinpointing the minimum wind speed. This minimum wind speed serves as the cyclone's centre, allowing us to map its latitude and longitude coordinates. When considering Mawar cyclone there were 11 L2B products considered and these were the results. In order to obtain this we are using inputs min wind speed, max wind speed from the masked wind speed and their latitudes and longitudes. The distance is calculated between Vmax and wind speed at the centre using haversine technique and the same process is followed for other cyclones.

Day	Latitude_center	Longitude_center	Windspedd	Latitude_vmax	Longitude_vmax	Vmax	Rmax	VDirection
22-May-2023_142_NS	9.02	142.15	11.38	8.65	147.31	33.46	44.74	SE
23-May-2023_143_NS	10.87	145.25	8.57	11.06	146.61	36.58	149.96	N
24-May-2023_144_NS	14.34	148.46	10.41	13.18	145.16	50	228.51	S
25-May-2023_145_SN	14.68	138.98	12.1	14.90	140.51	48.65	178.29	N
26-May-2023_146_NS	14.65	149.7	15.66	15.22	148.17	46.16	176.18	SW
27-May-2023_147_SN	16	139.28	11.91	17.34	140.59	67.9	204.14	N
28-May-2023_148_SN	18.77	177	16.91	14.85	129.5	66.99	409.14	S
29-May-2023_149_NS	19.39	125.89	11.21	19.73	125.36	44.54	57.7.5	
30-May-2023_150_SN	21.08	124.9	12.52	24.76	120.83	41.91	584.03	SW
31-May-2023_151_NS	22.07	125.29	10.62	22.77	125.22	35.77	78.17	SW
01-Jun-2023_152_NS	24.51	126.83	11.32	26.73	128.05	30.51	275.49	N

Figure 3.12- RV Mawar

3.4.2 Binarization Mawar

In studying the Mawar Cyclone, we identify the minimum wind speed by analysing its Binarized Matrix. To find the cyclone's centre, we examine the minimum value within the group of ones in the binarized data. This minimum wind speed indicates the cyclone's centre, enabling us to determine its latitude and

longitude coordinates. In the case of the Mawar Cyclone, we analysed 11 L2B products, and these findings yielded the results we observed.

Day	Latitude_center	Longitude_center	Windspeed	Latitude_vmax	Longitude_vmax	Vmax	Rmax	VDirection
22-May-2023_142_NS	9.02	147.15	11.39	8.65	147.31	33.46	28.9	SE
23-May-2023_143_NS	10.82	146.53	11.93	11.06	146.81	36.58	41.79	N
24-May-2023_144_NS	13.02	145.73	12.99	13.33	146.26	47.34	65.5	N
25-May-2023_145_SN	14.08	138.93	12.1	14.94	140.51	38.05	177.64	N
26-May-2023_146_NS	14.05	139.7	13.66	15.23	138.17	46.16	170.71	SW
27-May-2023_147_SN	15.4	133.6	10.74	17.34	130.59	37.59	364.57	SW
28-May-2023_148_SN	18.27	127	8.91	14.35	136.5	36.99	266.62	S
29-May-2023_149_NS	19.35	125.89	11.21	19.23	125.36	44.54	59.44	S
30-May-2023_150_SN	19.42	126.81	10.35	21.92	125.22	33.21	240.75	SW
31-May-2023_151_NS	22.07	125.29	10.62	22.77	125.22	35.77	45.6	SW
01-Jun-2023_152_NS	24.51	126.83	11.32	23.04	127.79	28.69	145.63	SE

Figure 3.13- Binarization Mawar

3.4.3 RV Biparjoy

When analysing the Biparjoy Cyclone, we determine the RV by identifying its peak vorticity. To locate the centre of the cyclone, we survey the surrounding area within a radius of 100 km, pinpointing the minimum wind speed. This minimum wind speed serves as the cyclone's centre, allowing us to map its latitude and longitude coordinates. When considering Mawar cyclone there were 5 L2B products considered and these were the results. In order to obtain this we are using inputs min wind speed, max wind speed from the masked wind speed and their latitudes and longitudes. The distance is calculated between Vmax and wind speed at the centre using haversine technique and the same process is followed for other cyclones.

Day	Latitude_center	Longitude_center	Windspeed	Latitude_vmax	Longitude_vmax	Vmax	Rmax	VDirection
06-Jun-2023_157_NS	13.42	67.28	7.92	13.5	64.34	39.34	318.06	SW
08-Jun-2023_159_NS	16.1	64.68	7.55	15.27	63.77	33.96	134.19	S
10-Jun-2023_161_NS	16.87	67.4	10.17	15.67	65.18	37.35	271.95	S
11-Jun-2023_162_NS	17.57	66.19	8.66	18.24	67.38	44.17	146.3	N
12-Jun-2023_163_NS	19.54	67.17	7.76	19.49	67.48	33.13	32.96	SE

Figure 3.14- RV Biparjoy

3.4.5 Binarization Biparjoy

In studying the Biparjoy Cyclone, we identify the minimum wind speed by analysing its Binarized Matrix. To find the cyclone's centre, we examine the minimum value within the group of ones in the binarized data. This minimum wind speed indicates the cyclone's centre, enabling us to determine its latitude and longitude coordinates. In the case of the Mawar Cyclone, we analysed 5 L2B products, and these findings yielded the results we observed.

Day	Latitude center	Longitude center	Windspeed	Latitude vmax	Longitude vmax	Vmax	Rmax	VDirection
06-Jun-2023_157_NS	13.96	66.45	11.11	13.5	64.34	39.34	235.58 S	
08-Jun-2023_158_NS	15.31	64.04	10.4	15.22	63.77	33.96	30.09 S	
10-Jun-2023_161_NS	16.87	67.4	10.17	15.67	65.18	37.35	252.6 S	
11-Jun-2023_162_NS	18.29	67.75	8.95	18.21	67.38	44.17	41.2 S	
12-Jun-2023_163_NS	19.54	67.17	7.76	19.49	67.48	33.13	34.54 SE	

Figure 3.15- Binarization Biparjoy

3.5. Characteristics along different quadrants

In the study of cyclones, particularly tropical cyclones, meteorologists utilise a quadrant-based approach to comprehensively analyse wind speed patterns and associated data. The central point of focus within a cyclone is typically identified as the minimum wind speed, commonly known as the eye of the storm. From this central point, four distinct quadrants are delineated: NorthWest, NorthEast, SouthWest, and SouthEast. Each quadrant serves as a unit of analysis, allowing meteorologists to examine various parameters such as maximum and mean wind speeds. Daily reports are generated for each quadrant, providing detailed insights into wind speed dynamics over time. Additionally, distance reports are compiled, detailing the distances between the central minimum wind speed point and the locations of maximum wind speeds within each quadrant.

Furthermore, comprehensive wind speed data is collected and analysed within a radius of 400 kilometres from the central point in each direction. This data includes precise measurements of wind speed at various locations, along with corresponding distances from the central point. Moreover, the latitude and longitude coordinates of these locations are recorded, enabling meteorologists to precisely map the spatial distribution of wind speeds within the cyclone. For inputs we have used masked wind speed with partitioning quadrants based on the cyclone range. The range is estimated in RV through analysing the cyclone and in binarization through positioning of the matrix edges.

3.5.1. RV

The max wind speed, mean wind speed can be used in assessing the average wind speed in each quadrant throughout the cyclone genesis.

Mawar Table

The major moment of the cyclone depends on which quadrant has the max wind speed. From 22 May to 01-June for mawar this specifies that the cyclones began at SE and ended at SW and for biparjoy day 6,8,10,11,12 June began at S and ended at SE.

Vmax ; max wind speed , VDirection : max wind speed direction.

Vmax	VDirection
33.46	SE
36.58	N
47.34	N
38.65	N
46.16	SW
37.59	SW
36.99	S
44.54	S
33.21	SW
35.77	SW
28.69	SE

Table 1.5- Vmax-Direction.

Biparjoy Table

Vmax	VDirection
39.34	S
33.96	S
37.35	S
44.17	S
33.13	SE

Table 1.6- Vmax-Direction.

RV - Mawar, Quadrant Wise - Max

Days	Quadrant1-NW	Quadrant2-NE	Quadrant3-SE	Quadrant4-SW
22-May-2023_142_NS	29.19m/s - {9.46 , 147.26}	32.59m/s - {9.22 , 147.31}	33.46m/s - {8.65 , 147.31}	24.4m/s - {8.91 , 146.66}
23-May-2023_143_NS	33.11m/s - {11.44 , 146.31}	36.58m/s - {11.06 , 146.61}	36.58m/s - {11.06 , 146.61}	38.58m/s - {11.06 , 146.61}
24-May-2023_144_NS	25.93m/s - {12.77 , 142.63}	47.94m/s - {13.33 , 146.26}	47.34m/s - {13.33 , 146.26}	42.62m/s - {13.02 , 145.16}
25-May-2023_145_SN	38.65m/s - {14.99 , 140.51}	38.65m/s - {14.99 , 140.51}	38.65m/s - {14.99 , 140.51}	32.38m/s - {12.74 , 139.47}
26-May-2023_146_NS	46.16m/s - {15.22 , 138.17}	46.16m/s - {15.22 , 138.17}	41.74m/s - {15.41 , 138.81}	46.16m/s - {15.22 , 138.17}
27-May-2023_147_SN	37.59m/s - {17.34 , 130.59}	37.59m/s - {17.34 , 130.59}	34.68m/s - {16.79 , 134.11}	32.74m/s - {17.1 , 129.57}
28-May-2023_148_SN	34.02m/s - {18.51 , 128.46}	31.29m/s - {19.53 , 128.21}	36.02m/s - {14.16 , 129.51}	36.99m/s - {14.35 , 126.5}
29-May-2023_149_NS	44.54m/s - {19.23 , 125.36}	34.83m/s - {19.53 , 126.54}	35.05m/s - {18.9 , 125.9}	44.54m/s - {19.23 , 125.36}
30-May-2023_150_SN	41.91m/s - {24.76 , 120.83}	33.21m/s - {21.92 , 125.22}	32.0m/s - {21.04 , 126.01}	28.02m/s - {21.26 , 124.72}
31-May-2023_151_NS	35.77m/s - {22.77 , 125.22}	35.77m/s - {22.77 , 125.22}	30.3m/s - {18.88 , 125.7}	30.3m/s - {18.88 , 125.2}
01-Jun-2023_152_NS	30.51m/s - {26.73 , 128.05}	30.51m/s - {26.73 , 128.05}	28.69m/s - {23.04 , 127.79}	28.69m/s - {23.04 , 127.79}

Figure 3.16- RV - Mawar, Quadrant Wise - Max

Quadrant Wise - Mean

Days	Quadrant1-NW	Quadrant2-NE	Quadrant3-SE	Quadrant4-SW
22-May-2023_142_NS	15.06680707	15.73510331	16.38997807	13.36376252
23-May-2023_143_NS	14.99456325	16.01877027	15.67852381	14.63179598
24-May-2023_144_NS	13.81652715	15.32465028	16.7294837	14.88390083
25-May-2023_145_SN	13.93637607	16.80562245	16.56577624	12.96348854
26-May-2023_146_NS	16.96171556	18.41112727	19.36678236	16.33600129
27-May-2023_147_SN	18.62827396	20.62046703	15.29078632	16.1924158
28-May-2023_148_SN	19.40030827	20.88252344	18.0550224	18.90911606
29-May-2023_149_NS	18.85368321	16.85116397	18.4292115	18.9610327
30-May-2023_150_SN	16.96417464	16.15181452	18.94243728	19.3675213
31-May-2023_151_NS	18.81408886	16.84812539	17.37638624	17.78912932
01-Jun-2023_152_NS	16.86707063	13.96928401	14.67810672	14.46838563

Figure 3.17- RV - Mawar, Quadrant Wise - Mean

RV - Biparjoy, Quadrant Wise - Max

Days	Quadrant1-NW	Quadrant2-NE	Quadrant3-SE	Quadrant4-SW
06-Jun-2023_157_NS	15.04696429	15.04696429	15.18100733	15.18100733
08-Jun-2023_159_NS	12.09156379	12.09156379	15.01647748	15.01647748
10-Jun-2023_161_NS	18.46653226	18.46653226	18.47991497	18.47991497
11-Jun-2023_162_NS	17.36686147	17.36686147	17.36416785	17.36416785
12-Jun-2023_163_NS	10.36646179	15.42140762	17.86336842	16.10551316

Figure 3.18- RV - Mawar, Quadrant Wise - Max

Quadrant Wise - Mean

Days	Quadrant1-NW	Quadrant2-NE	Quadrant3-SE	Quadrant4-SW
06-Jun-2023_157_NS	39.34m/s - {13.5 , 64.34}	39.34m/s - {13.5 , 64.34}	28.25m/s - {11.5 , 66.15}	28.25m/s - {11.5 , 66.15}
08-Jun-2023_159_NS	33.96m/s - {15.27 , 63.77}	33.96m/s - {15.27 , 63.77}	33.17m/s - {14.47 , 65.84}	33.17m/s - {14.47 , 65.84}
10-Jun-2023_161_NS	35.68m/s - {17.11 , 67.32}	35.68m/s - {17.11 , 67.32}	36.63m/s - {16.22 , 68.55}	36.63m/s - {16.22 , 68.55}
11-Jun-2023_162_NS	44.17m/s - {18.24 , 67.38}	44.17m/s - {18.24 , 67.38}	29.69m/s - {17.22 , 68.15}	29.69m/s - {17.22 , 68.15}
12-Jun-2023_163_NS	25.79m/s - {19.38 , 65.64}	33.13m/s - {19.49 , 67.48}	33.13m/s - {19.49 , 67.48}	33.13m/s - {19.49 , 67.48}

Figure 3.19- RV - Mawar, Quadrant Wise - Mean

3.5.2. Binarization

Binarization - Mawar, Quadrant Wise - Max

Days	Quadrant1-NW	Quadrant2-NE	Quadrant3-SE	Quadrant4-SW
22-May-2023_142_NS	29.19m/s - (9.46 , 147.26)	33.46m/s - (8.65 , 147.31)	33.46m/s - (8.65 , 147.31)	24.4m/s - (8.51 , 146.66)
23-May-2023_143_NS	36.58m/s - (11.06 , 146.61)	36.58m/s - (11.06 , 146.61)	36.58m/s - (11.06 , 146.61)	29.4m/s - (10.15 , 146.66)
24-May-2023_144_NS	42.62m/s - (13.02 , 145.16)	47.34m/s - (13.33 , 146.26)	26.74m/s - (12.34 , 146.18)	42.62m/s - (13.02 , 145.16)
25-May-2023_145_SN	38.65m/s - (14.99 , 140.51)	38.65m/s - (14.99 , 140.51)	38.65m/s - (14.99 , 140.51)	32.38m/s - (12.74 , 139.47)
26-May-2023_146_NS	45.16m/s - (15.22 , 138.17)	46.16m/s - (15.22 , 138.17)	32.71m/s - (14.54 , 139.1)	42.85m/s - (14.98 , 138.24)
27-May-2023_147_SN	37.59m/s - (17.34 , 130.59)	34.68m/s - (16.79 , 134.11)	30.19m/s - (15.18 , 135.11)	37.59m/s - (17.34 , 130.59)
28-May-2023_148_SN	34.02m/s - (18.51 , 126.46)	31.29m/s - (19.53 , 128.21)	36.99m/s - (14.35 , 126.5)	36.99m/s - (14.35 , 126.5)
29-May-2023_149_NS	44.54m/s - (19.23 , 125.36)	36.0m/s - (19.31 , 125.89)	35.09m/s - (18.5 , 125.9)	44.54m/s - (19.23 , 125.36)
30-May-2023_150_SN	32.0m/s - (21.64 , 126.61)	32.0m/s - (21.04 , 126.61)	27.85m/s - (19.64 , 127.61)	28.47m/s - (18.3 , 126.89)
31-May-2023_151_NS	35.77m/s - (22.77 , 125.22)	35.77m/s - (22.77 , 125.22)	30.3m/s - (18.88 , 125.2)	27.57m/s - (22.36 , 123.47)
01-Jun-2023_152_NS	26.49m/s - (24.94 , 126.41)	30.51m/s - (26.73 , 128.05)	28.69m/s - (23.04 , 127.79)	28.69m/s - (23.04 , 127.79)

Figure 3.20- Binarization - Mawar, Quadrant Wise - Max

Quadrant Wise - Mean

Days	Quadrant1-NW	Quadrant2-NE	Quadrant3-SE	Quadrant4-SW
22-May-2023_142_NS	17.63535014	18.99508403	16.15161538	15.29
23-May-2023_143_NS	16.69878788	20.16767059	17.16887955	14.85304094
24-May-2023_144_NS	18.17879357	20.28287379	15.14821839	15.76179657
25-May-2023_145_SN	16.84635429	19.59326389	17.13709366	15.11296552
26-May-2023_146_NS	19.24170975	20.61686869	16.53268191	15.46172619
27-May-2023_147_SN	18.12569816	17.70655411	13.99653846	16.10715086
28-May-2023_148_SN	16.17065033	20.04745098	18.43981884	17.76570827
29-May-2023_149_NS	19.78518187	18.8796748	17.09225821	18.01055447
30-May-2023_150_SN	17.37370748	17.07689024	17.29692308	18.30183908
31-May-2023_151_NS	17.81405579	18.68155611	16.23591185	14.71118365
01-Jun-2023_152_NS	18.056475	17.8473913	16.70792969	16.55328571

Figure 3.21- Binarization - Mawar, Quadrant Wise - Mean

Binarization - Biparjoy, Quadrant Wise - Max

Days	Quadrant1-NW	Quadrant2-NE	Quadrant3-SE	Quadrant4-SW
06-Jun-2023_157_NS	39.34m/s - (13.5 , 64.34)	39.34m/s - (13.5 , 64.34)	30.14m/s - (10.9 , 64.82)	39.34m/s - (13.5 , 64.34)
08-Jun-2023_159_NS	33.96m/s - (15.27 , 63.77)	33.17m/s - (14.47 , 65.84)	33.17m/s - (14.47 , 65.84)	33.96m/s - (15.27 , 63.77)
10-Jun-2023_161_NS	37.35m/s - (15.67 , 65.18)	36.63m/s - (16.22 , 68.55)	36.63m/s - (16.22 , 68.55)	37.35m/s - (15.67 , 65.18)
11-Jun-2023_162_NS	44.17m/s - (18.24 , 67.38)	35.67m/s - (18.42 , 68.26)	35.67m/s - (18.08 , 68.32)	44.17m/s - (18.24 , 67.38)
12-Jun-2023_163_NS	29.1m/s - (19.05 , 64.95)	33.13m/s - (19.49 , 67.48)	33.13m/s - (19.49 , 67.48)	33.13m/s - (19.49 , 67.48)

Figure 3.22- Binarization - Mawar, Quadrant Wise - Max

Quadrant Wise - Mean

Days	Quadrant1-NW	Quadrant2-NE	Quadrant3-SE	Quadrant4-SW
06-Jun-2023_157_NS	15.70594675	17.67325103	17.195338	15.37744805
08-Jun-2023_159_NS	14.81207283	19.41717687	17.99855556	15.03266106
10-Jun-2023_161_NS	16.675825	18.23292929	16.63153153	16.49676768
11-Jun-2023_162_NS	18.48282609	19.19289474	17.59709939	17.61651515
12-Jun-2023_163_NS	16.56345238	18.44929147	17.07851393	17.26684982

Figure 3.23- Binarization - Mawar, Quadrant Wise - Mean

4. Results

MIN WindSpeed and MAX WindSpeed are calculated and compared with the both methods. The L2B pass data is about cyclones Mawar and Biparjoy. All the data is shown in the below Figures.

Daily Wise Data For RV Mawar

Day	julian_day	Center_WS	North	South	West	East	NorthEast	SouthEast	NorthWest	SouthWest	Maxspeed	Direction
Day_1	142_NS	11.39	26.54	25.58	19.97	24.71	28.52	24.79	27.98	26.03	28.52	NorthEast
Day_2	143_NS	8.57	16.83	17.34	16.72	26.19	25.02	23.4	18.29	14.83	26.15	East
Day_3	144_NS	10.41	18.77	20.25	16.2	20.81	14.81	28.58	18.23	20.05	28.56	SouthEast
Day_4	145_SN	12.1	20.19	19.1	19.02	26.37	26.52	21.85	17.76	19.77	26.52	NorthEast
Day_5	146_NS	13.66	25.69	27.88	28.43	24.48	26.03	21.55	40.59	27.83	40.59	NorthWest
Day_6	147_SN	11.91	28.08	21.28	22.69	31.19	13.58	21.44	20.92	21.19	33.58	NorthEast
Day_7	148_SN	8.91	27.85	29.28	32.02	30.48	31.29	31.08	28.4	33.57	33.57	SouthWest
Day_8	149_NS	11.21	36	35.08	35.81	29.53	27.54	26.55	36.04	30.2	36	North
Day_9	150_SN	12.52	27.34	25.04	24.98	32	26.87	21.08	41.91	22.84	41.91	NorthWest
Day_10	151_NS	10.62	26.7	29.48	26.75	23.84	27	25.31	26.37	22.74	29.46	South
Day_11	152_NS	11.32	21.32	20.51	22.52	25.2	23.55	25.69	26.49	19.65	26.49	NorthWest

Figure 4.1- Day 142-162 Pass with max wind speed in each quadrants

RV Biparjoy

Day	julian_day	Center_WS	North	South	West	East	NorthEast	SouthEast	NorthWest	SouthWest	Maxspeed	Direction
Day_1	157_NS	7.97	18.89	17.28	29.74	22.27	14.28	12.28	26.97	30.14	30.14	SouthWest
Day_2	158_NS	7.56	10.45	20.58	20.87	17.04	8.97	19.87	11.07	33.96	33.96	SouthWest
Day_3	161_NS	10.17	32.64	21.66	29.57	26.14	22.51	26.85	30.26	36.05	36.05	East
Day_4	162_NS	8.66	17.54	21.11	18.84	28.22	23.84	20.7	16.75	18.88	28.22	East
Day_5	163_NS	7.76	22.23	24.54	24.04	27.97	26.96	30.5	23.28	24.1	30.5	SouthEast

Figure 4.2- Day 157,9-161-163 Pass with max wind speed in each quadrants

Binarization Mawar

Day	julian_day	Center_WS	North	South	West	East	NorthEast	SouthEast	NorthWest	SouthWest	Maxspeed	Direction
Day_1	142_NS	11.39	26.54	25.58	18.97	24.71	28.52	24.79	27.98	26.03	28.52	NorthEast
Day_2	143_NS	11.93	26.81	28.67	20.29	21.01	28.38	21.66	21.45	23.4	28.38	NorthEast
Day_3	144_NS	12.99	38.68	23.53	42.62	27.54	32.04	25.45	39.83	31.39	42.62	West
Day_4	145_SN	12.1	20.19	19.1	19.02	26.37	28.52	21.85	17.76	19.77	26.52	NorthEast
Day_5	146_NS	13.66	25.69	27.88	28.43	24.48	26.03	21.55	40.59	27.83	40.59	NorthWest
Day_6	147_SN	10.74	24.71	33.93	22.24	22.46	22.38	24.18	28.57	15.63	28.57	NorthWest
Day_7	148_SN	8.91	27.85	29.29	32.03	30.96	31.29	31.08	28.4	33.57	33.57	SouthWest
Day_8	149_NS	11.21	36	35.08	35.81	28.53	22.54	26.55	34.04	30.2	36	North
Day_9	150_SN	10.75	34.93	22.07	22.08	21.21	22.0	19.78	25.61	26.17	25.61	NorthWest
Day_10	151_NS	10.02	26.7	29.48	26.75	23.84	27	25.31	24.37	22.74	29.46	South
Day_11	152_NS	11.32	21.32	20.51	22.52	25.2	23.55	25.69	26.49	19.65	26.49	NorthWest

Figure 4.3- Day 142-162 Pass with max wind speed in each quadrants

Binarization Biparjoy

Day	julian_day	Center_WS	North	South	West	East	NorthEast	SouthEast	NorthWest	SouthWest	Maxspeed	Direction
Day_1	157_NS	11.11	33.23	25.01	26.82	15.79	24.79	26.42	27.17	23.85	33.21	North
Day_2	158_NS	10.4	20.65	27.91	33.96	16.8	20.86	25.6	16.94	23.74	33.96	West
Day_3	161_NS	10.17	32.64	25.68	39.57	16.54	22.51	26.85	30.55	26.85	36.54	East
Day_4	162_NS	8.95	36.5	21.71	34.17	30.97	28.84	30.43	28.81	21.85	44.17	West
Day_5	163_NS	7.76	22.23	24.54	34.04	27.97	26.96	30.5	23.28	24.1	30.5	SouthEast

Figure 4.4- Day 157,9-161-163 Pass with max wind speeds in each quadrants

4.1. RV

The below images describe the Mawar cyclone from Day 142-162 Pass and Biparjoy cyclone from Day 157,9-161-163 Pass covering in three formats. The First part covers the cyclone wind velocity pattern of the cyclone. The Second part covers the min speed and max speed positioning of min wind speed and max wind speed. The Third part covers the positioning of the RV in the cyclone. Here the mawar region is covered in a region of 0° to 35° latitude and 110° to 170° longitude. Here the biparjoy region is covered in a region of 0° to 60° latitude and 20° to 80° longitude. The details of the centre and the max are mentioned 3.7, 3.8, 3.9, 3.10. The inputs for plotting we used Masked wind speed, Latitudes, Longitudes, Masked zonal wind speeds, Masked meridional wind speeds. We plotted min wind speed, max wind speed, max vorticity.

RV - Mawar

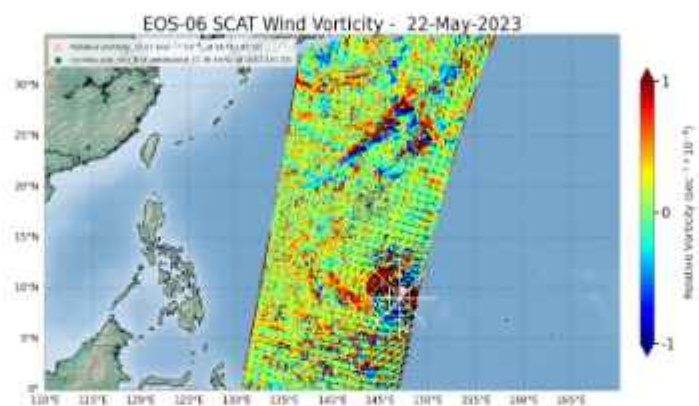
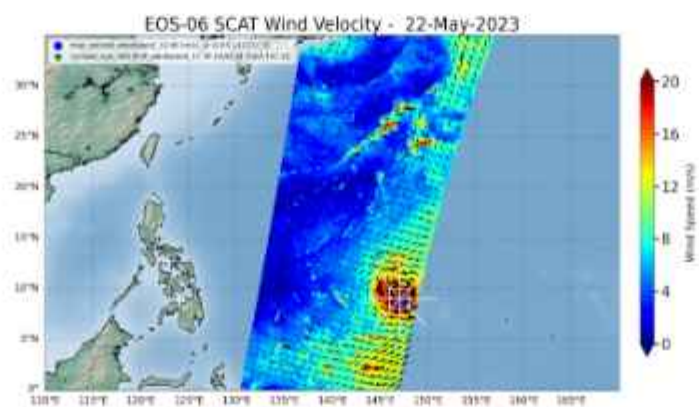
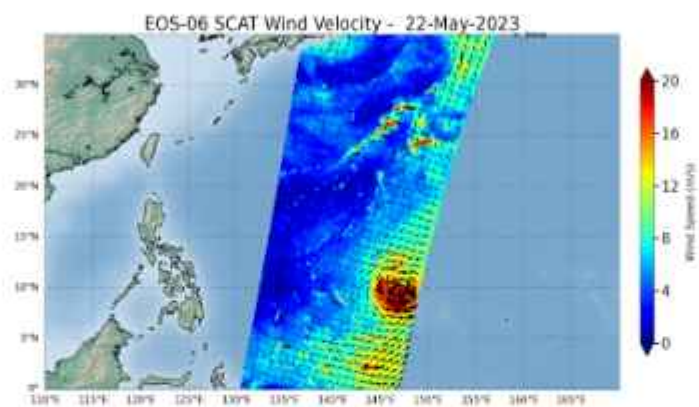


Figure 4.5- Day 22 142 Pass with min 11.39 , max 33.36, vorticity 12.29 ws

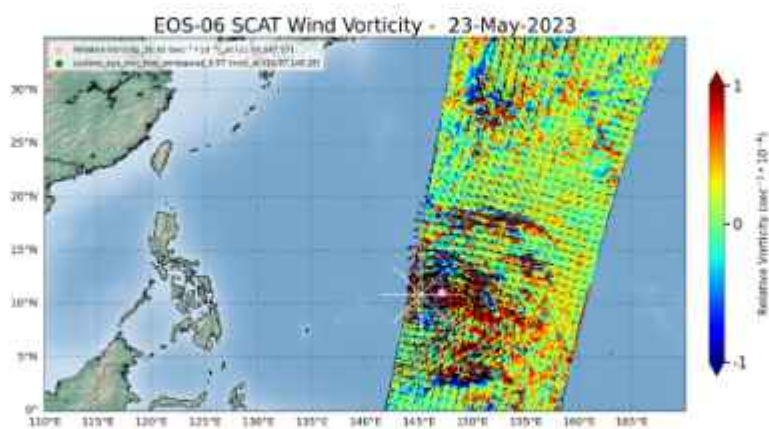
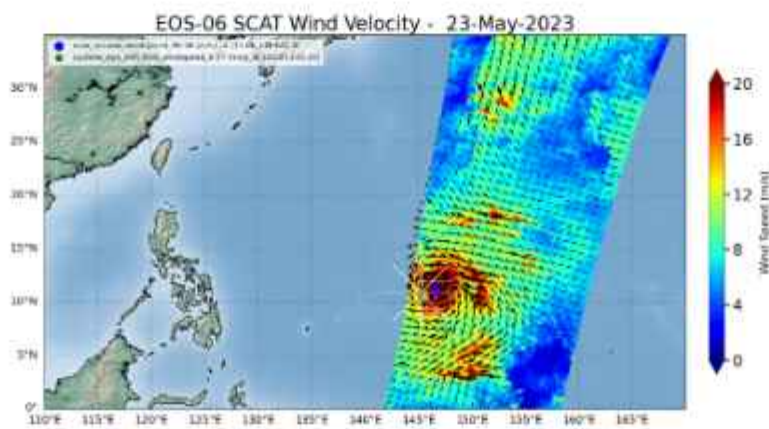
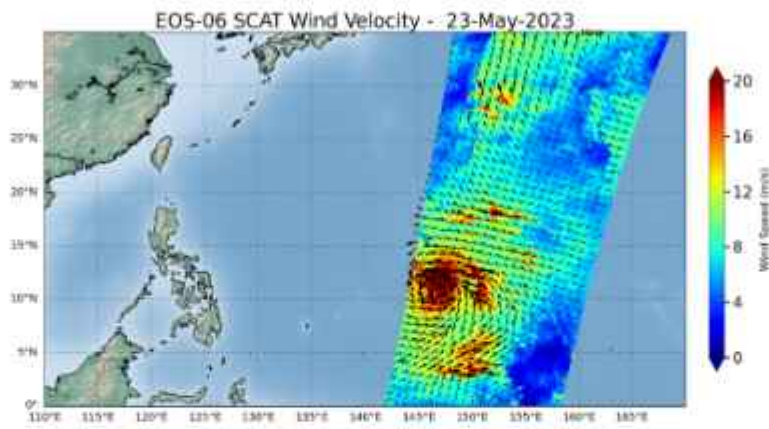


Figure 4.1.2- Day 23 143 Pass with min 8.57, max 36.58, vorticity 21.92 ws

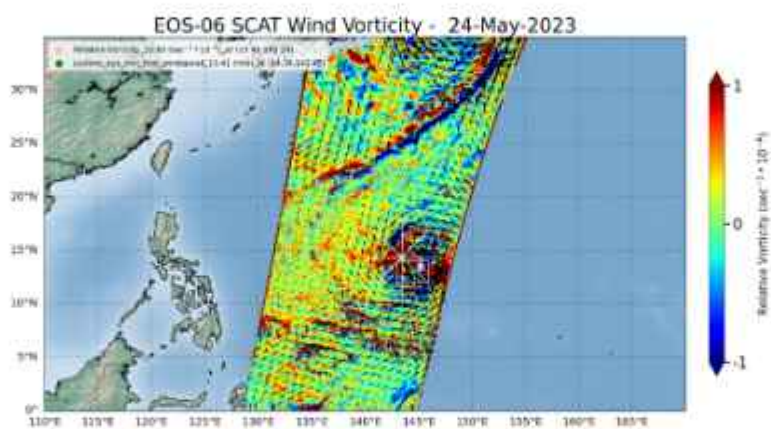
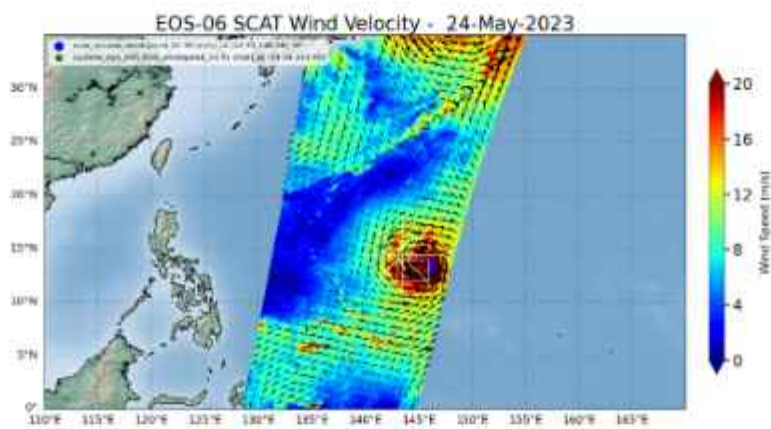
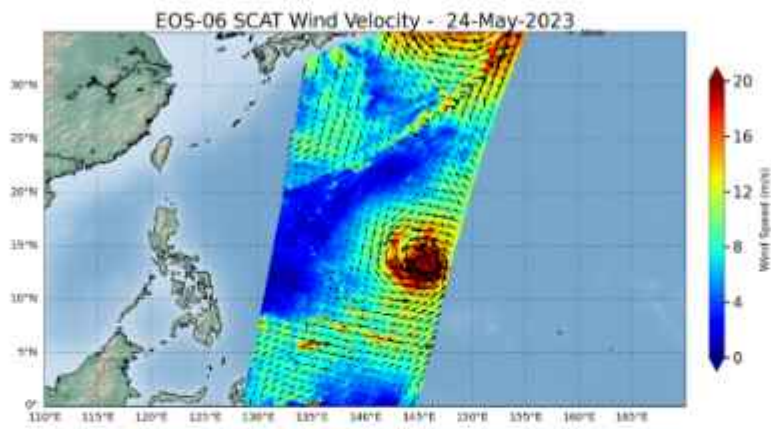


Figure 4.6- Day 24 144 Pass with min 10.41, max 47.34, vorticity 13.80 ws

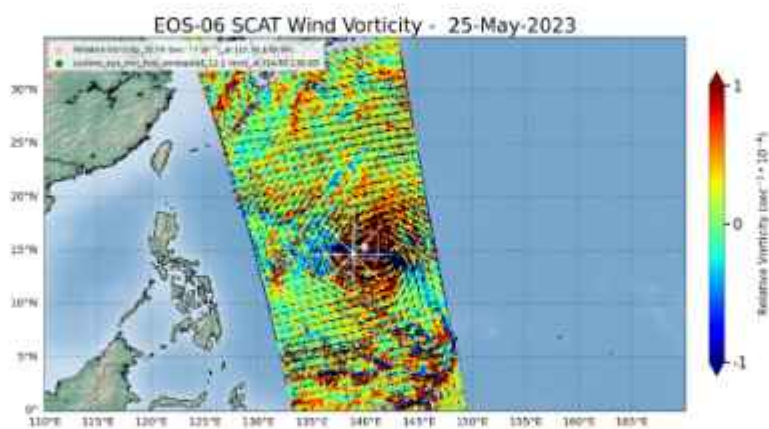
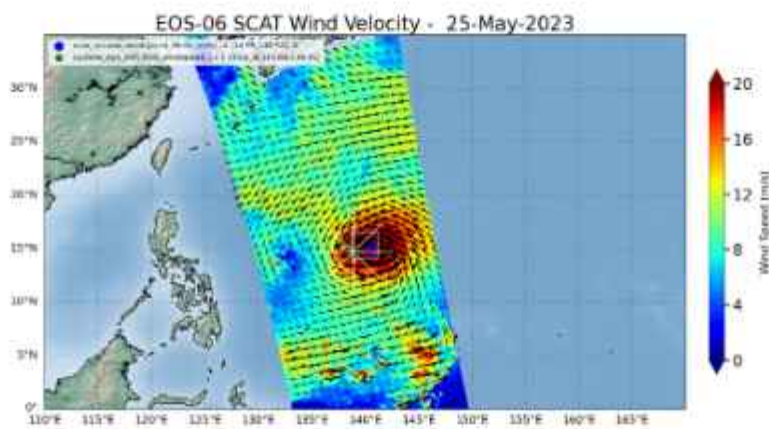
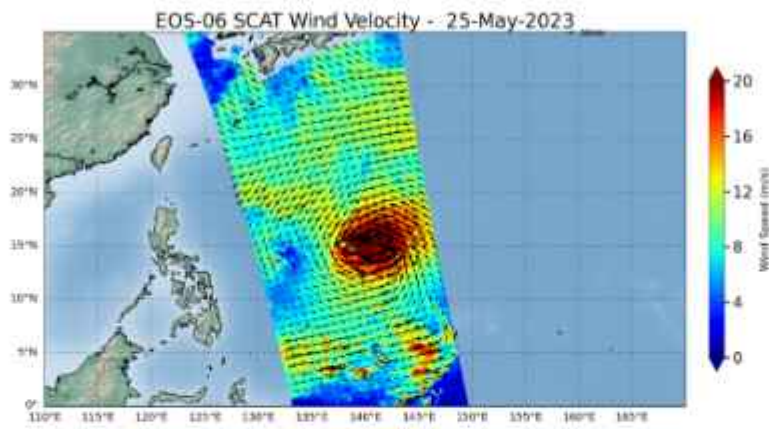


Figure 4.7- Day 25 145 Pass with min 12.1, max 38.65, vorticity 15.79 ws

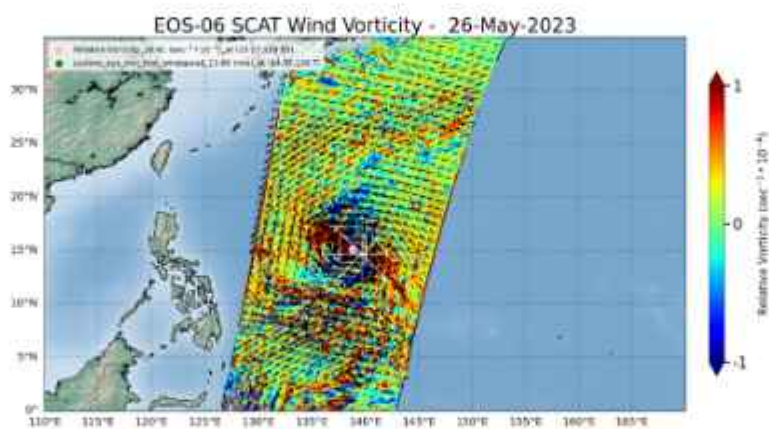
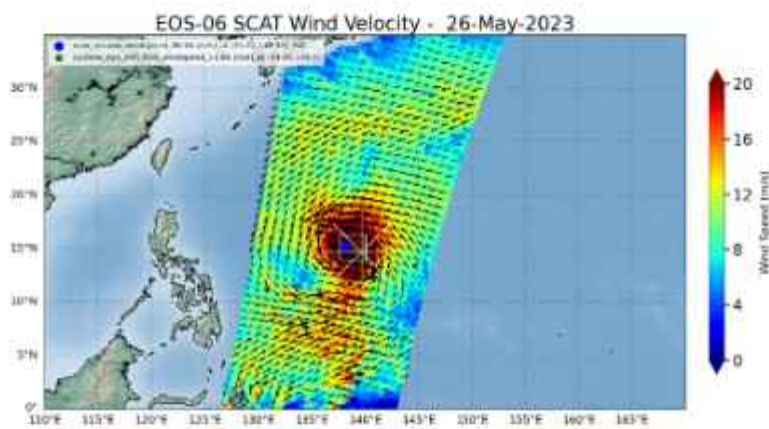
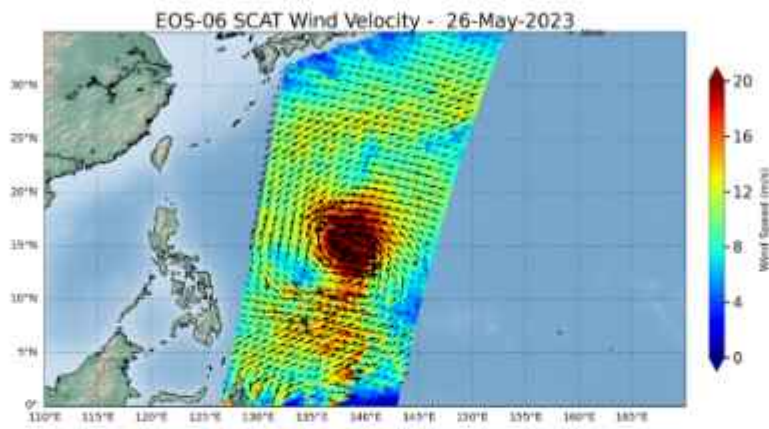


Figure 4.8- Day 26 146 Pass with min 13.66, max 46.16, vorticity 18.41

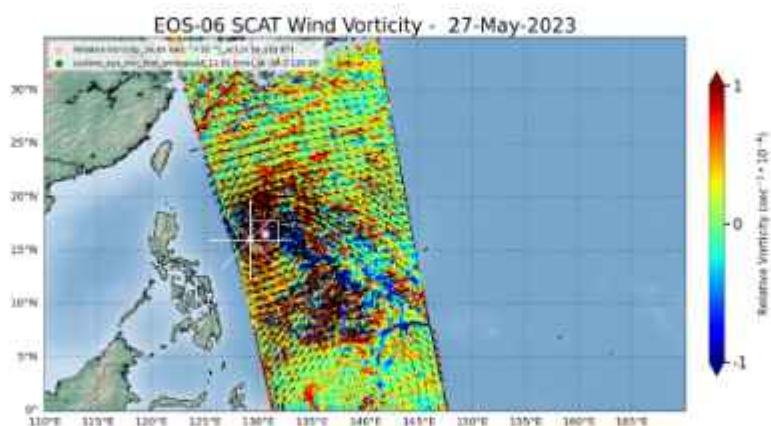
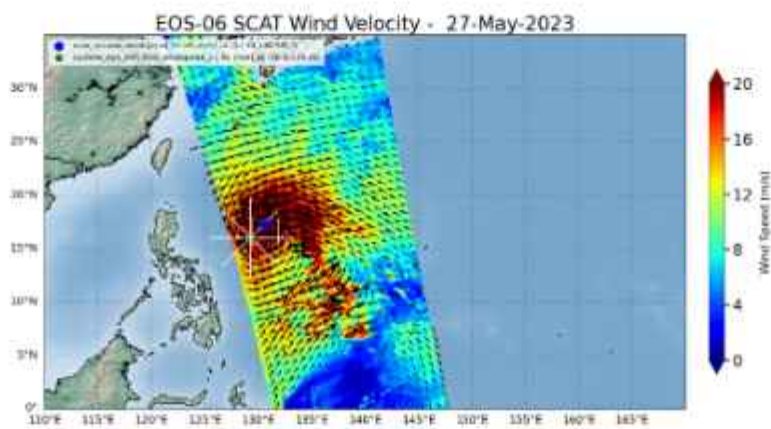
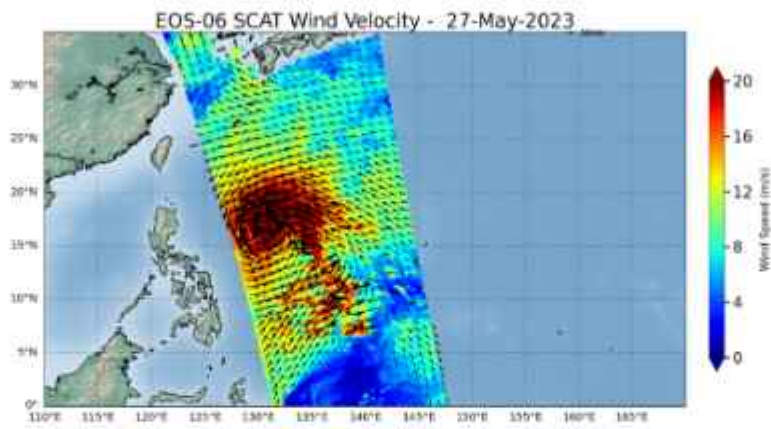


Figure 4.9- Day 27 147 Pass with min 11.91, max 37.59, vorticity 14.69 ws

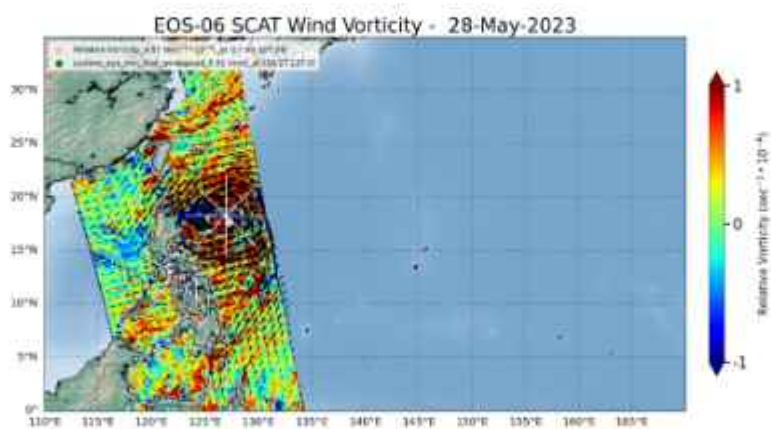
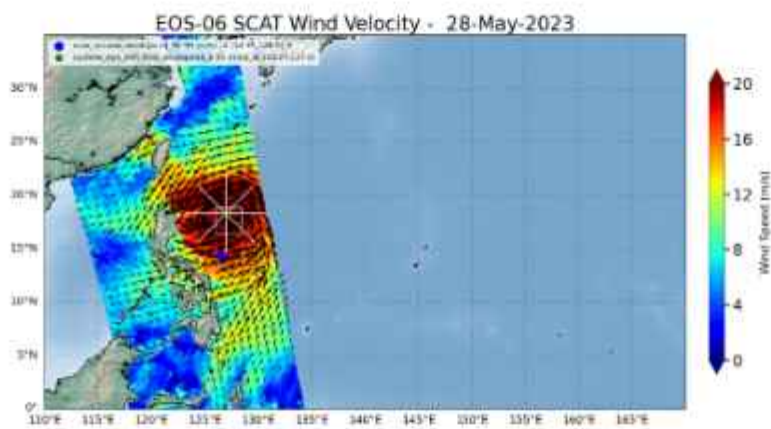
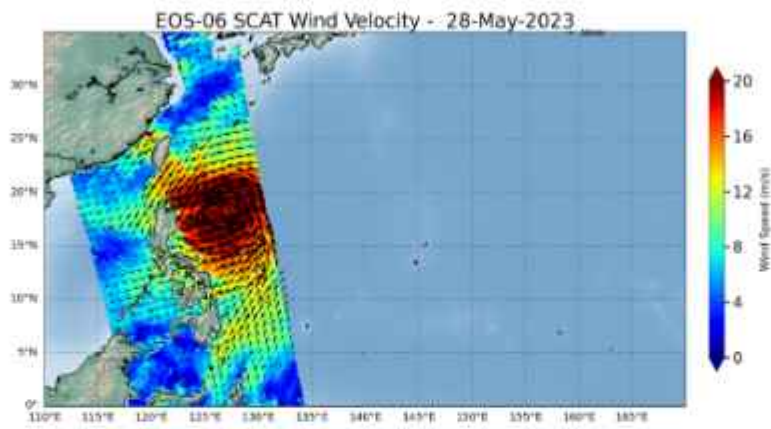


Figure 4.10- Day 28 148 Pass with min 8.91, max 36.99, vorticity 4.57 ws

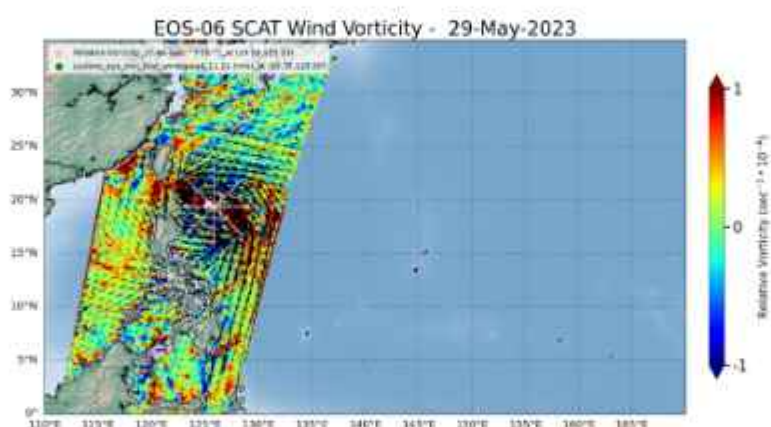
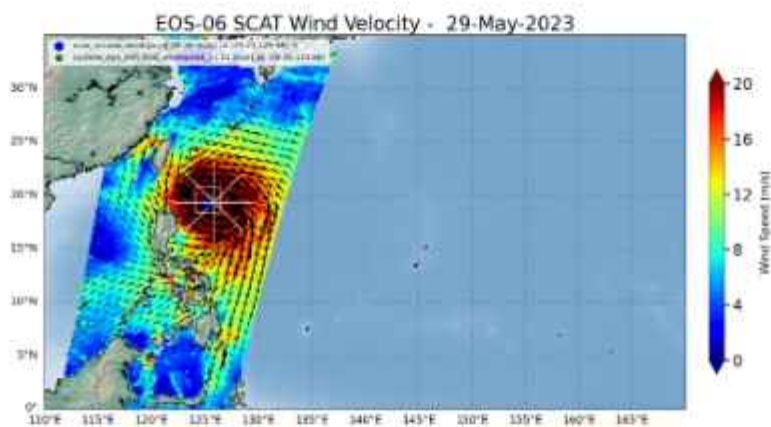
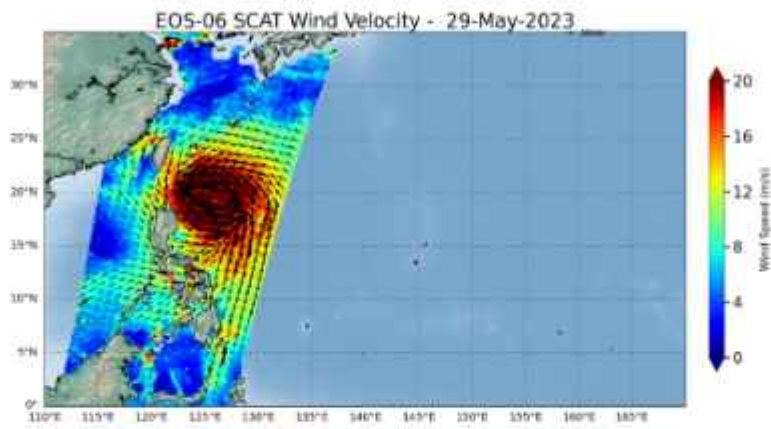


Figure 4.11- Day 29 149 Pass with min 11.21, max 44.54, vorticity 17.66 ws

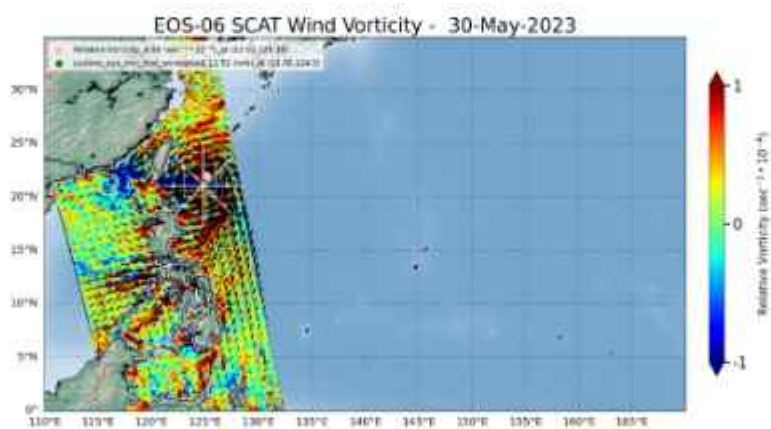
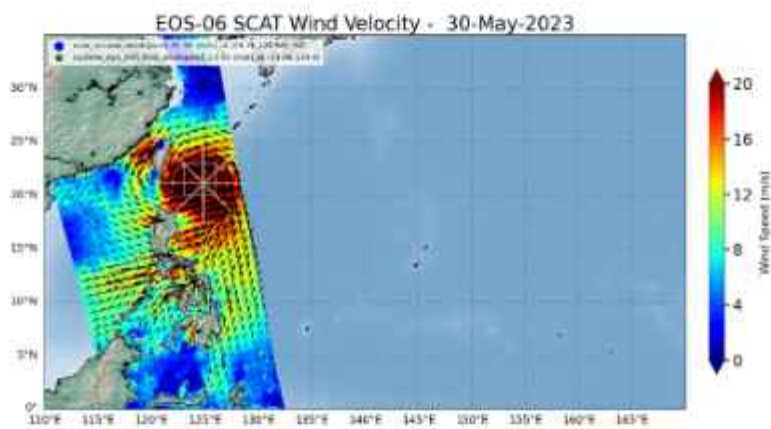
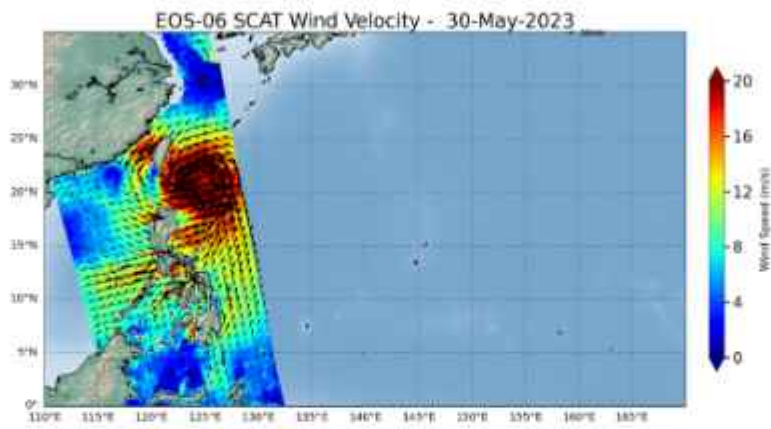


Figure 4.12- Day 30 150 Pass with min 12.52, max 41.91, vorticity 6.98 ws

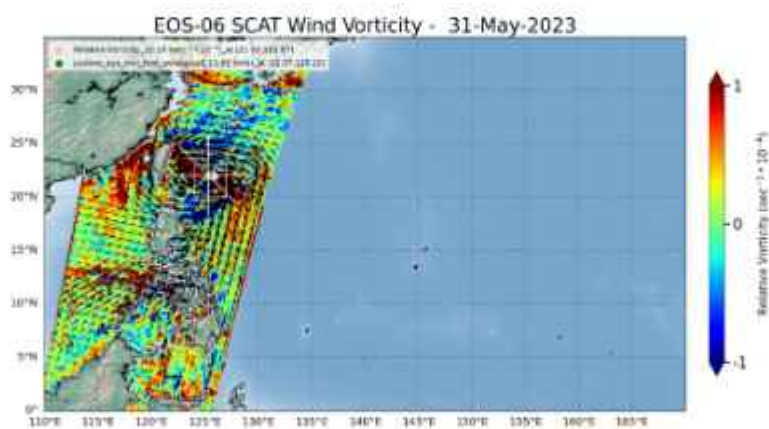
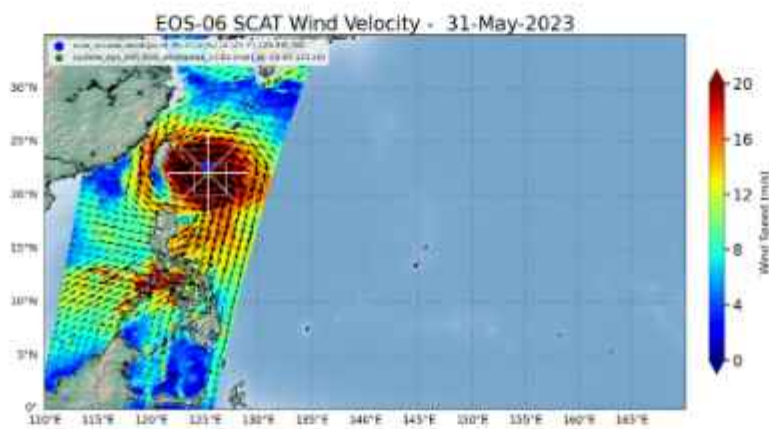
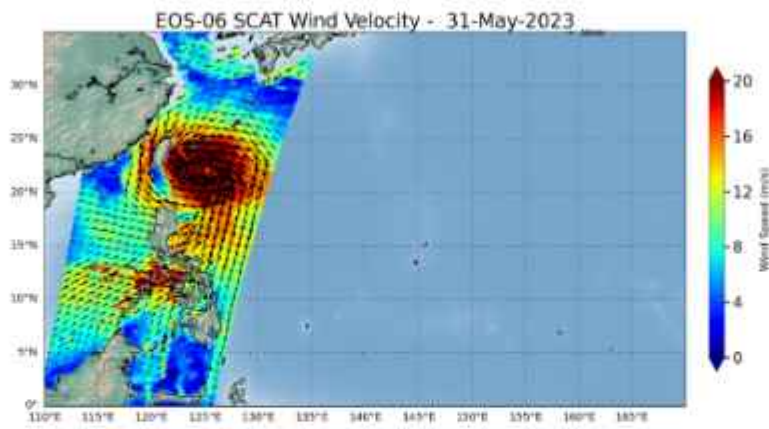


Figure 4.13- Day 31 151 Pass with min 10.62, max 35.77, vorticity 12.69 ws

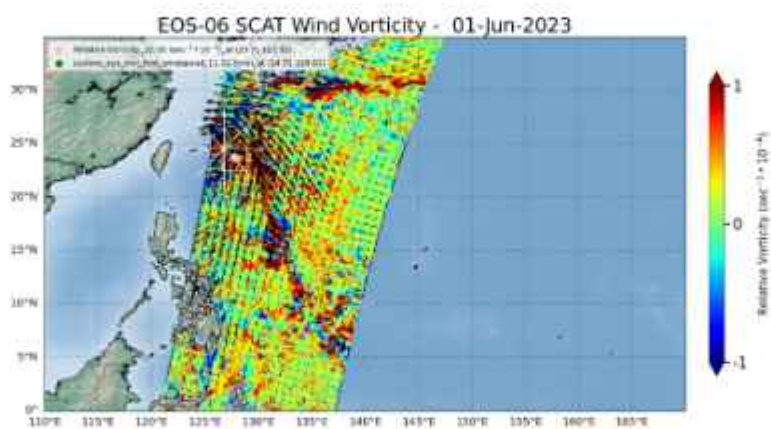
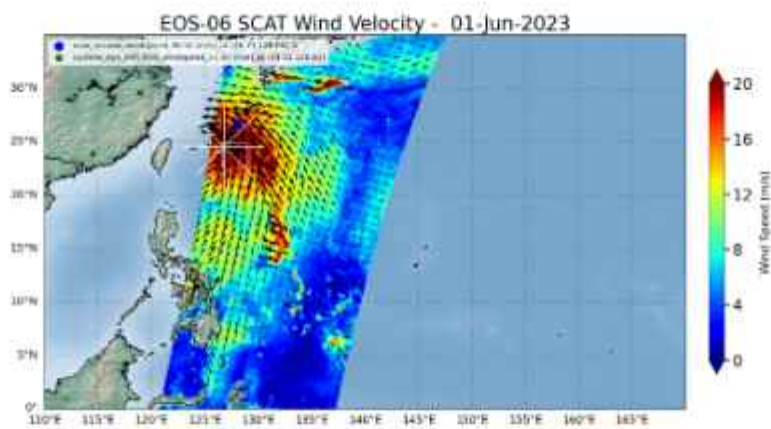
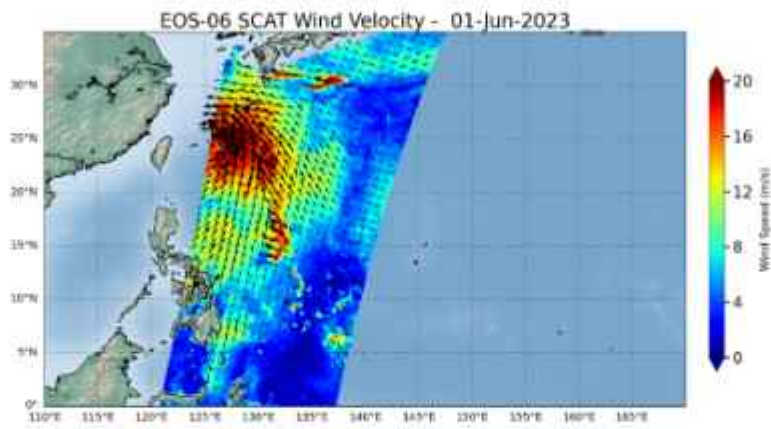


Figure 4.14- Day 01 152 Pass with min 11.32, max 30.51, vorticity 12.36 ws

RV - Biparjoy

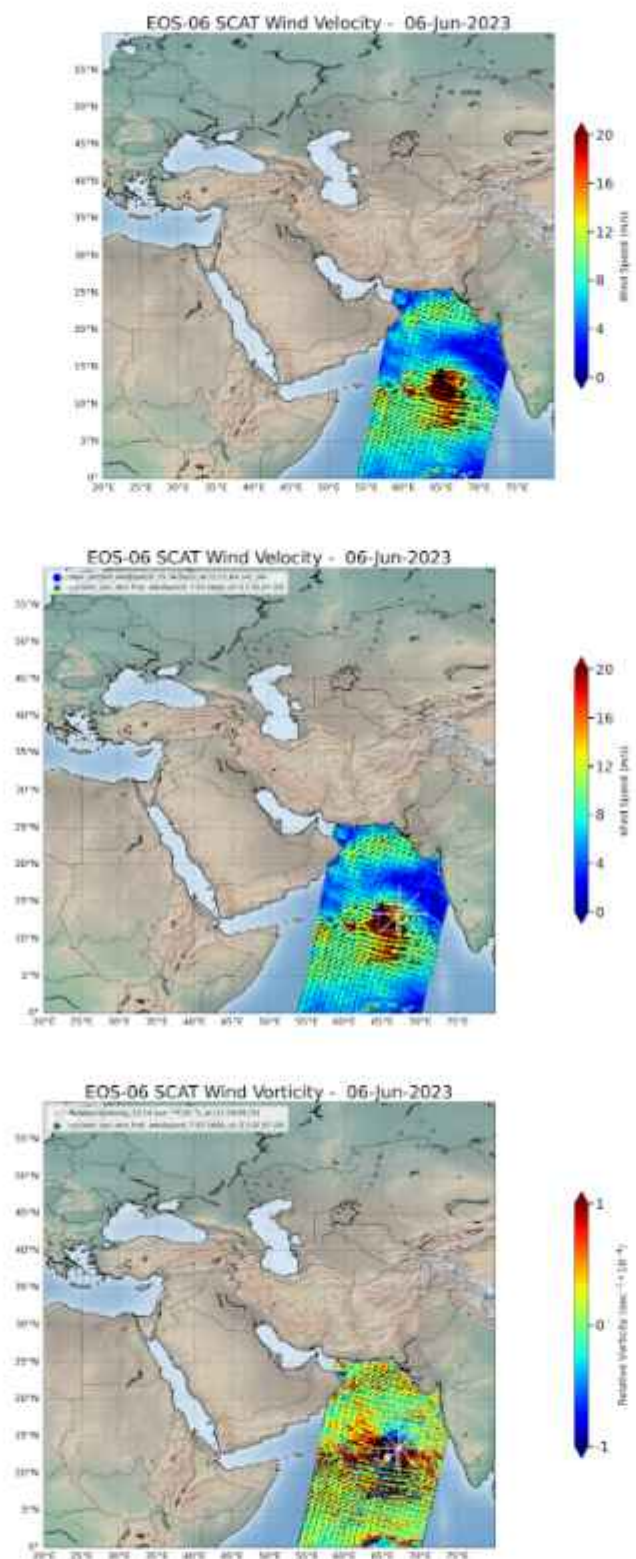


Figure 4.15- Day 06 157 Pass with min 7.92, max 39.34, vorticity 13.24 ws

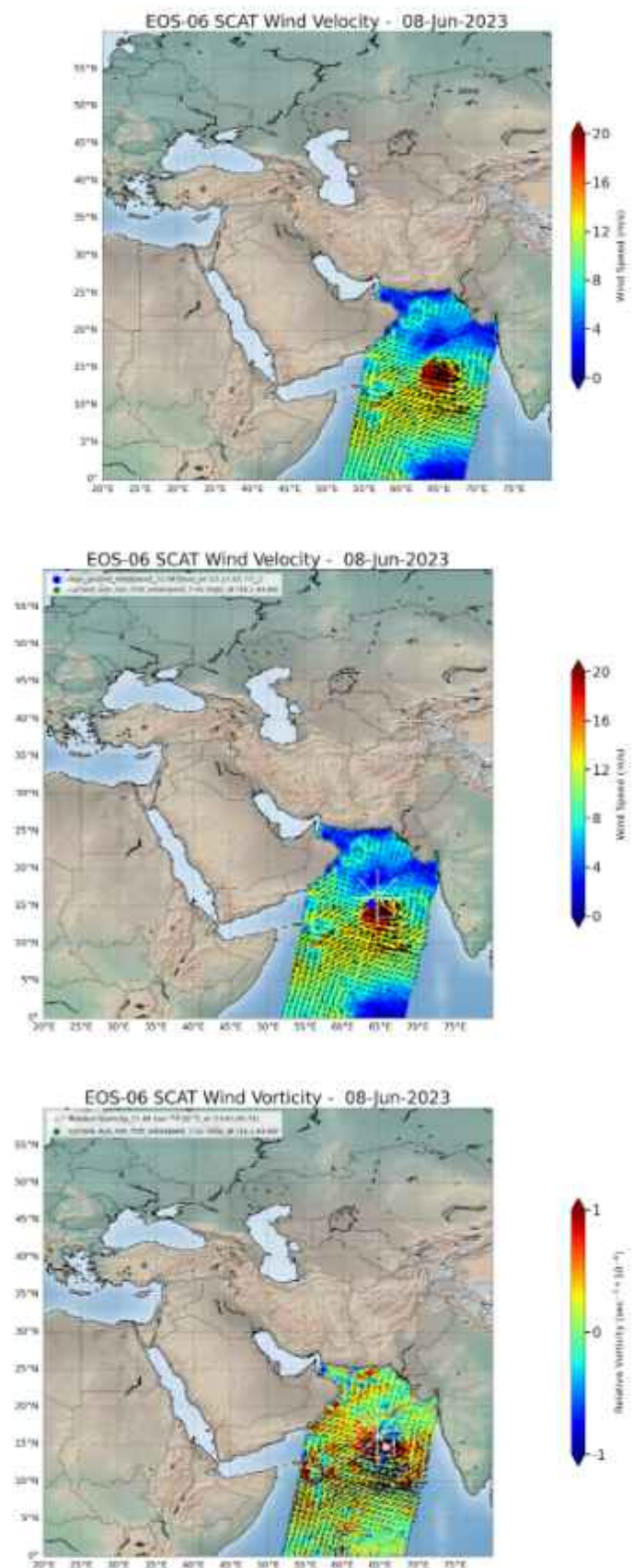


Figure 4.16- Day 08 159 Pass with min 7.55, max 33.96, vorticity 11.69 ws

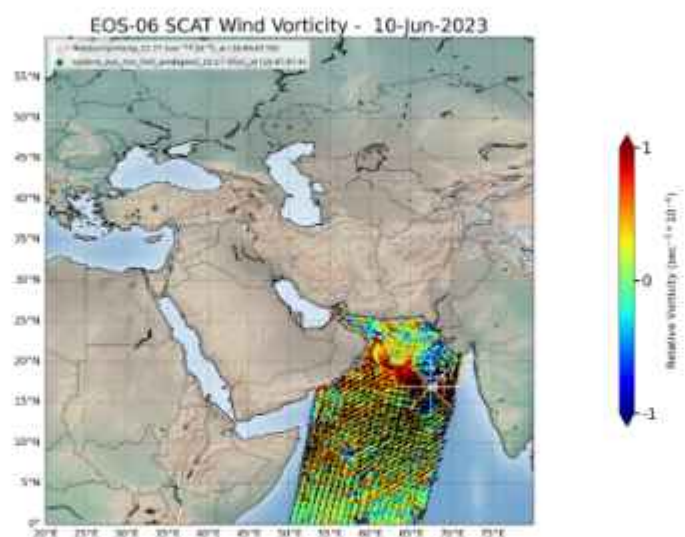
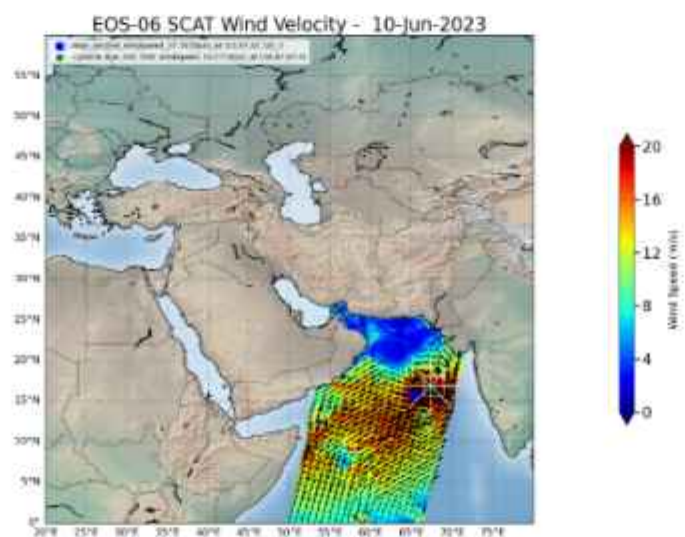
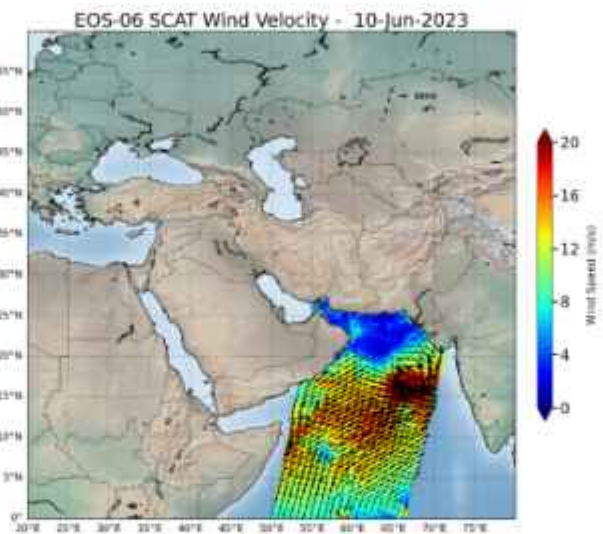


Figure 4.17- Day 10 161 Pass with min 10.17, max 37.35, vorticity 11.27 ws

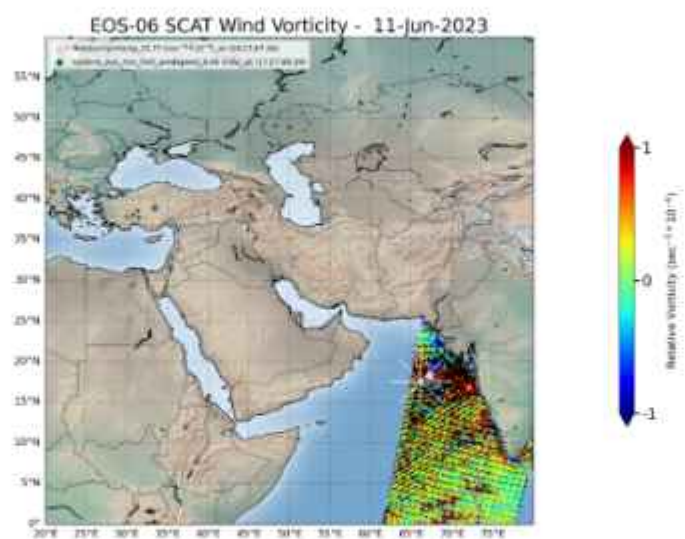
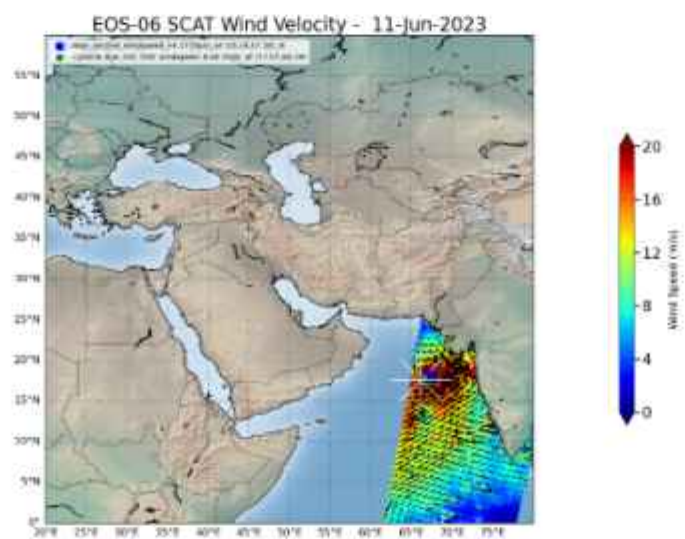
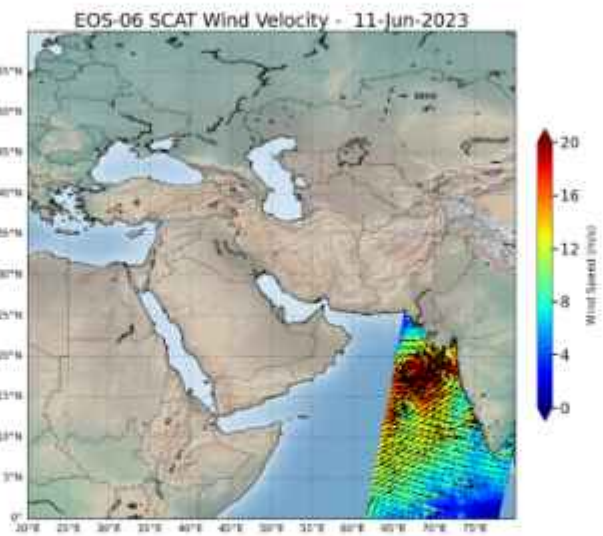


Figure 4.18- Day 11 162 Pass with min 8.66, max 44.17, vorticity 21.77 ws

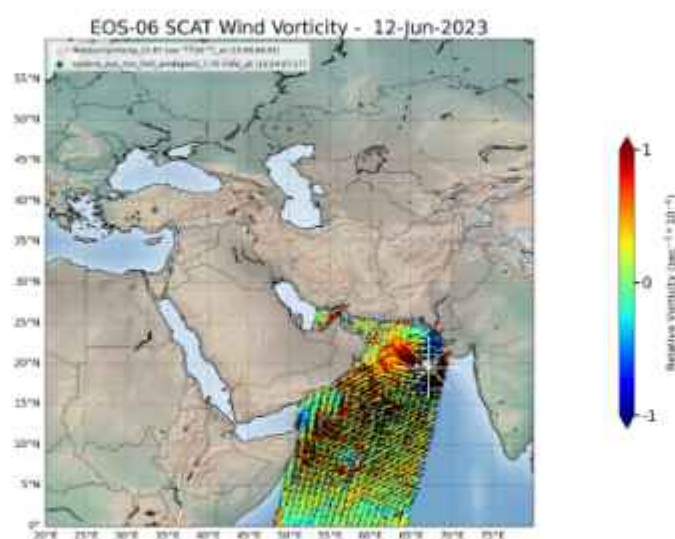
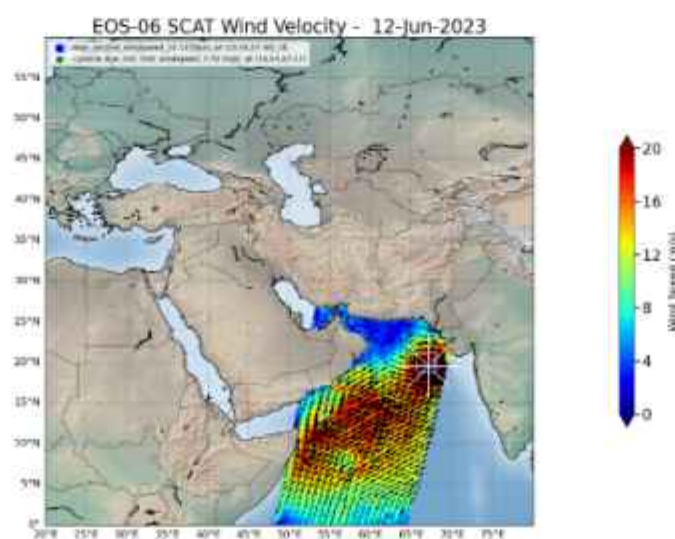
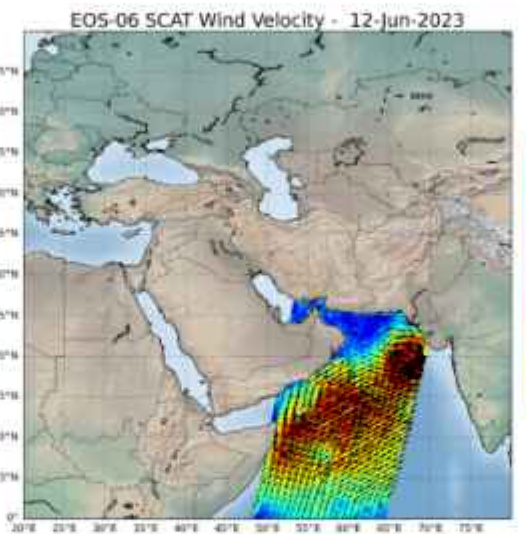


Figure 4.19- Day 12 163 Pass with min 7.76, max 33.13, vorticity 11.87 ws

4.2. Binarization

Binarization - Mawar

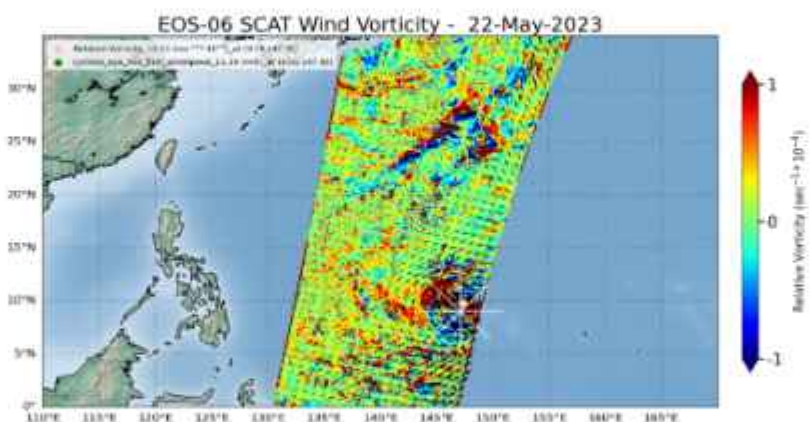
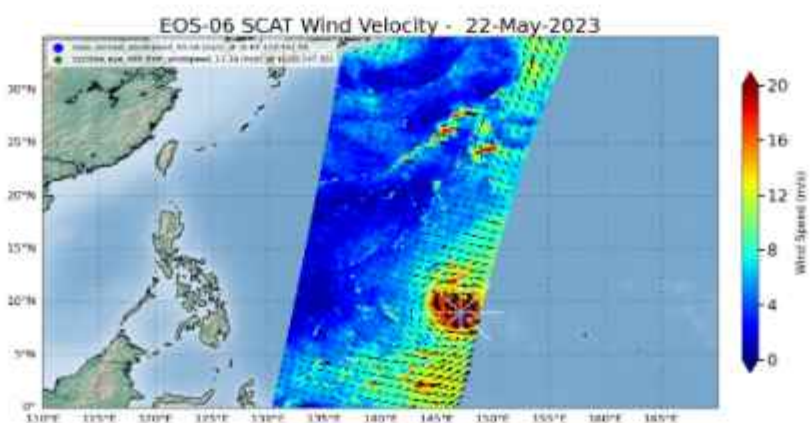
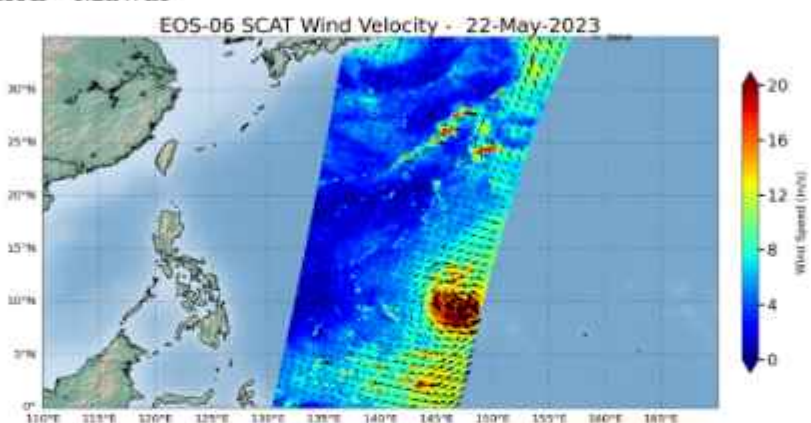


Figure 4.20- Day 22 142 Pass with min 11.39, max 33.46, vorticity 12.21 ws

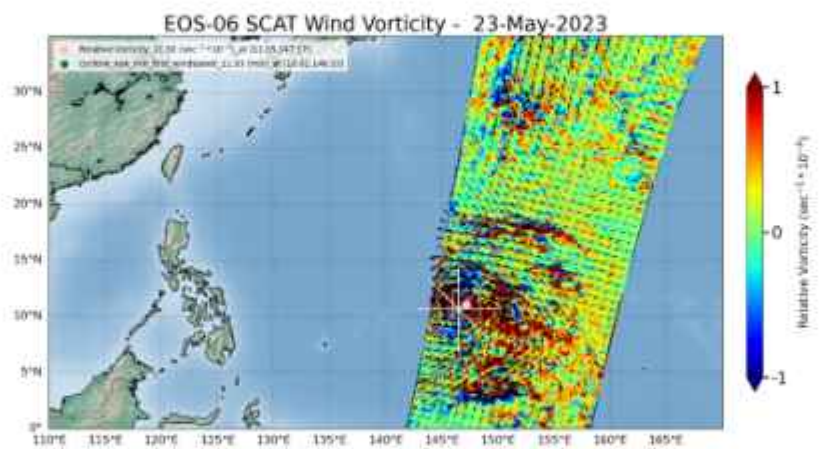
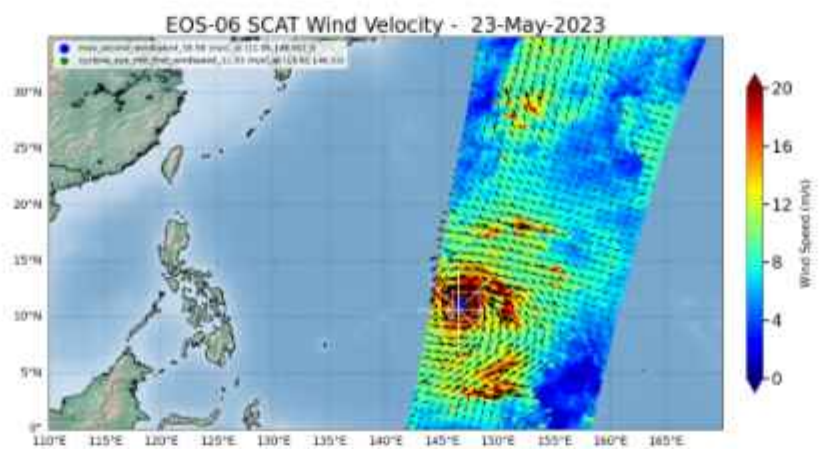
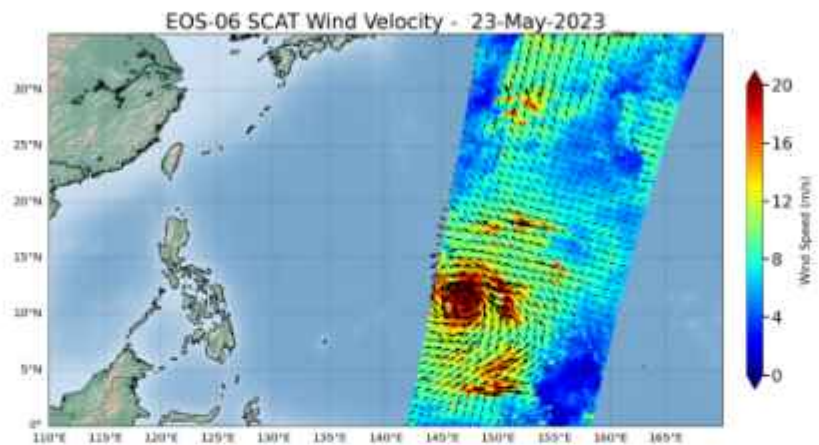


Figure 4.21- Day 23 143 Pass with min 11.93, max 36.58, vorticity 21.92 ws

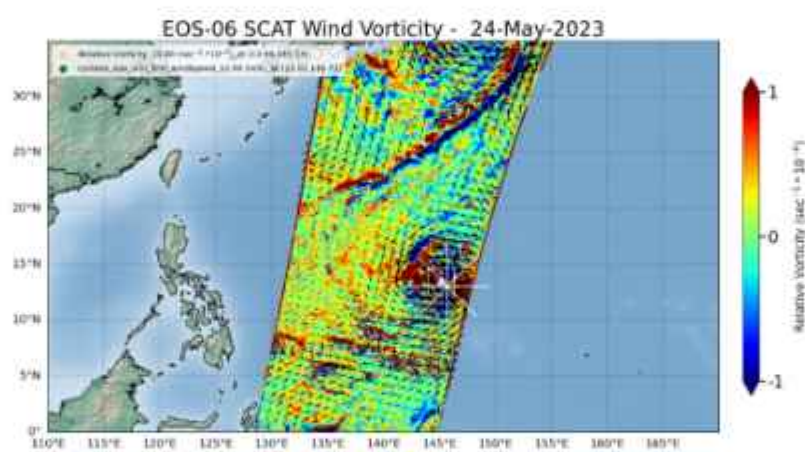
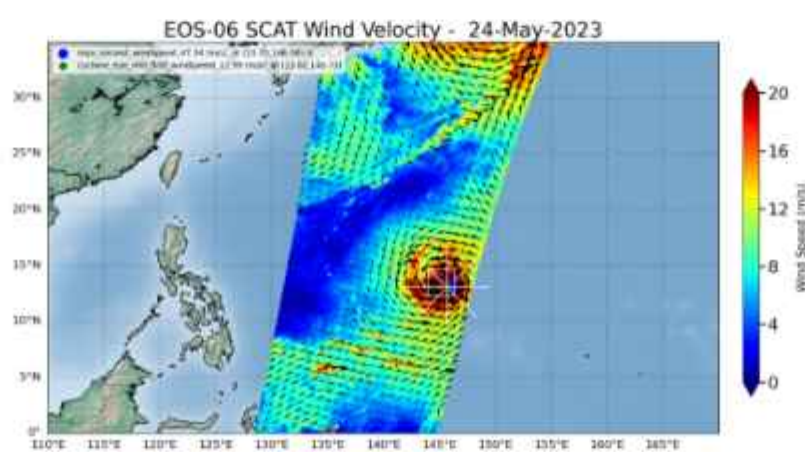
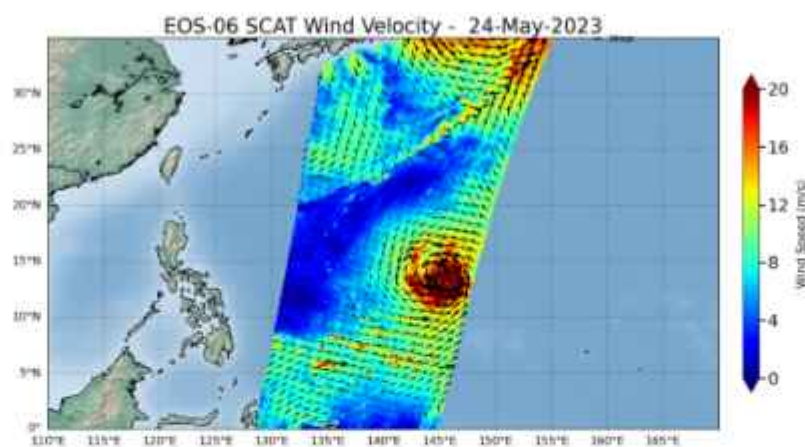


Figure 4.22- Day 24 144 Pass with min 12.99, max 47.34, vorticity 13.80 ws

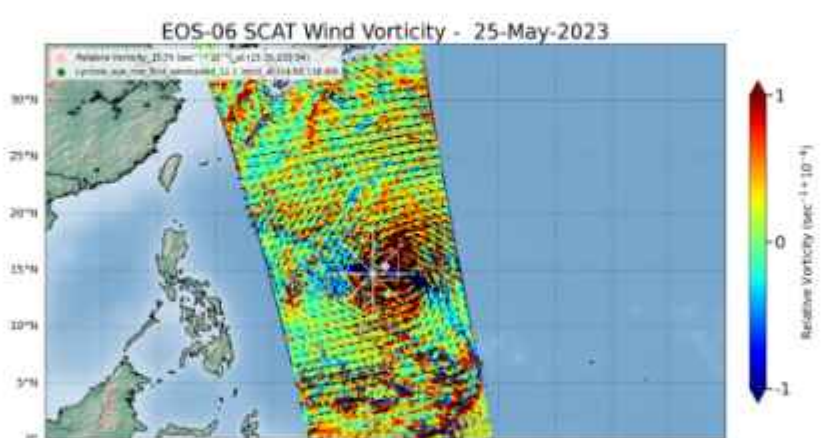
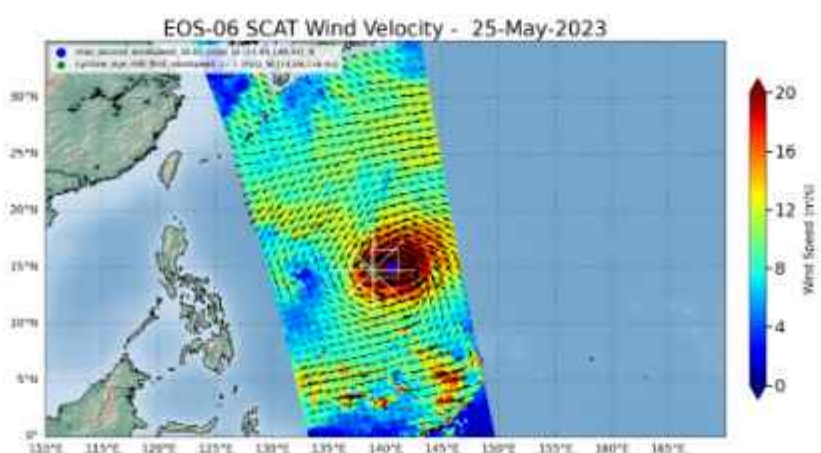
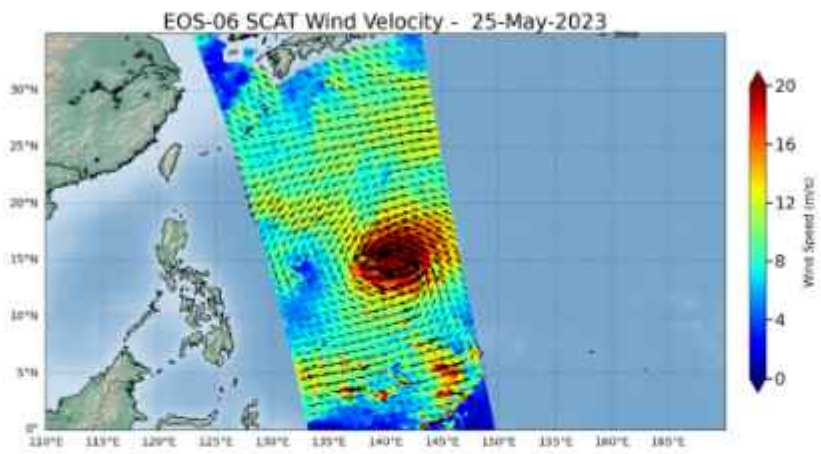


Figure 4.23- Day 25 145 Pass with min 12.1, max 38.65 , vorticity 15.79 ws

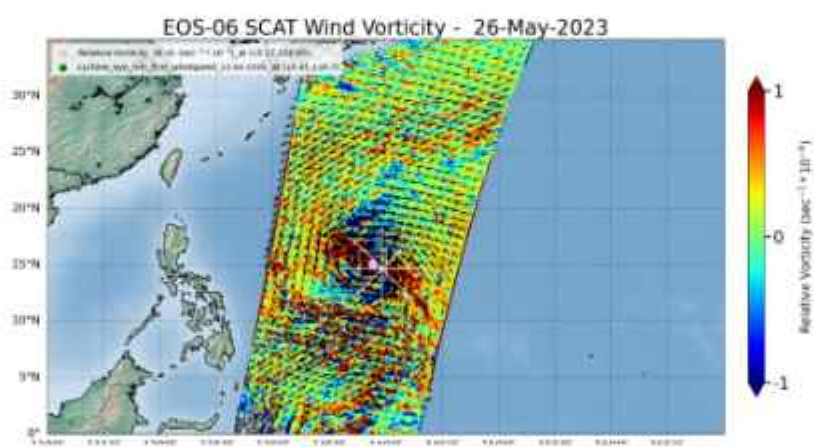
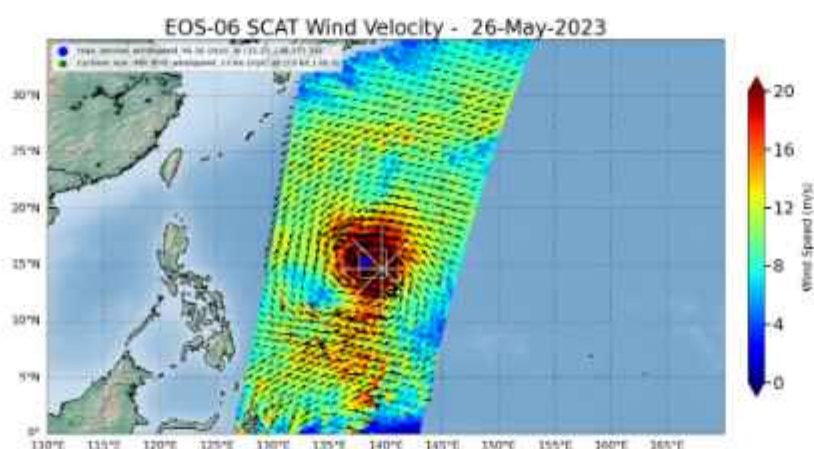
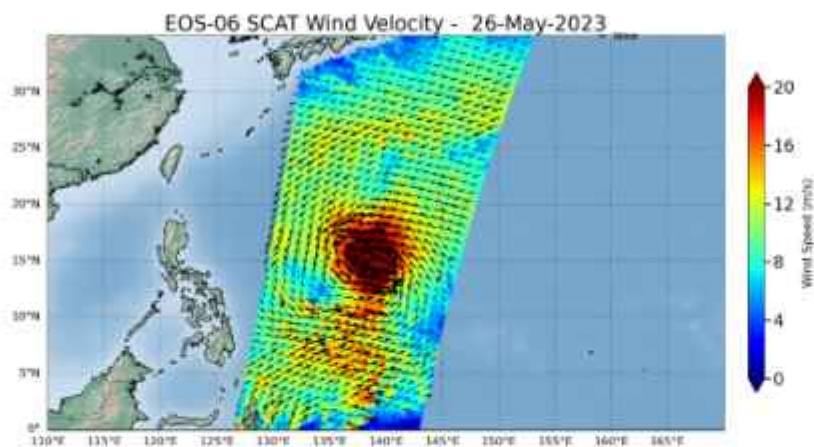


Figure 4.24- Day 26 146 Pass with min 13.66 , max 46.16, vorticity 18.41 ws

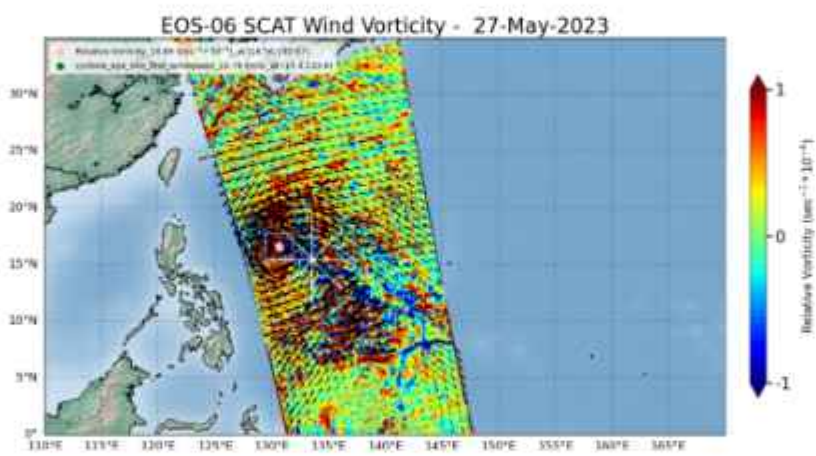
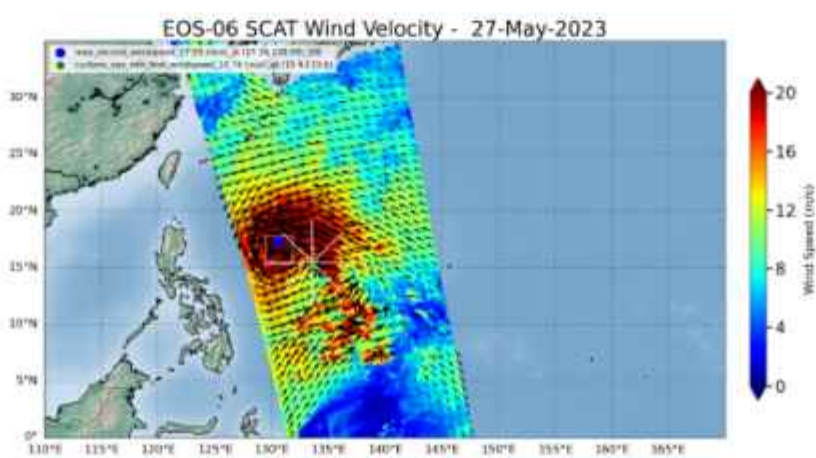
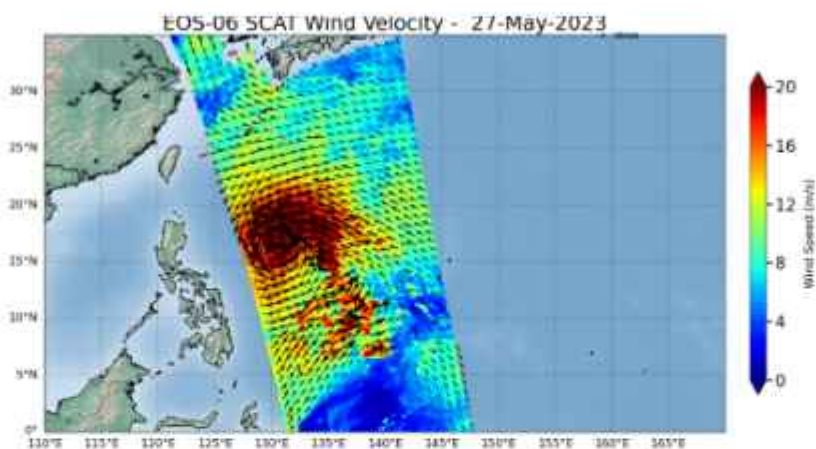


Figure 4.25- Day 27 147 Pass with min 10.74, max 37.59, vorticity 14.96 ws

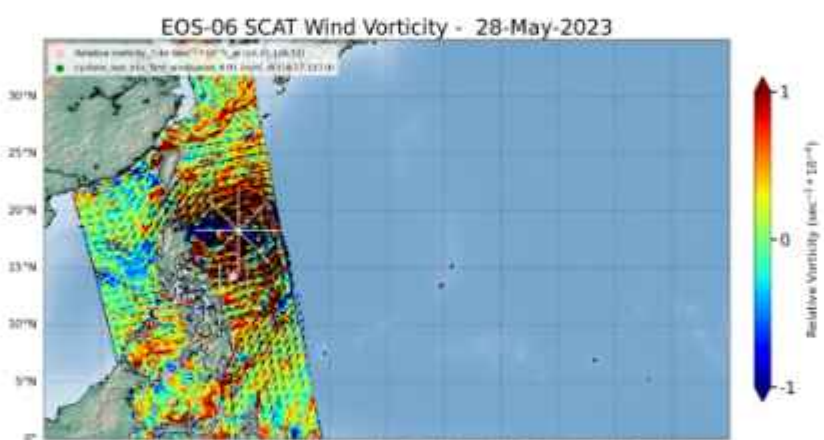
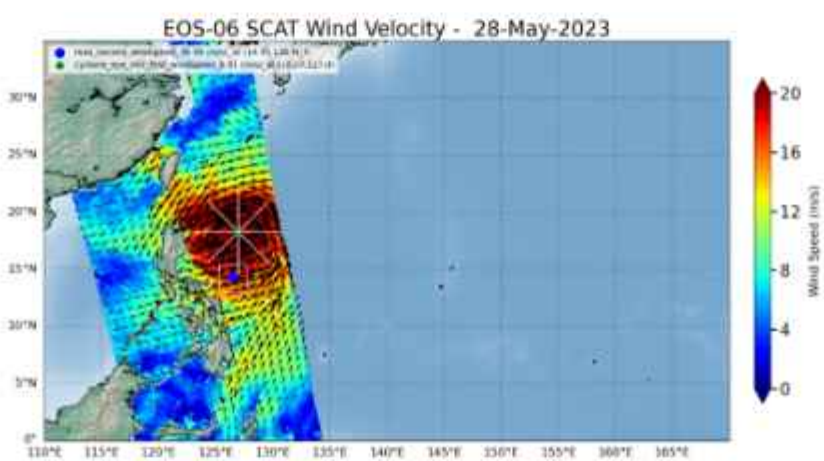
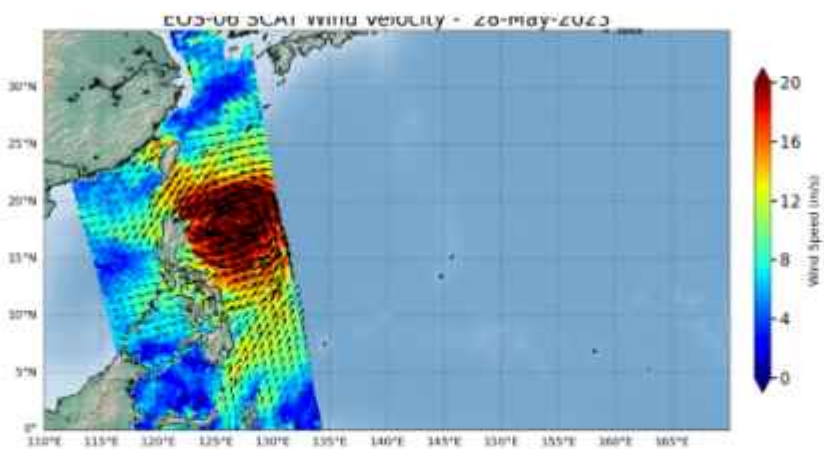


Figure 4.26- Day 28 148 Pass with min 8.91, max 36.99, vorticity 7.44 ws

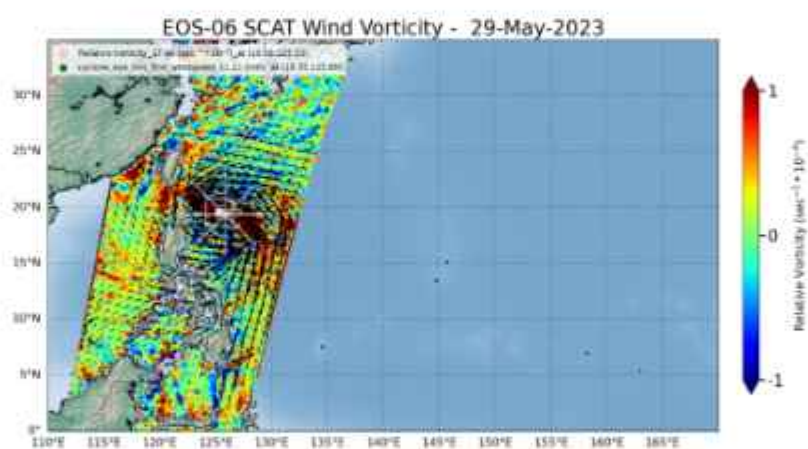
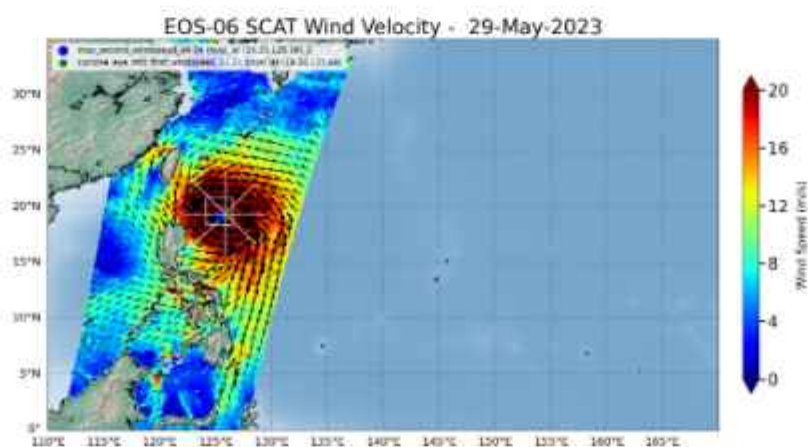
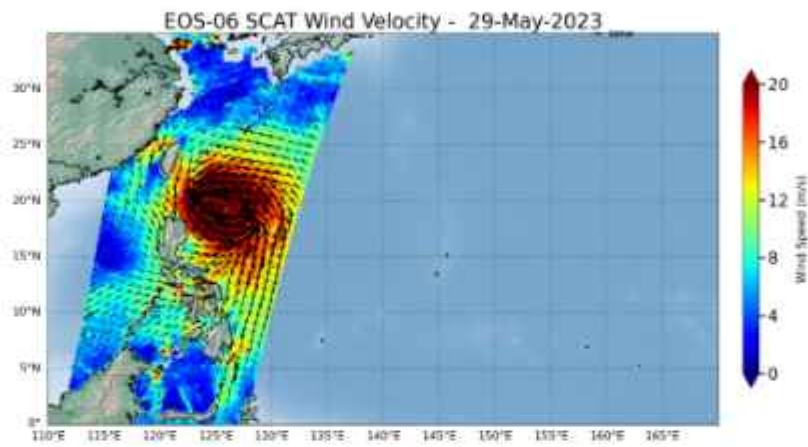


Figure 4.27- Day 29 149 Pass with min 11.21, max 44.54, vorticity 17.66 ws

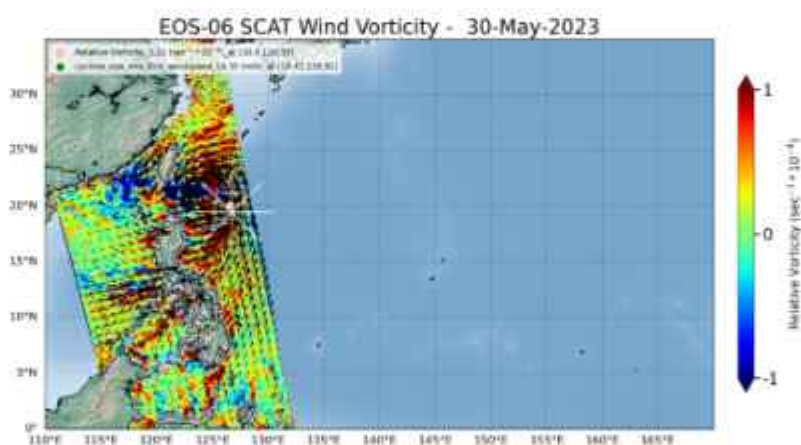
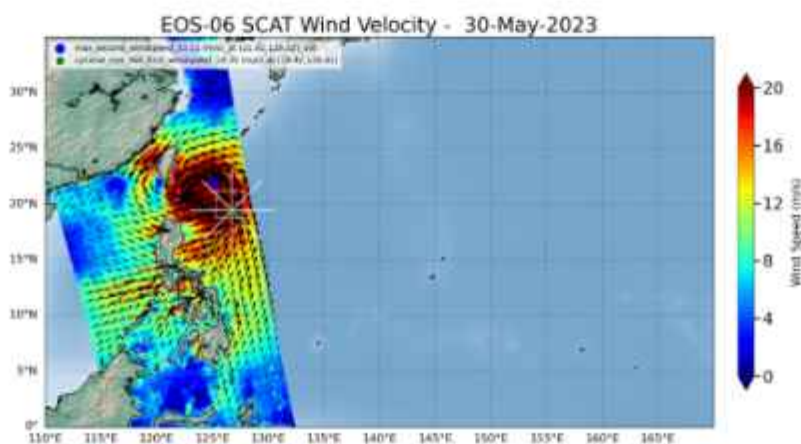
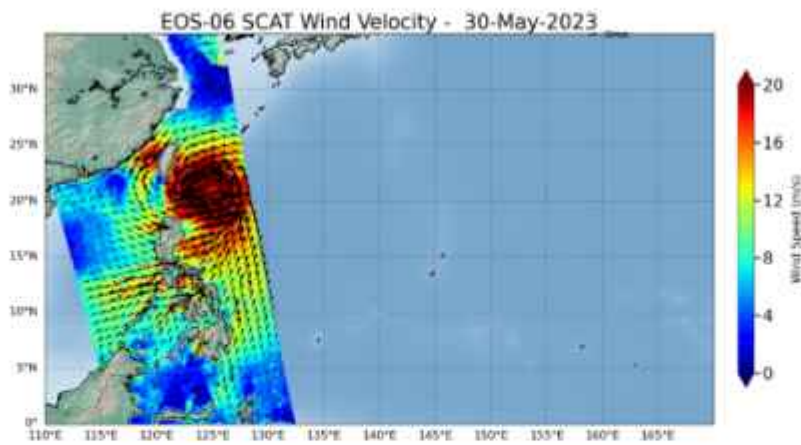


Figure 4.28- Day 30 150 Pass with min 10.35, max 33.21, vorticity 5.22 ws

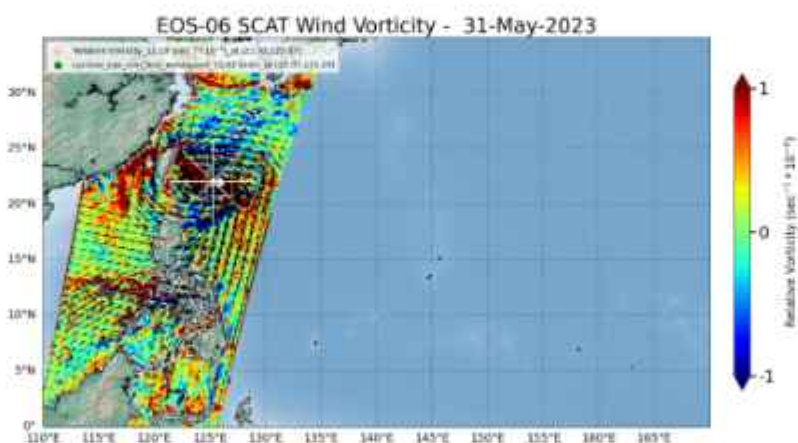
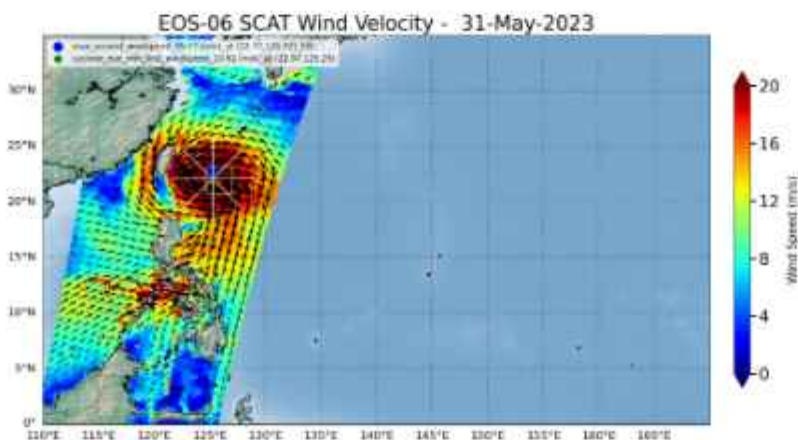
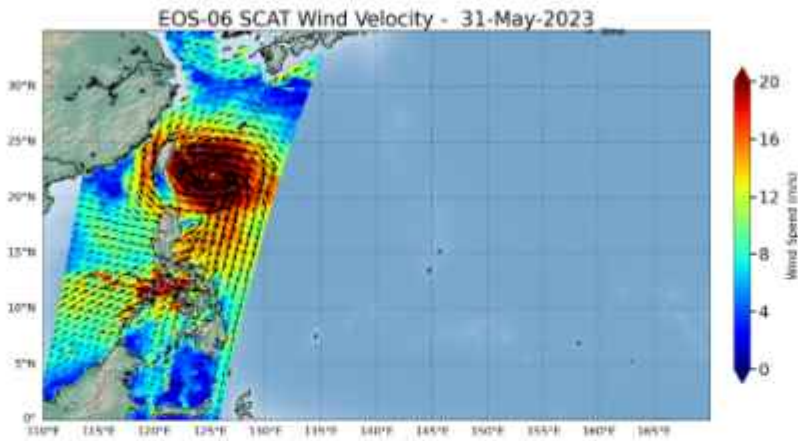


Figure 4.29- Day 31 151 Pass with min 10.62, max 35.77, vorticity 12.19 ws

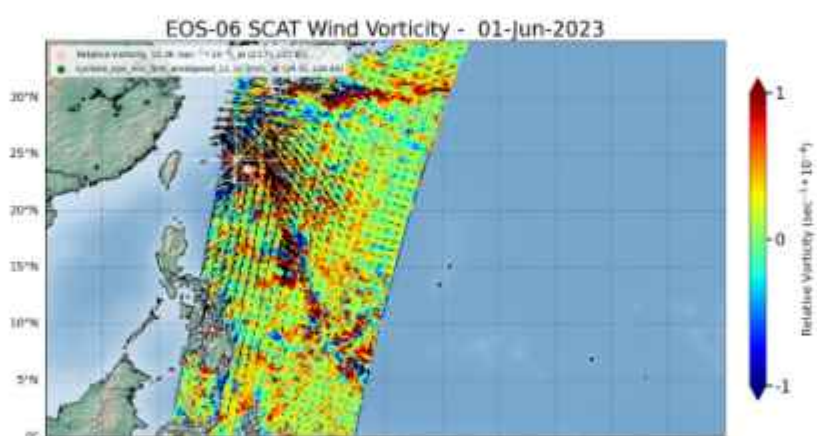
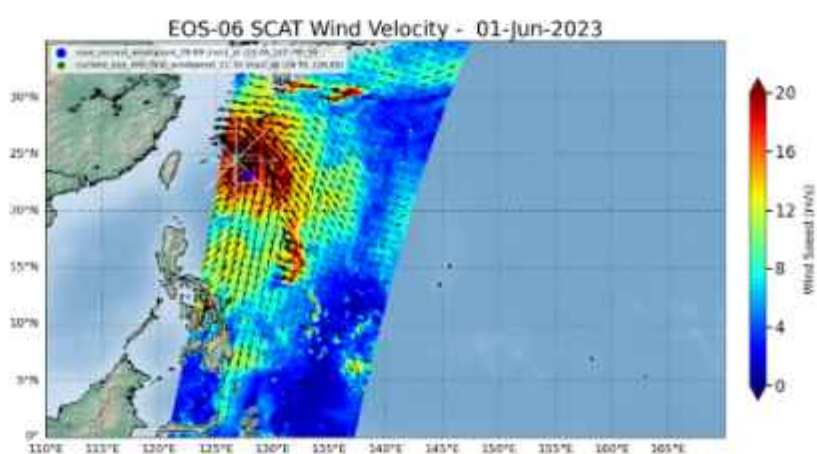
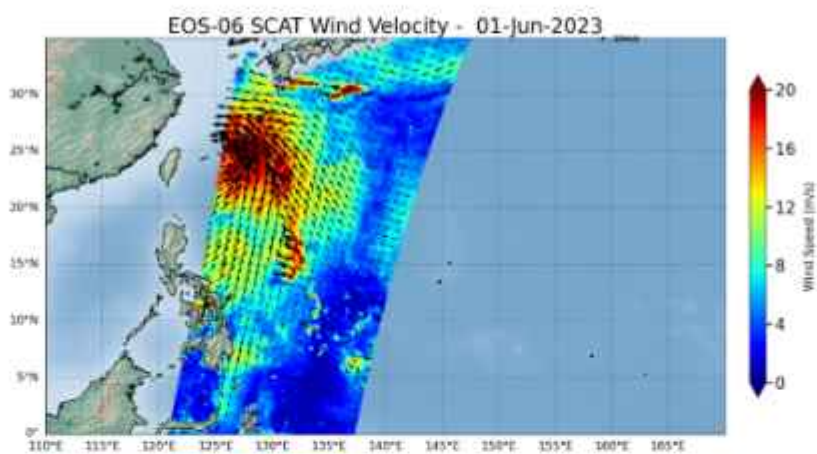


Figure 4.30- Day 32 152 Pass with min 11.32, max 28.69, vorticity 12.36 ws

Binarization - Biparjoy

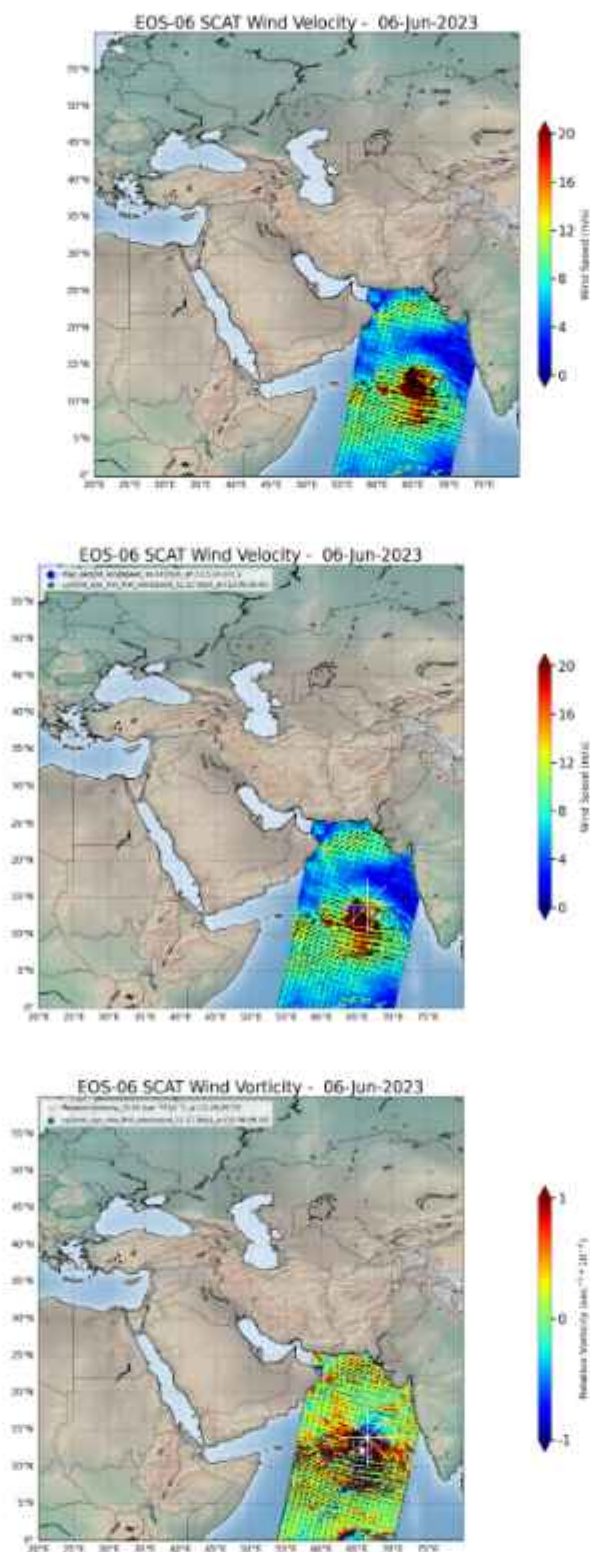


Figure 4.31- Day 06 157 Pass with min 11.11, max 39.34, vorticity 13.24 ws

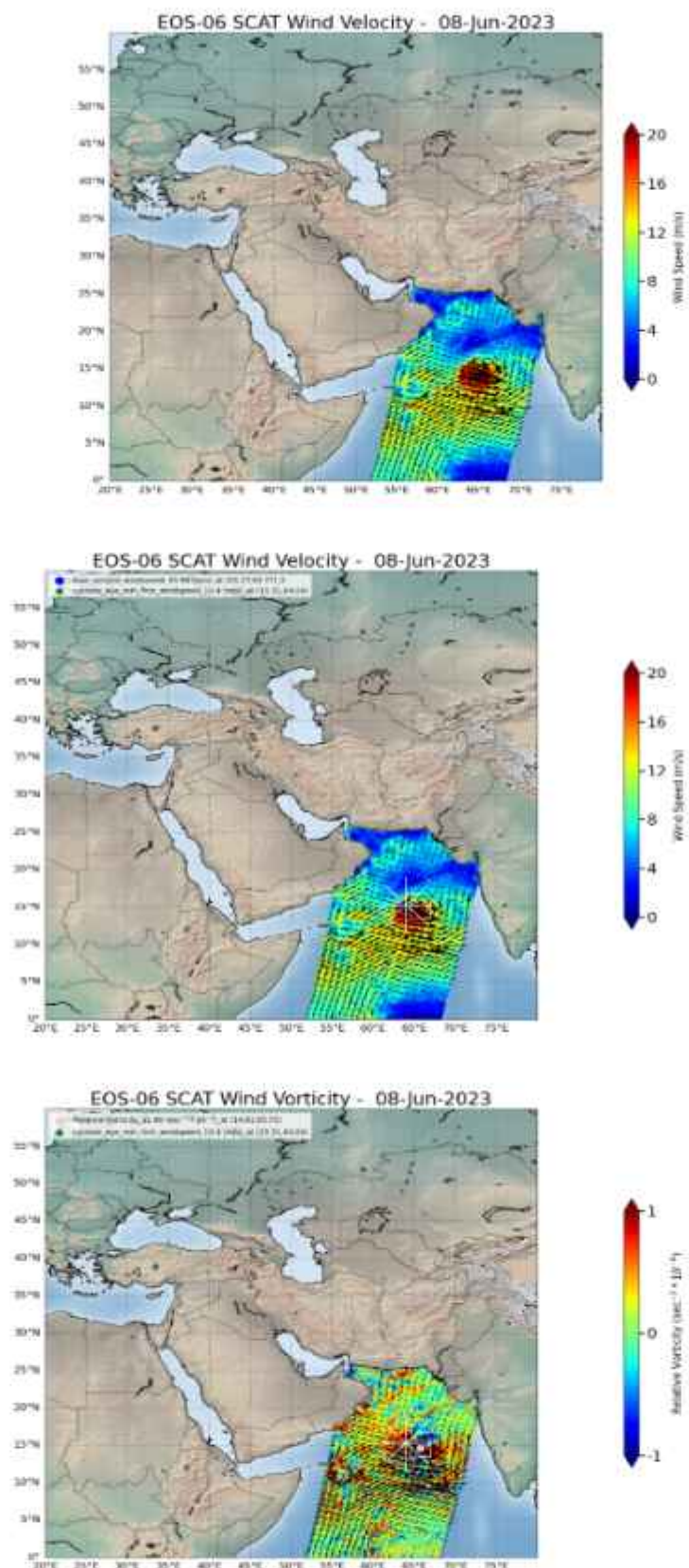


Figure 4.32- Day 08 159 Pass with min 10.4, max 33.96, vorticity 11.69 ws

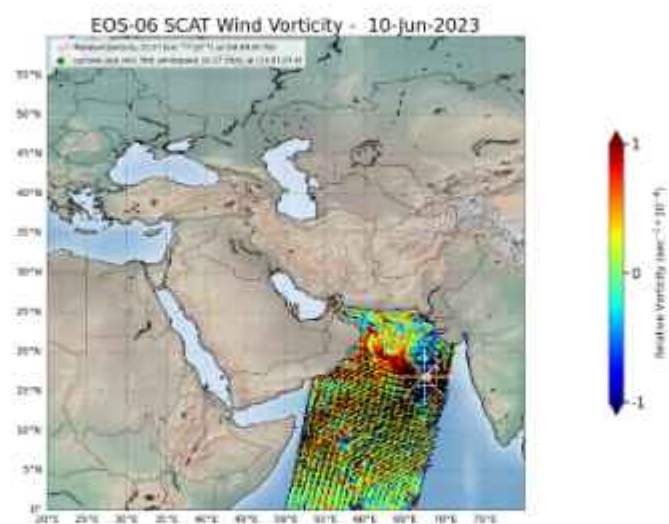
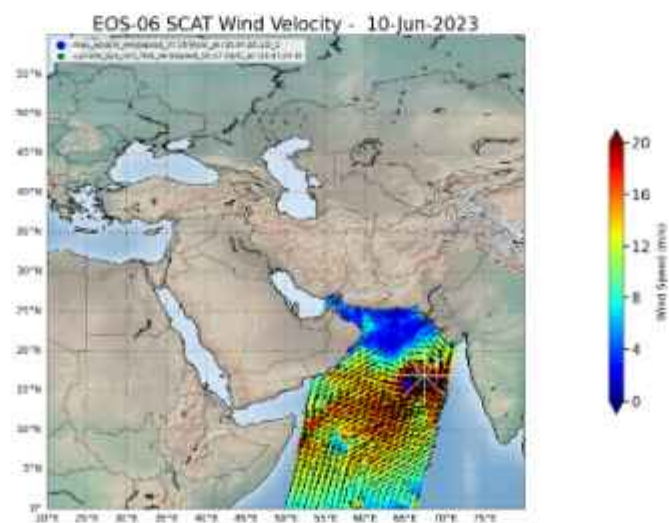
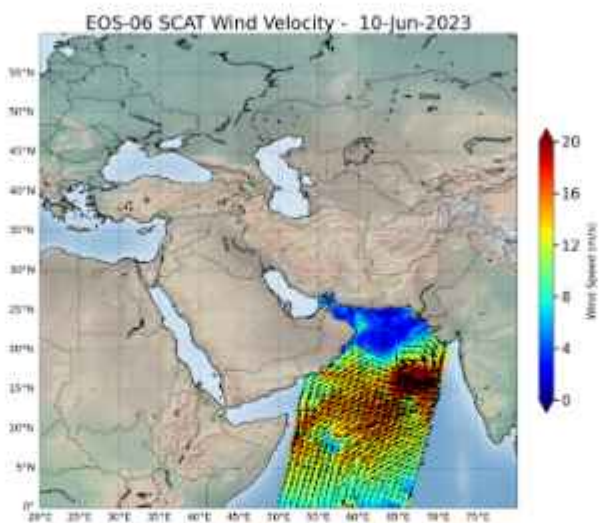


Figure 4.33- Day 10 161 Pass with min 10.17, max 37.35, vorticity 11.27 ws

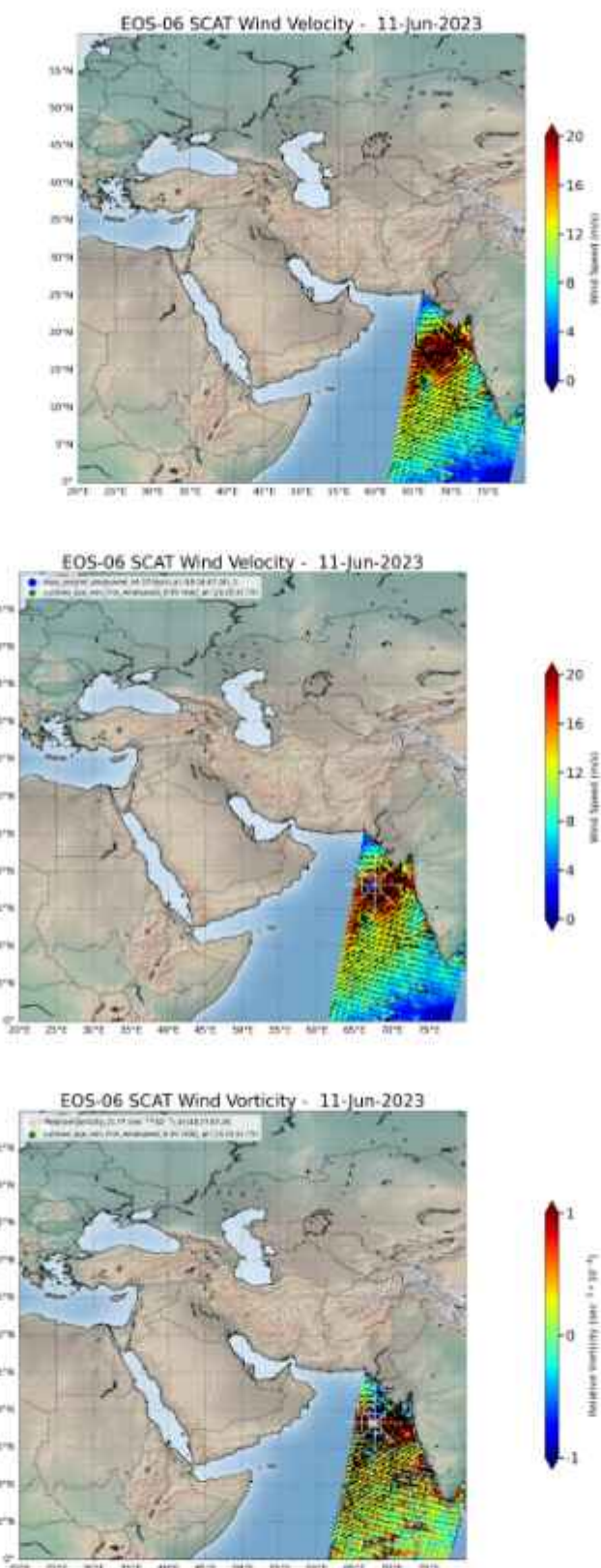


Figure 4.34- Day 11 162 Pass with min, max, vorticity ws

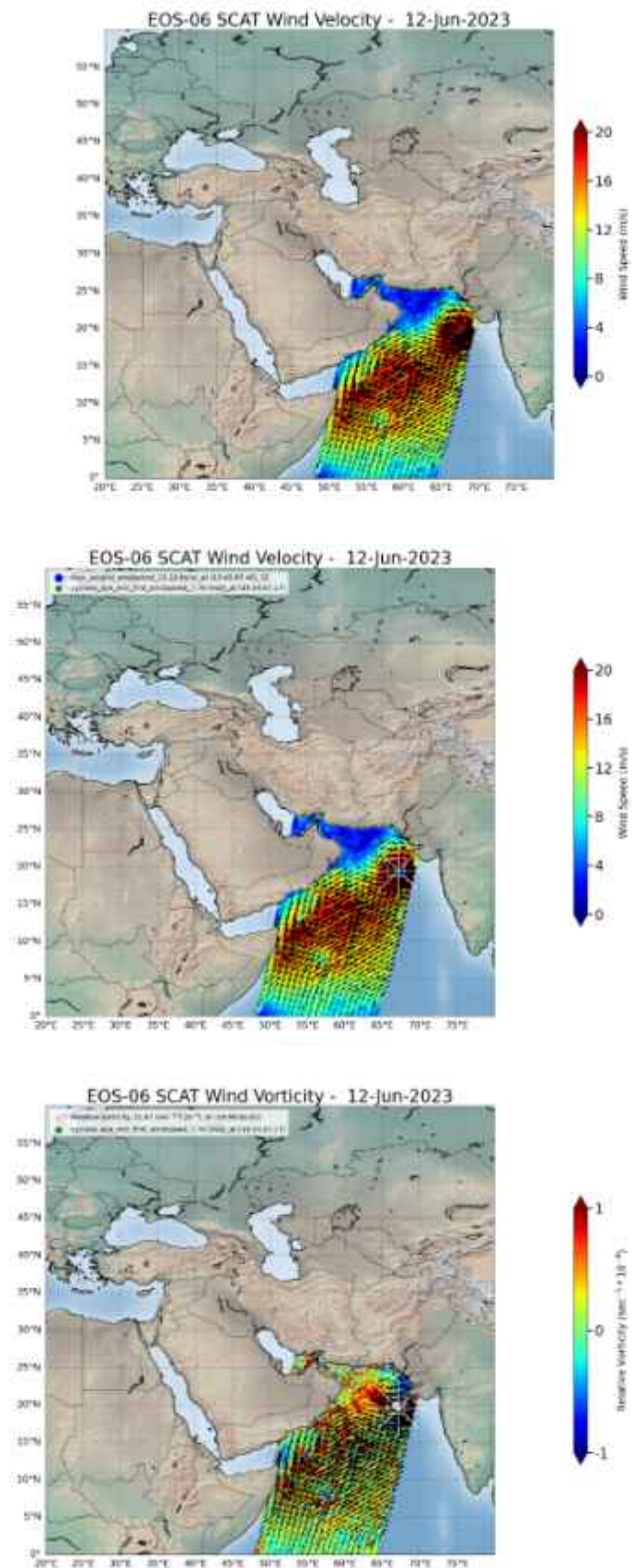


Figure 4.35- Day 12 162 Pass with min 8.95, max 44.17, vorticity 21.77 ws

4.3. Track Plot

The track plot generated through RV tracking, represented by a white line, focuses on quantifying the local rotation of air within the cyclone and plotting all the centres of 11 days. In contrast, binarization tracking, depicted by a black line and plotting all the centres of 11 days. Both tracking methods offer valuable perspectives on the cyclone's behaviour over the 11-day period. These track plots serve as essential at aiding in forecasting its path and impact.



Figure 4.36- Track data of RV and binarization for mawar

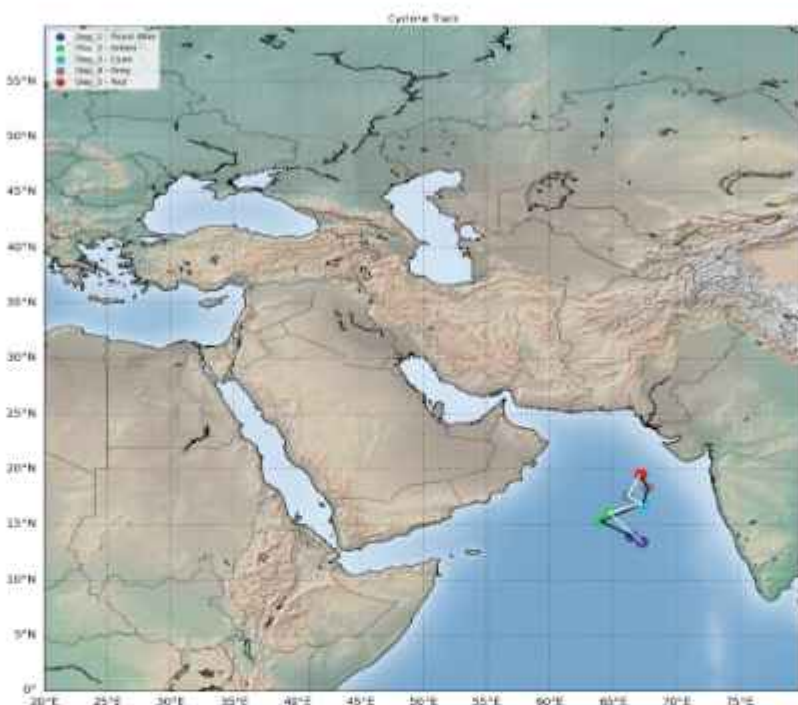


Figure 4.37- Track data of RV and binarization for biparjoy

The track plot compares three methods over 11 days: RV (white line), binarization (black line), and India Meteorological Department (IMD) centre track data (brown line). RV focuses on air rotation, while binarization distinguishes cyclonic and anticyclonic regions. IMD centre track data provides additional context. These comparisons offer insights into cyclone movement and aid in forecasting and response efforts.



Figure 4.38- Track data of RV and binarization for mawar

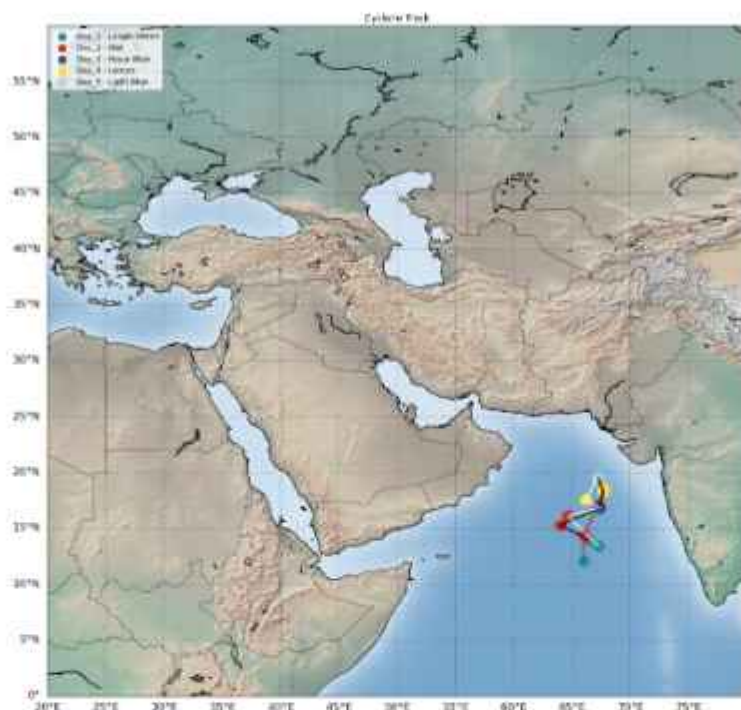


Figure 4.39- Track data of RV and binarization for biparjoy

The below data provides detailed information about the centre comparison with IMD and BI trackdata and IMD and RV track data.

IMD	IMD_to_BI	IMD_to_RV
Day_1_{10.0, 146.9 }	Day_1_{9.02, 147.15 }_(112.37)	Day_1_{9.02, 147.15 }_(112.37)
Day_2_{12.2, 146.1 }	Day_2_{10.62, 146.53 }_(181.83)	Day_2_{10.87, 145.25 }_(174.49)
Day_3_{13.8, 144.7 }	Day_3_{13.02, 145.73 }_(141.19)	Day_3_{14.34, 143.45 }_(147.59)
Day_4_{14.3, 143.5 }	Day_4_{14.68, 138.93 }_(493.80)	Day_4_{14.68, 138.93 }_(493.80)
Day_5_{15.7, 136.5 }	Day_5_{14.65, 139.7 }_(362.71)	Day_5_{14.65, 139.7 }_(362.71)
Day_6_{16.4, 133.3 }	Day_6_{15.4, 133.6 }_(115.73)	Day_6_{16.0, 129.28 }_(431.55)
Day_7_{17.3, 128.7 }	Day_7_{18.27, 127.0 }_(209.84)	Day_7_{18.27, 127.0 }_(209.84)
Day_8_{19.7, 125.6 }	Day_8_{19.35, 125.89 }_(49.38)	Day_8_{19.35, 125.89 }_(49.38)
Day_9_{20.4, 125.1 }	Day_9_{19.42, 126.81 }_(209.37)	Day_9_{21.08, 124.9 }_(78.42)
Day_10_{22.7, 125.5 }	Day_10_{22.07, 125.29 }_(73.30)	Day_10_{22.07, 125.29 }_(73.30)
Day_11_{25.8, 127.1 }	Day_11_{24.51, 126.83 }_(145.99)	Day_11_{24.51, 126.83 }_(145.99)

Figure 4.40- Track data of centre between IMD and RVand BI for Marwr

IMD	IMD_to_BI	IMD_to_RV
Day_1_{12.1, 66.0 }	Day_1_{13.96, 66.45 }_(212.49)	Day_1_{13.42, 67.28 }_(202.02)
Day_2_{14.4, 66.0 }	Day_2_{15.31, 64.04 }_(233.70)	Day_2_{16.1, 64.68 }_(236.19)
Day_3_{17.1, 67.3 }	Day_3_{16.87, 67.4 }_(27.70)	Day_3_{16.87, 67.4 }_(27.70)
Day_4_{18.6, 67.7 }	Day_4_{18.29, 67.75 }_(34.87)	Day_4_{17.57, 66.19 }_(196.45)
Day_5_{19.6, 67.3 }	Day_5_{19.54, 67.17 }_(15.17)	Day_5_{19.54, 67.17 }_(15.17)

Figure 4.41- Track data of centre between IMD and RVand BI for Biparjoy

4.4. Contour R34, R50, R60

The contour data obtained through which we can analyse the cyclones behaviour.
the input considered is masked wind speed with threshold being

R64 : 64 knots or 32.9 m/s

R50 : 50 knots or 25.7 m/s

R34 : 34 knots or 17.5 m/s

based on the threshold we are analysing wind speeds in each quadrants.

Days	QUAD-1	QUAD-2	QUAD-3	QUAD-4
22-May-2023_142_NN	(R34: 97.29, R50: 52.31, R64: 'nan')	(R34: 88.10, R50: 28.84, R64: 28.34)	(R34: 108.44, R50: 28.84, R64: 'nan')	(R34: 108.44, R50: 'nan', R64: 'nan')
23-May-2023_142_NE	(R34: 215.94, R50: 111.46, R64: 'nan')	(R34: 265.04, R50: 111.46, R64: 'nan')	(R34: 104.11, R50: 84.02, R64: 'nan')	(R34: 125.04, R50: 'nan', R64: 'nan')
24-May-2023_144_NE	(R34: 189.89, R50: 98.27, R64: 79.14)	(R34: 189.47, R50: 98.01, R64: 79.14)	(R34: 169.37, R50: 77.71, R64: 'nan')	(R34: 211.07, R50: 170.68, R64: 101.07)
25-May-2023_145_NN	(R34: 113.34, R50: 73.49, R64: 33.51)	(R34: 113.24, R50: 37.18, R64: 23.51)	(R34: 370.02, R50: 220.17, R64: 238.71)	(R34: 118.03, R50: 97.01, R64: 323.47)
26-May-2023_146_NE	(R34: 471.99, R50: 254.49, R64: 165.71)	(R34: 284.40, R50: 154.49, R64: 165.01)	(R34: 290.02, R50: 74.82, R64: 65.71)	(R34: 473.11, R50: 182.21, R64: 145.01)
27-May-2023_147_NN	(R34: 357.44, R50: 182.72, R64: 473.29)	(R34: 443.20, R50: 140.17, R64: 'nan')	(R34: 106.80, R50: 173.19, R64: 'nan')	(R34: 151.27, R50: 285.30, R64: 169.89)
28-May-2023_148_NE	(R34: 336.56, R50: 74.58, R64: 84.67)	(R34: 339.89, R50: 208.02, R64: 'nan')	(R34: 176.80, R50: 47.67, R64: 50.69)	(R34: 220.27, R50: 94.58, R64: 34.67)
29-May-2023_149_NN	(R34: 411.11, R50: 57.32, R64: 121.00)	(R34: 333.98, R50: 58.68, R64: 121.00)	(R34: 215.59, R50: 72.02, R64: 58.30)	(R34: 211.92, R50: 171.22, R64: 52.59)
30-May-2023_150_NN	(R34: 287.37, R50: 156.91, R64: 181.34)	(R34: 264.52, R50: 156.91, R64: 181.34)	(R34: 198.87, R50: 156.91, R64: 'nan')	(R34: 87.95, R50: 156.91, R64: 'nan')
31-May-2023_151_NE	(R34: 510.39, R50: 98.88, R64: 'nan')	(R34: 345.62, R50: 147.88, R64: 'nan')	(R34: 341.82, R50: 88.88, R64: 'nan')	(R34: 312.18, R50: 98.88, R64: 'nan')
01-Jun-2023_152_NN	(R34: 248.39, R50: 43.47, R64: 'nan')	(R34: 472.42, R50: 34.23, R64: 'nan')	(R34: 286.07, R50: 31.31, R64: 'nan')	(R34: 140.42, R50: 31.31, R64: 'nan')

Days	QUAD-1	QUAD-2	QUAD-3	QUAD-4
06-Jun-2023_157_NN	(R34: 239.47, R50: 237.08, R64: 'nan')	(R34: 548.86, R50: 217.08, R64: 'nan')	(R34: 113.47, R50: 178.81, R64: 'nan')	(R34: 100.05, R50: 217.08, R64: 'nan')
08-Jun-2023_159_NN	(R34: 57.11, R50: 11.07, R64: 'nan')	(R34: 530.07, R50: 218.72, R64: 'nan')	(R34: 259.08, R50: 218.72, R64: 'nan')	(R34: 251.07, R50: 112.05, R64: 'nan')
10-Jun-2023_161_NN	(R34: 308.42, R50: 83.12, R64: 23.01)	(R34: 278.62, R50: 99.07, R64: 28.05)	(R34: 322.72, R50: 99.07, R64: 'nan')	(R34: 328.49, R50: 22.21, R64: 225.81)
11-Jun-2023_162_NN	(R34: 237.85, R50: 56.17, R64: 18.07)	(R34: 311.44, R50: 56.17, R64: 133.07)	(R34: 322.58, R50: 317.09, R64: 133.07)	(R34: 313.12, R50: 317.09, R64: 133.07)
12-Jun-2023_163_NN	(R34: 232.68, R50: 73.07, R64: 'nan')	(R34: 388.77, R50: 77.07, R64: 39.07)	(R34: 238.79, R50: 181.57, R64: 'nan')	(R34: 212.07, R50: 181.57, R64: 'nan')

Chapter 5

5. Conclusion

The HDF5 dataset provided by the NRSC serves as a crucial resource for cyclone analysis, enabling the identification of cyclone centres through two distinct methods: RV and binarization. These methods allow us to pinpoint the core of cyclonic activity and characterise the cyclone into four quadrants, providing insights into maximum and mean wind speeds within each quadrant. By leveraging this dataset, we establish a comprehensive framework for automatically tracking cyclone movements and assessing wind speed intensities over time.

The plotted track data derived from these methods is then compared to IMD track data, facilitating a rigorous validation process and ensuring the reliability of our analysis. This comparative approach not only enhances the accuracy of cyclone tracking but also enables us to establish trends and patterns in cyclone behaviour. Through daily analysis, we gain a deeper understanding of cyclone dynamics, empowering meteorologists to make informed forecasts and effectively communicate potential risks to communities in vulnerable areas.

In summary, the integration of HDF5 dataset analysis, cyclone centre identification, analysing the daily characteristics of cyclones such as rv, Vmax, distance from centre, mean wind speeds, R34, R50, R64 and track data comparison with IMD track data establishes a robust methodology for cyclone monitoring and intensity assessment. This approach enables us to automate this process and obtain a detailed report on how to analyse cyclones characteristics and monitor its moments.

7. References

- [1]. "Scatterometer" (2023, December 15). In Wikipedia.
(<https://en.wikipedia.org/wiki/Scatterometer>)
- [2]. Atmospheric pressure and winds.
(<https://www.britannica.com/science/climate-meteorology/Atmospheric-pressure-and-wind>)
- [3]. Atmospheric circulation and weather systems.
(<https://www.ncert.nic.in/ncerts/l/kegy210.pdf>)
- [4]. Global tropical cyclone tracks
(https://en.wikipedia.org/wiki/File:Global_tropical_cyclone_tracks-edit2.jpg)
- [5]. Prediction of Tropical Cyclogenesis Using Scatterometer Data Neeru Jaiswal and C. M. Kishtawa.
- [6]. Stoffelen, Ad, 1998, Thesis "Scatterometry".
(<http://igitur-archive.library.uu.nl/dissertations/01840669/inhoud.htm>).
- [7]. Observation and Tracking of Tropical Cyclones Using Resolution Enhanced Scatterometry Richard Ryan Halterman.
- [8]. EOS06-SCAT-3 Wind Products V1.

Process DataSet

Automated Data Set Processing

This appendix documents the tools and procedure for generating the co- location and centre x data sets for oceansat3 winds and IMD best-tracks. The procedure is broken down into three principal steps: co-location and image creation, track determination, and visualisation. Tools used employ a combination of Python libraries Matplotlib, basemap. They are outlined below.

Co-location and image creation

First, process the HDF5 file to extract specific fields including Latitude, Longitude, Wind speed selection, and wind direction selection. Subsequently, compute the meridional and zonal wind speeds. Upon extraction, convert values of 327.67 and 655.35 to NaN (Not a Number) to mitigate effects stemming from non-cyclone areas such as land and water.

After that apply two methods :

RV:

First calculate max vorticity and in the radius of 100 km calculate min wind speed then consider it as the centre of the cyclone. After that consider the four quadrants around the centre NorthEast, NorthWest, SouthEast, SouthWest. Then calculate the max, mean wind speeds in each quadrant.

Binarization:

First binarize the data it gives the cyclone areas as 1's extract the largest group of ones and consider it the area of cyclone. Then calculate the min wind speed in that area and consider it as the centre of the cyclone. After that consider the four quadrants around the centre NorthEast, NorthWest, SouthEast, SouthWest. Then calculate the max, mean wind speeds in each quadrant.